

Spring School on Numerical Relativity and Gravitational Wave Physics

Gravitational Waves from colliding Compact Star Binaries in the context of Strange/Exotic Matter

*ROOM 6620
ITP NEW BUILDING, BEIJING
15.-25. MAY, 2017*

MATTHIAS HANAUSKE

*FRANKFURT INSTITUTE FOR ADVANCED STUDIES
JOHANN WOLFGANG GOETHE UNIVERSITY
INSTITUTE OF THEORETICAL PHYSICS
DEPARTEMENT OF RELATIVISTIC ASTROPHYSICS
D-60438 FRANKFURT AM MAIN
GERMANY*

Chapter 3

Contents of the whole Lecture

- **Chapter 1**

- General Relativity of Black Holes and Compact Stars
- Elementary Particle Physics and the Interior of a Compact Star

- **Chapter 2**

- Numerical Relativity and Relativistic Hydrodynamics
- The Einstein Toolkit

- **Chapter 3**

- Binary Mergers of Compact Stars
- Gravitational Waves and Internal Properties of Hypermassive Neutron Stars

[Intro 介绍](#)

[Chapter I 第一章](#)

[Chapter II 第二章](#)

[Chapter III 第三章](#)

[e-learning 电子学习](#)

Spring School on Numerical Relativity and Gravitational Wave Physics

15th-25th May 2017, Beijing
Room 6620, ITP New Building, Beijing



Invited Lecturers:

Niels Warburton (University College Dublin)
Andrea Taracchini (Max Planck Institute for Gravitational Physics)
David Hilditch (Theoretical Physics Institute, University of Jena)
David Weir (Helsinki Institute of Physics, University of Helsinki)
Koutarou Kyutoku (KEK, IPNS)
Matthias Hanauskę (Goethe University Frankfurt)

(Spring School on Numerical Relativity and Gravitational Wave Physics)

Vorlesungsreihe (6 Vorlesungen) über
Gravitationswellen von kollidierenden kompakten Sternen und die
Eigenschaften seltsamer Materie
(Gravitational waves from colliding compact star binaries in the context of
strange/exotic matter)
致密星碰撞引起的引力波和奇异物质的性质
Beijing, China, 15.-25. May 2017

Die im Jahre 2017 gehaltene Vorlesungsreihe führt einerseits in die Allgemeine Relativitätstheorie ein, andererseits fokussiert sie sich auf den speziellen Teilaspekt der relativistischen Astrophysik kollidierender hybrider Neutronensterne, in deren innerem Bereich es zur Bildung seltsamer und exotischer Materie kommen kann. Kollabiert ein instabiler Neutronenstern zu einem schwarzen Loch oder zu einem Quark Stern? Wie kann man anhand des ausgesandten Gravitationswellen-Signals zweier kollidierender kompakter Sterne die Eigenschaften der Nuklearen- und Quark-Materie entschlüsseln?

(The series of lectures held in 2017. Topics: theory of general relativity theory, relativistic astrophysics of colliding hybrid neutron stars, strange and exotic matter in the interior of compact stars. Questions: Does an unstable neutron star collapse to a black hole or quark star? How can we extract the strange properties of high density nuclear and quark matter by means of the emitted gravitational wave signal of two colliding compact stars?)

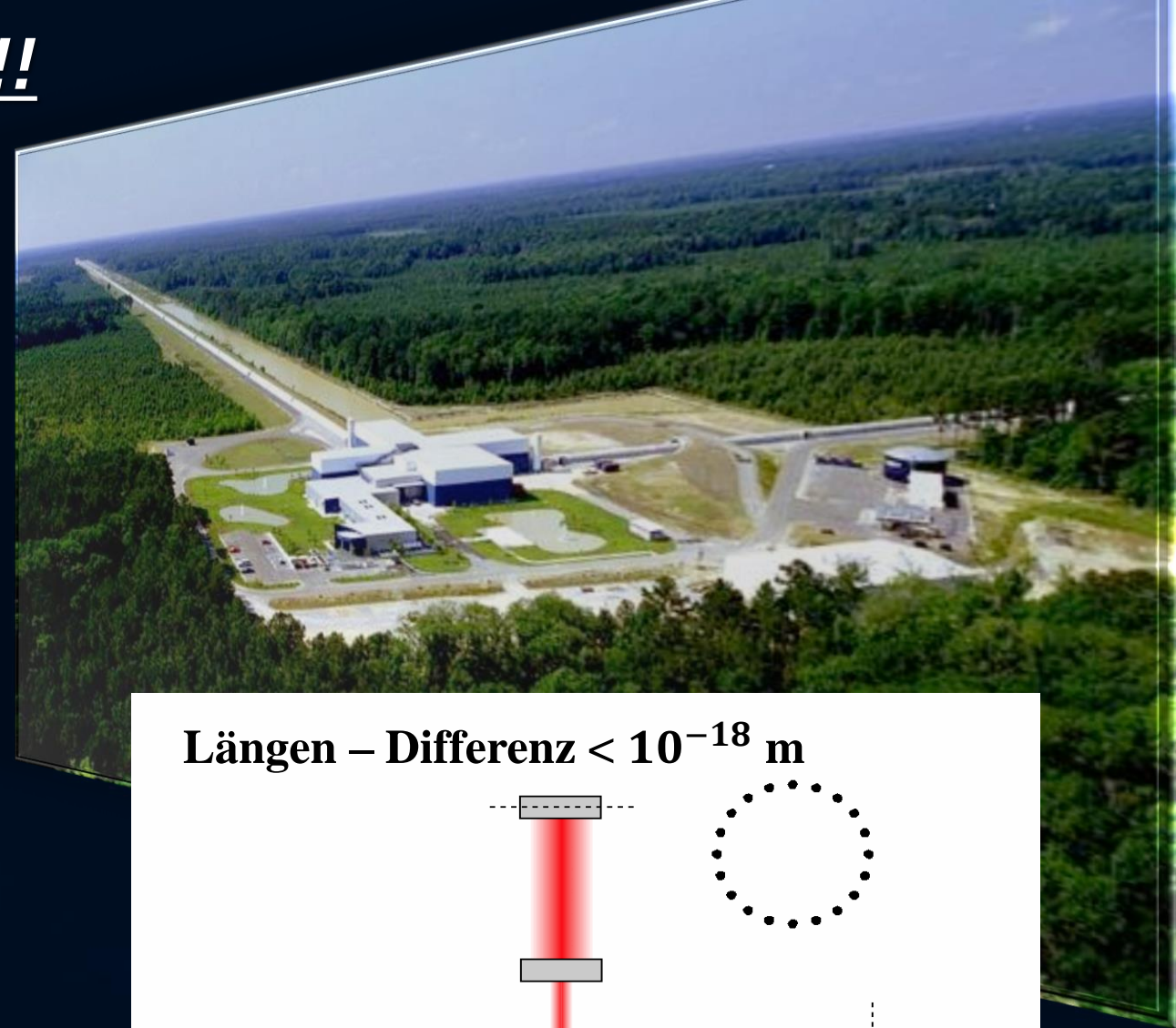
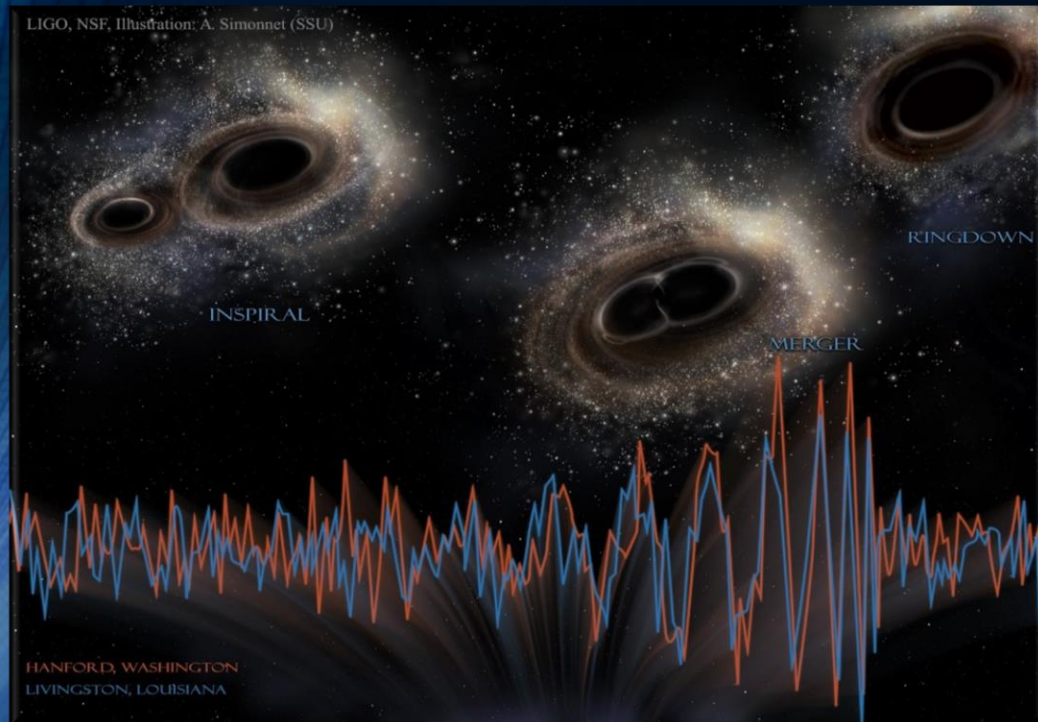
在2017年开设的课程,一方面介绍广义相对论理论,另一方面聚焦于相对论天体物理中的一个特殊部分:混合致密星碰撞,以及在其内部可能生成的奇异和异常物质。一个不稳定的中子星是会坍缩成黑洞还是夸克星?如何根据两个致密星碰撞发射的引力波信号来解码核物质和夸克物质的奇异特性?

Gravitational Waves detected!!!

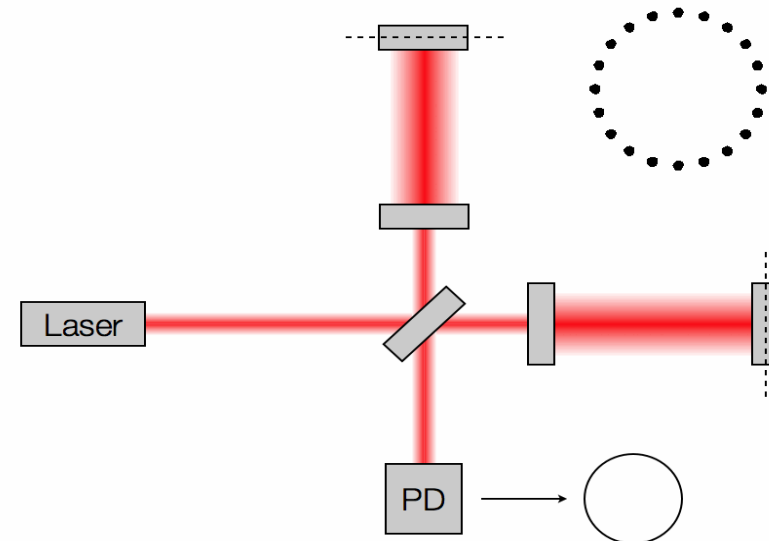
Collision of two Black Holes GW150914

Masses: 36 & 29 Sun masses

Distance to the earth 410 Mpc
(1.34 Billion Light Years)



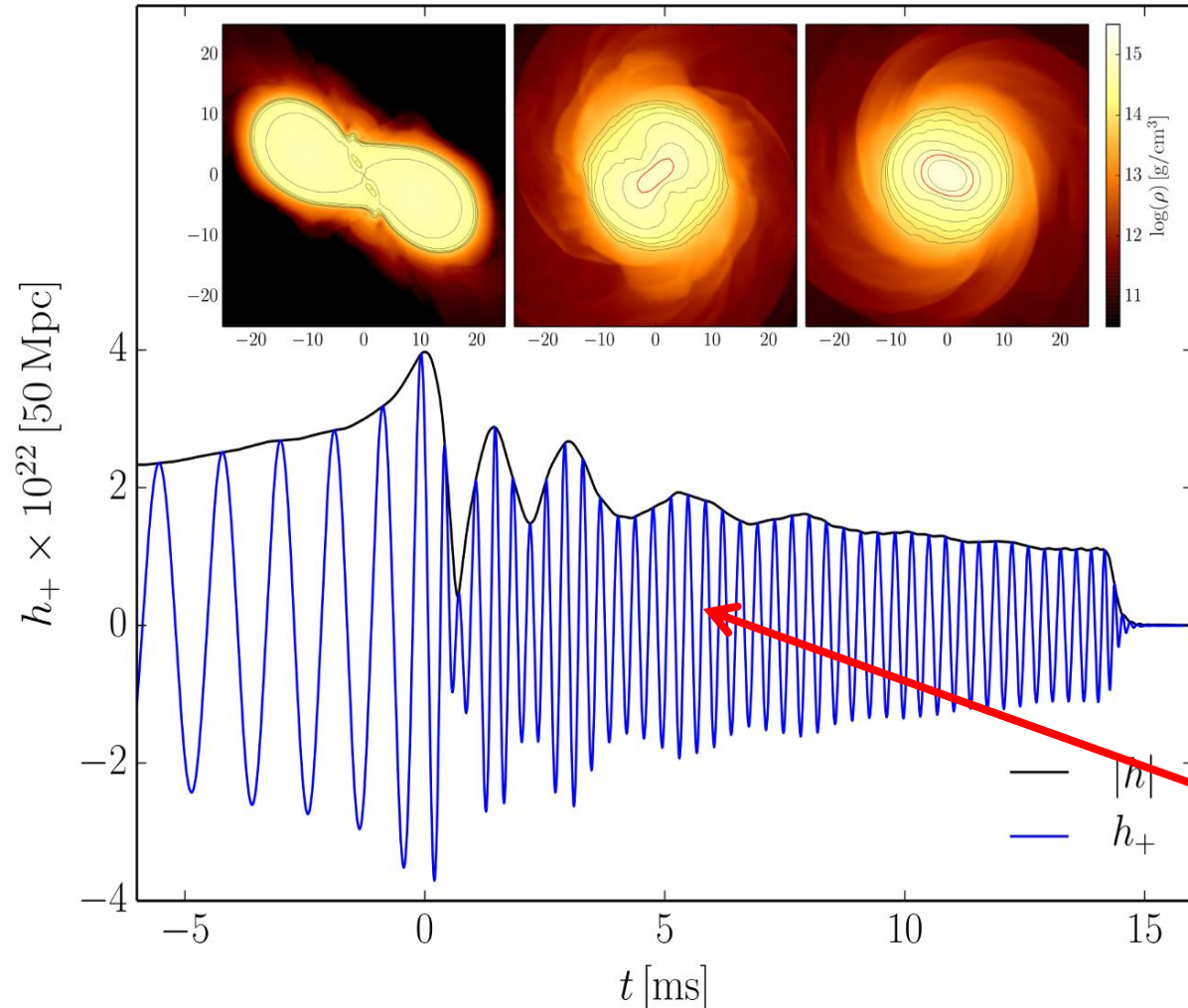
Längen – Differenz $< 10^{-18}$ m



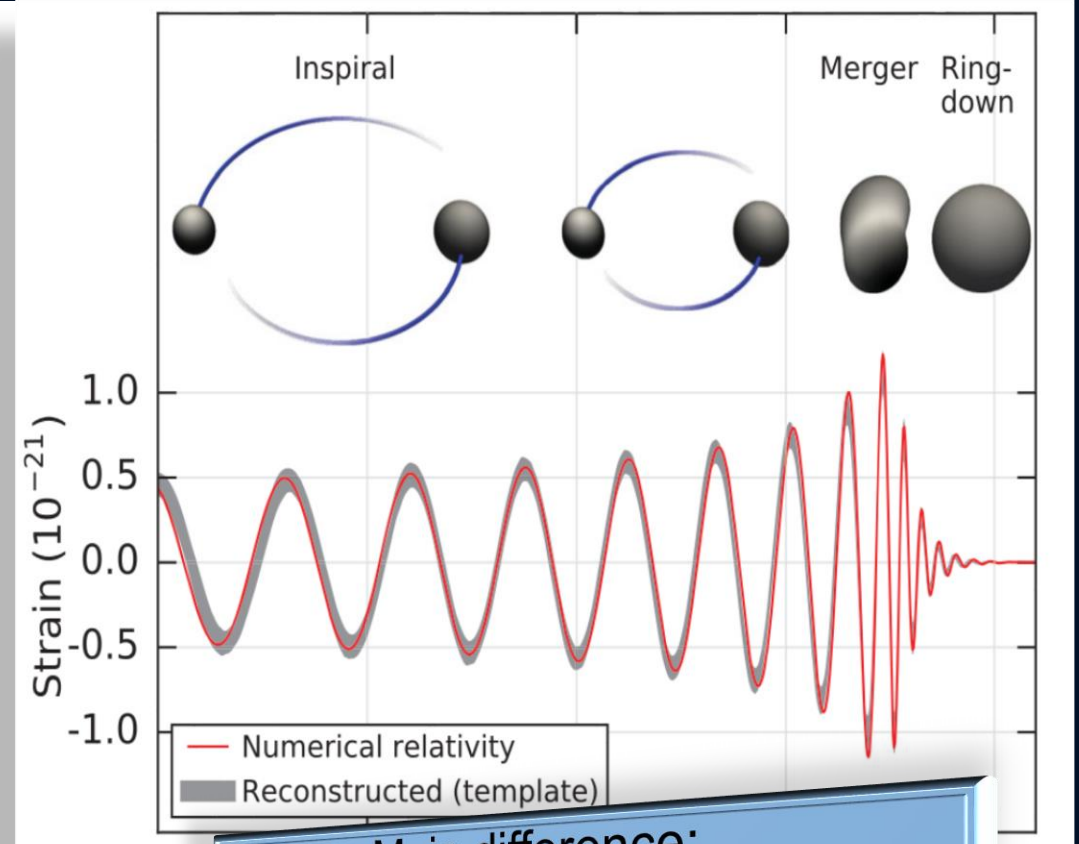
Credit: Les Wade from Kenyon College

Gravitational Waves from Neutron Star Mergers

Neutron Star Collision (Simulation)



Collision of two Black Holes



Main difference:
In binary neutron star mergers a **Post-Merger Phase** often exists

The Einstein Equation

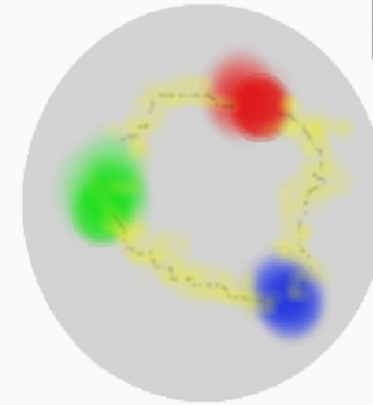
ART	<u>Yang-Mills-Theories</u>
$D_\beta v^\alpha = \partial_\beta v^\alpha + \Gamma_{\sigma\beta}^\alpha v^\sigma$	$D_{\beta a}{}^b = \partial_\beta 1_a{}^b + ig A_{\beta a}{}^b$
$R^\delta{}_{\mu\alpha\beta} v^\mu = [D_\alpha, D_\beta] v^\delta$	$F_{\alpha\beta a}{}^b = \frac{1}{ig} [D_{\alpha a}{}^c, D_{\beta c}{}^b]$
$R^\delta{}_{\mu\alpha\beta} = \Gamma_{\mu\alpha \beta}^\delta - \Gamma_{\mu\beta \alpha}^\delta$ $+ \Gamma_{\nu\beta}^\delta \Gamma_{\mu\alpha}^\nu + \Gamma_{\nu\alpha}^\delta \Gamma_{\mu\beta}^\nu$	$= A_{\beta a}{}^b _\alpha - A_{\alpha a}{}^b _\beta$ $+ \frac{1}{ig} [A_{\alpha a}{}^c, A_{\beta c}{}^b]$
$\mathcal{L}_G = R + \underbrace{(c_1 R_{\mu\nu} R^{\mu\nu} + \dots)}_{\equiv 0 \text{ for ART}}$	$\mathcal{L}_{YM} = \frac{1}{4} F_{\mu\nu a}{}^b F^{\mu\nu}{}_a{}^b$

Quantum ChromoDynamic:

($SU(3)_{(c)}$ - Color Yang-Mills-Gauge Theory)

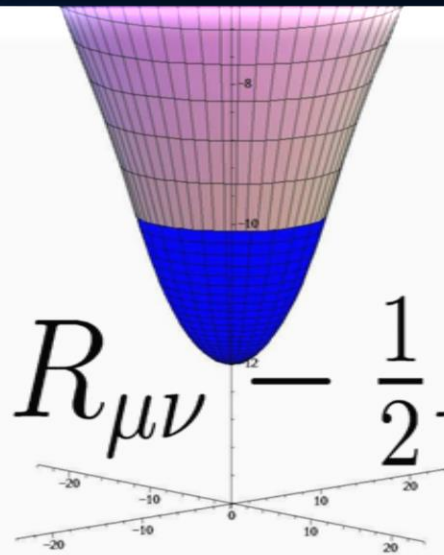
$$D_{\beta A}{}^B = \partial_\beta 1_A{}^B + ig G_{\beta A}{}^B$$

$A, B = \text{red, green, blue}$



$$\psi_A^f = \begin{pmatrix} \psi_r^f \\ \psi_g^f \\ \psi_b^f \end{pmatrix}$$

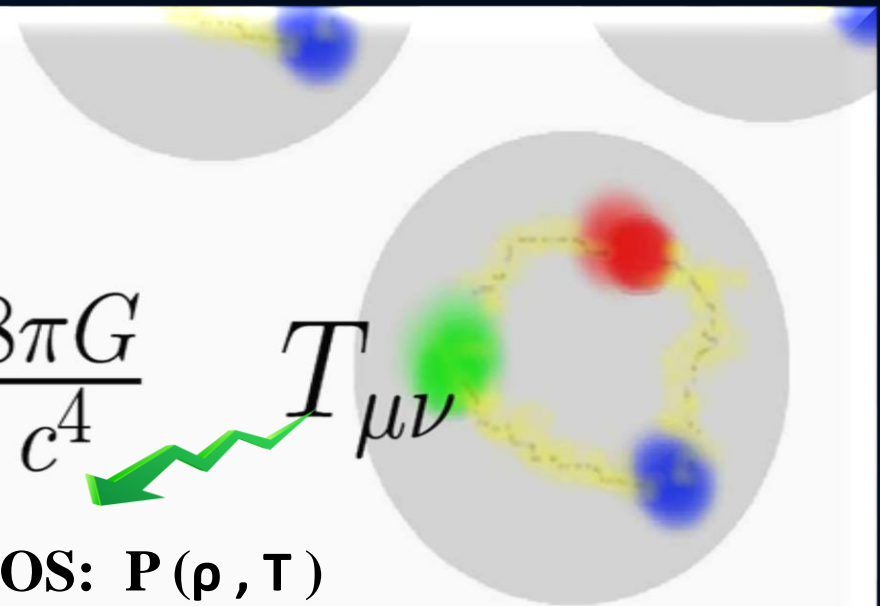
Confinement
chiral symmetry, ...



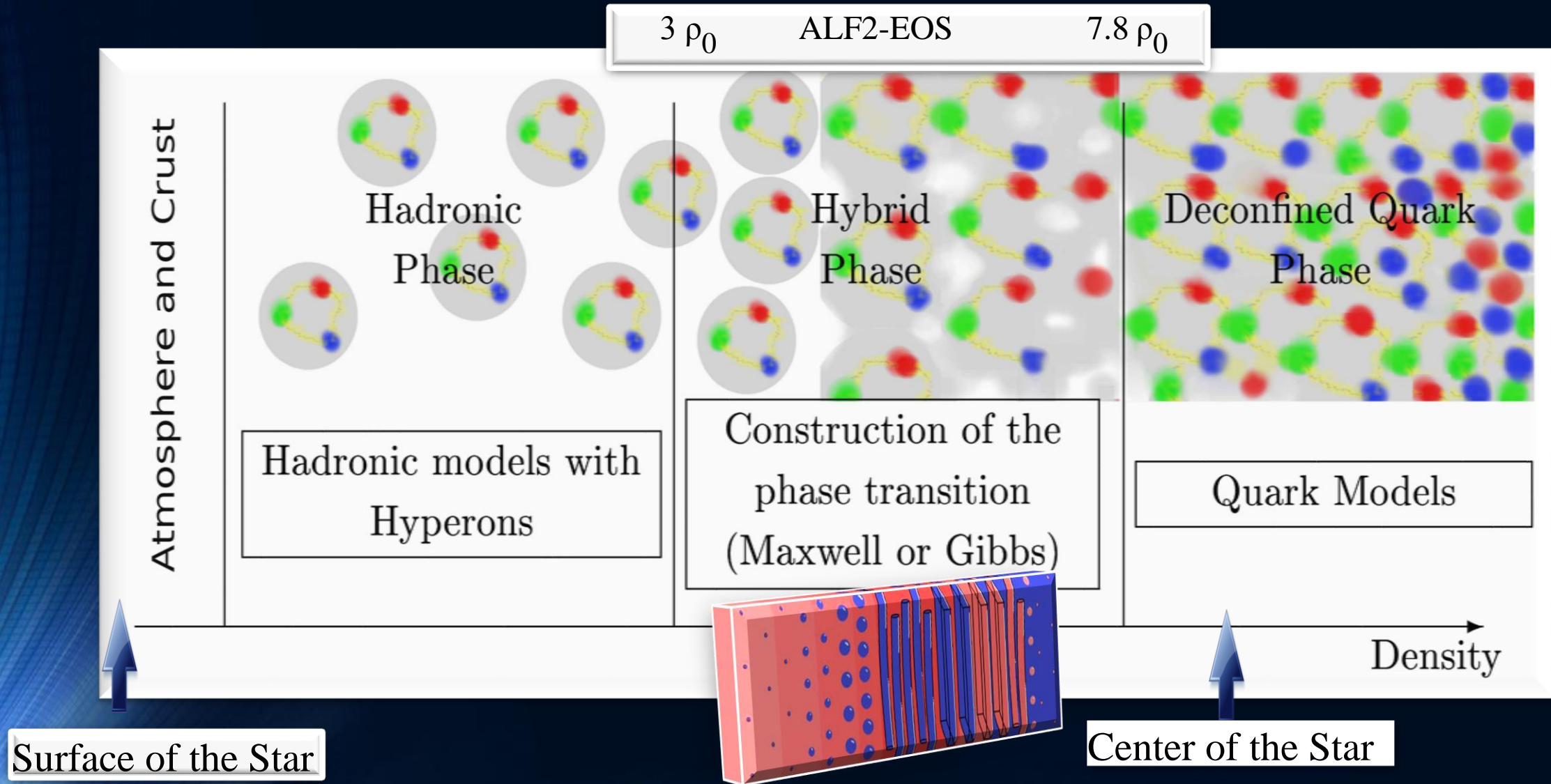
$$R_{\mu\nu} - \frac{1}{2} R g_{\mu\nu} =$$

$$\frac{8\pi G}{c^4} T_{\mu\nu}$$

EOS: $P(\rho, T)$

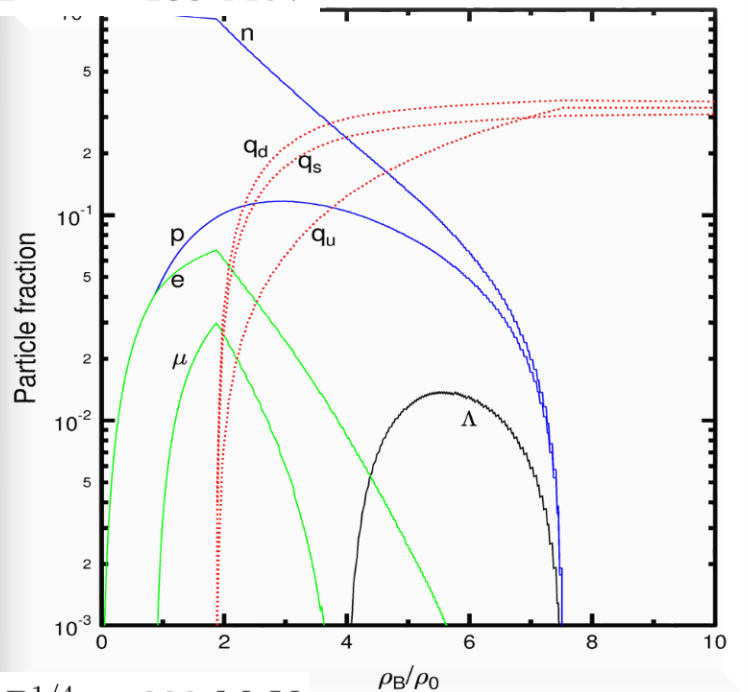


The QCD – Phase Transition and the Interior of a Hybrid Star

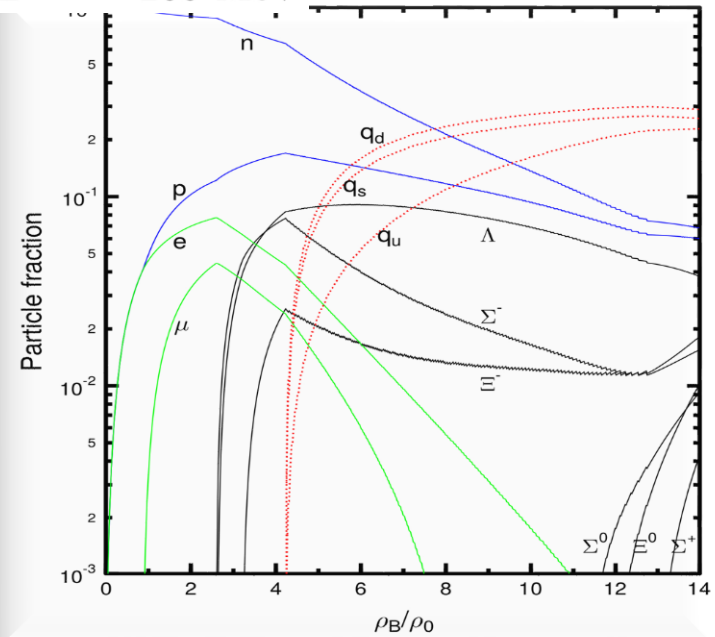


See: *Stable hybrid stars within a SU(3) Quark-Meson-Model*,
A.Zacchi, M.Hanuske, J.Schaffner-Bielich, PRD 93, 065011 (2016)

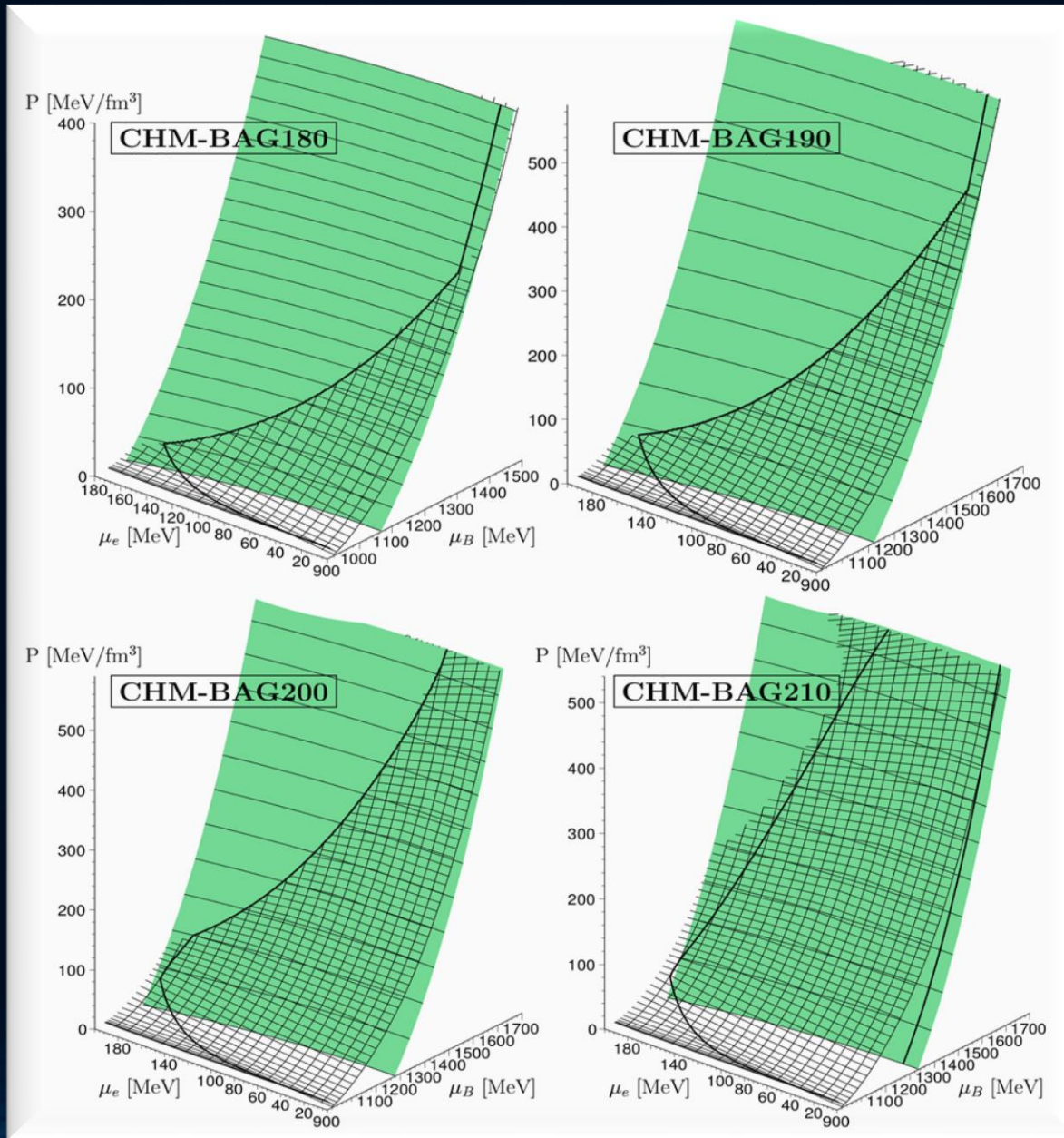
$B^{1/4} = 180 \text{ MeV}$



$B^{1/4} = 200 \text{ MeV}$



The Gibbs Construction



Numerical Relativity and Relativistic Hydrodynamics of Binary Neutron Star Mergers

A realistic numerical simulation of a twin star collapse, a merger of two compact stars or a collapse to a black hole needs to go beyond a static, spherically symmetric TOV-solution of the Einstein- and hydrodynamical equations.

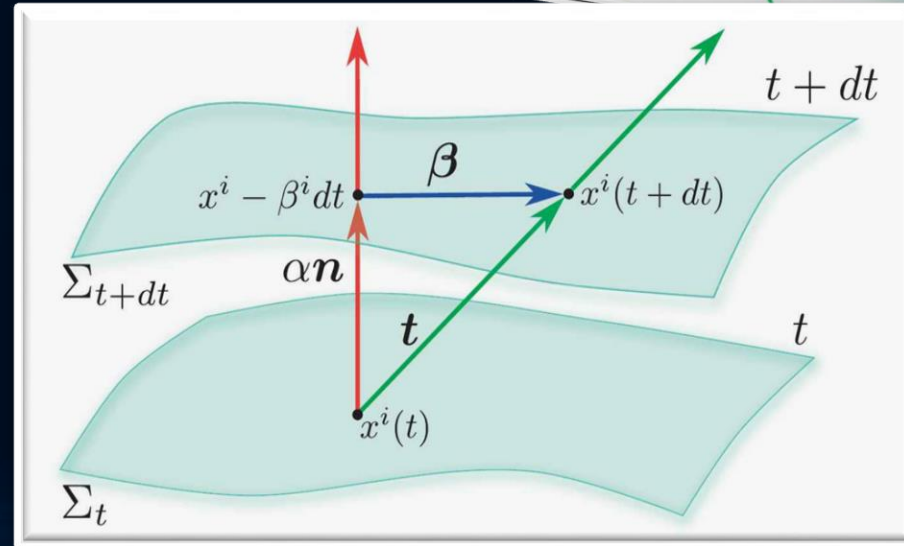
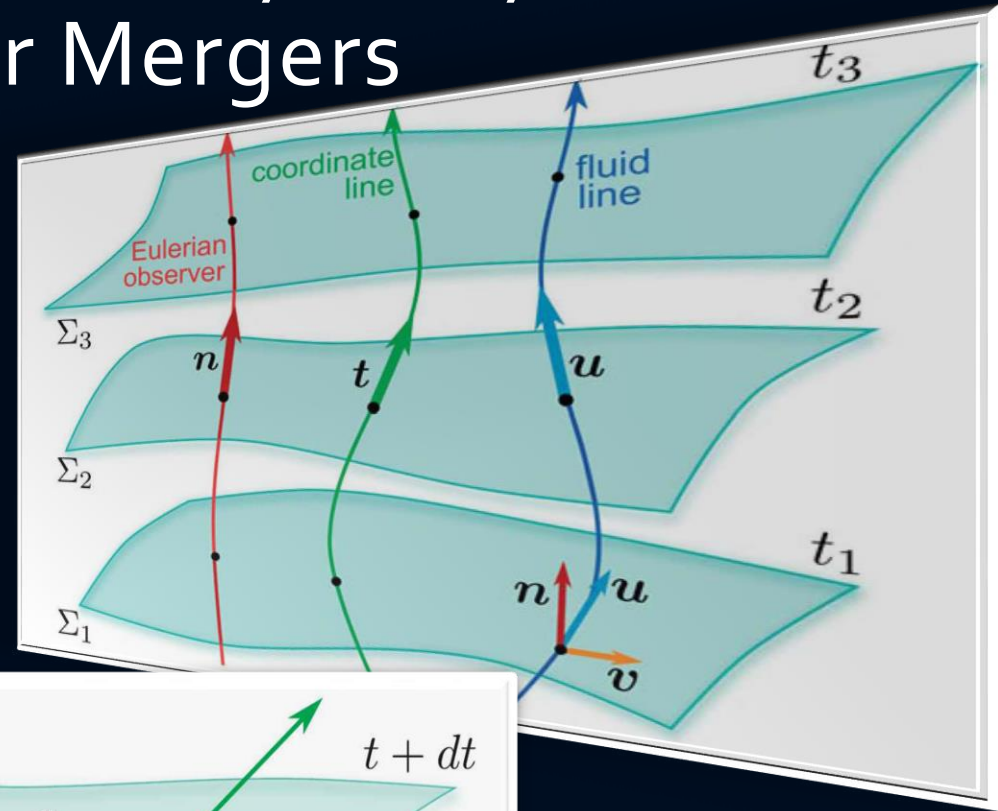
$$R_{\mu\nu} - \frac{1}{2}g_{\mu\nu}R = 8\pi T_{\mu\nu}$$

$$\begin{aligned}\nabla_{\mu}(\rho u^{\mu}) &= 0, \\ \nabla_{\nu}T^{\mu\nu} &= 0.\end{aligned}$$

(3+1) decomposition of spacetime

$$g_{\mu\nu} = \begin{pmatrix} -\alpha^2 + \beta_i\beta^i & \beta_i \\ \beta_i & \gamma_{ij} \end{pmatrix}$$

$$d\tau^2 = \alpha^2(t, x^j)dt^2 \quad x^i_{t+dt} = x^i_t - \beta^i(t, x^j)dt$$



The ADM equations

The ADM (Arnowitt, Deser, Misner) equations come from a reformulation of the Einstein equation using the (3+1) decomposition of spacetime.

$$\begin{aligned}\partial_t \gamma_{ij} &= -2\alpha K_{ij} + \mathcal{L}_\beta \gamma_{ij} \\ &= -2\alpha K_{ij} + D_i \beta_j + D_j \beta_i\end{aligned}$$

$$\begin{aligned}\partial_t K_{ij} &= -D_i D_j \alpha + \beta^k \partial_k K_{ij} + K_{ik} \partial_j \beta^k + K_{kj} \partial_i \beta^k \\ &+ \alpha \left({}^{(3)}R_{ij} + K K_{ij} - 2K_{ik} K^k_j \right) + 4\pi\alpha [\gamma_{ij} (S - E) - 2S_{ij}]\end{aligned}$$

Time evolving part of ADM

$$D_j (K^{ij} - \gamma^{ij} K) = 8\pi S^i$$

$${}^{(3)}R + K^2 - K_{ij} K^{ij} = 16\pi E$$

Constraints on each hypersurface

Three dimensional covariant derivative

$$D_\nu := \gamma^\mu_\nu \nabla_\mu = (\delta^\mu_\nu + n_\nu n^\mu) \nabla_\mu$$

Three dimensional Riemann tensor

$${}^{(3)}R^\mu_{\nu\kappa\sigma} = \partial_\kappa {}^{(3)}\Gamma^\mu_{\nu\sigma} - \partial_\sigma {}^{(3)}\Gamma^\mu_{\nu\kappa} + {}^{(3)}\Gamma^\mu_{\lambda\kappa} {}^{(3)}\Gamma^\lambda_{\nu\sigma} - {}^{(3)}\Gamma^\mu_{\lambda\sigma} {}^{(3)}\Gamma^\lambda_{\nu\kappa}$$

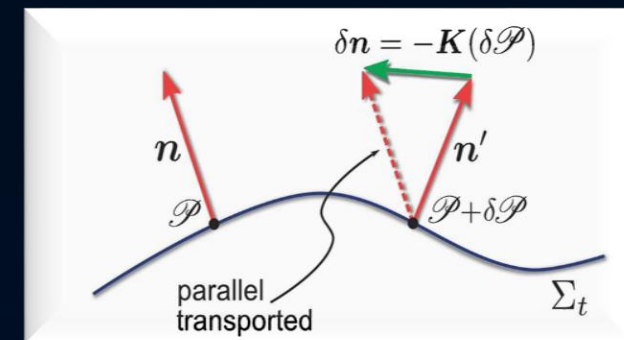
$${}^{(3)}\Gamma^\alpha_{\beta\gamma} = \frac{1}{2} \gamma^{\alpha\delta} (\partial_\beta \gamma_{\gamma\delta} + \partial_\gamma \gamma_{\delta\beta} - \partial_\delta \gamma_{\beta\gamma})$$

Spatial and normal projections of the energy-momentum tensor:

$$\begin{aligned}S_{\mu\nu} &:= \gamma^\alpha_\mu \gamma^\beta_\nu T_{\alpha\beta}, \\ S_\mu &:= -\gamma^\alpha_\mu n^\beta T_{\alpha\beta}, \\ S &:= S^\mu_\mu, \\ E &:= n^\alpha n^\beta T_{\alpha\beta},\end{aligned}$$

Extrinsic Curvature:

$$K_{\mu\nu} := -\gamma^\lambda_\mu \nabla_\lambda n_\nu$$



From ADM to BSSNOK

Unfortunately the ADM equations are only weakly hyperbolic (mixed derivatives in the three dimensional Ricci tensor) and therefore not "well posed". It can be shown that by using a conformal traceless transformation, the ADM equations can be written in a hyperbolic form. This reformulation of the ADM equations is known as the BSSNOK (Baumgarte, Shapiro, Shibata, Nakamuro, Oohara, Kojima) formulation of the Einstein equation. Most of the numerical codes use this (or even better the CCZ4) formulation.

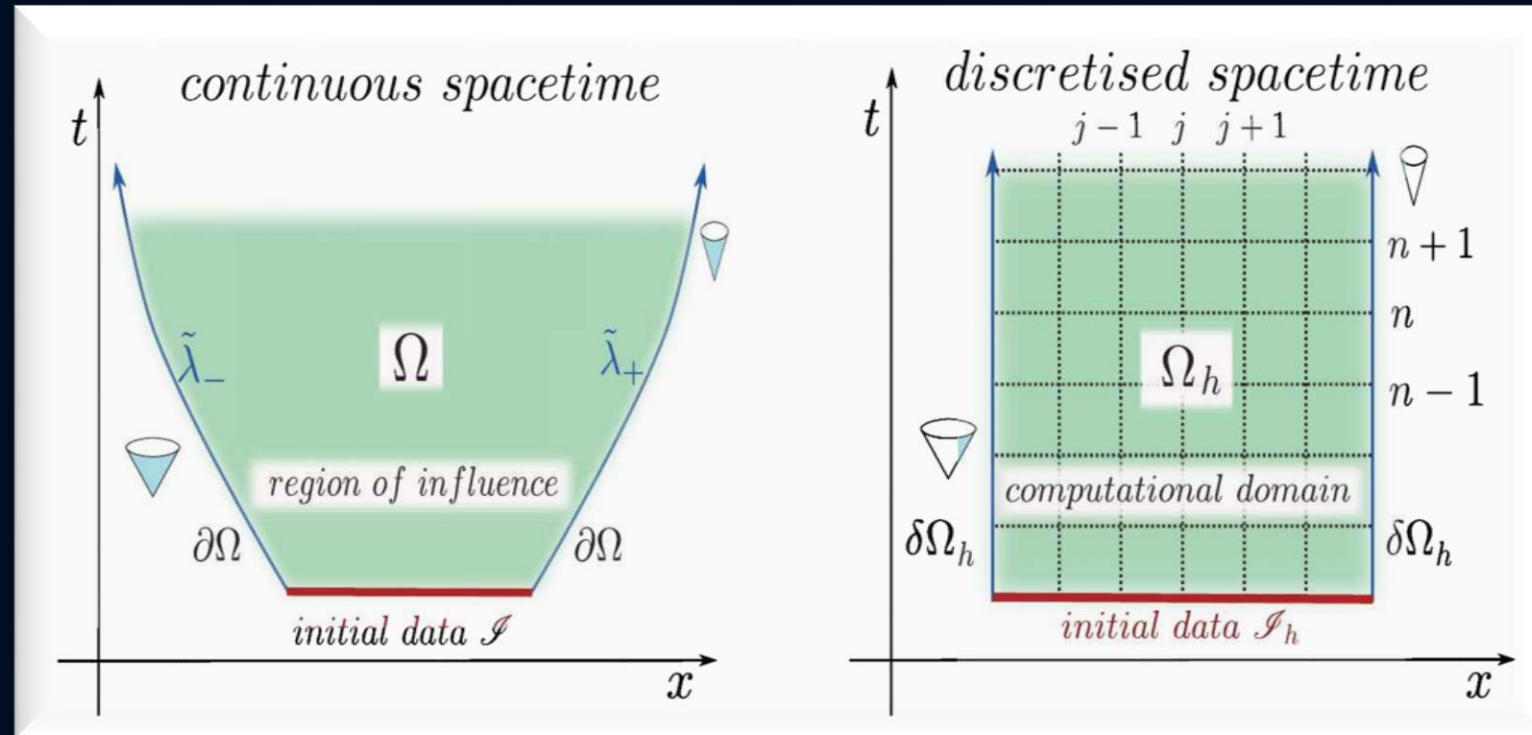
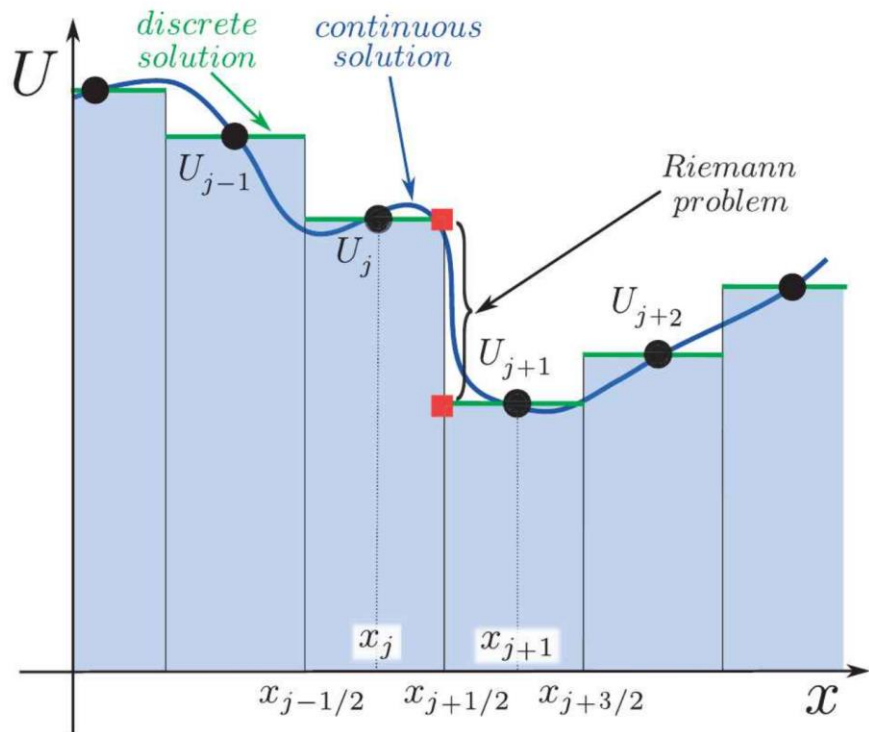
The 3+1 Valencia Formulation of the Relativistic Hydrodynamic Equations

$$\begin{aligned}\nabla_{\mu}(\rho u^{\mu}) &= 0, \\ \nabla_{\nu}T^{\mu\nu} &= 0.\end{aligned}$$

To guarantee that the numerical solution of the hydrodynamical equations (the conservation of rest mass and energy-momentum) converge to the right solution, they need to be reformulated into a conservative formulation. Most of the numerical "hydro codes" use here the 3+1 Valencia formulation.

Finite difference methods

Discretisation of a hyperbolic initial value boundary problem.



High resolution shock capturing methods (HRSC methods) are needed, when Riemann problems of discontinuous properties and shocks needs to be evolved accurately.

Gauge Conditions

On each spatial hypersurface, four additional degrees of freedom need to be specified: A slicing condition for the lapse function and a spatial shift condition for the shift vector need to be formulated to close the system. In an optimal gauge condition, singularities should be avoided and numerical calculations should be less time consuming.

Bona-Massó family of slicing conditions:

$$\partial_t \alpha - \beta^k \partial_k \alpha = -f(\alpha) \alpha^2 (K - K_0)$$

“1+log” slicing condition:

$$f = 2/\alpha$$

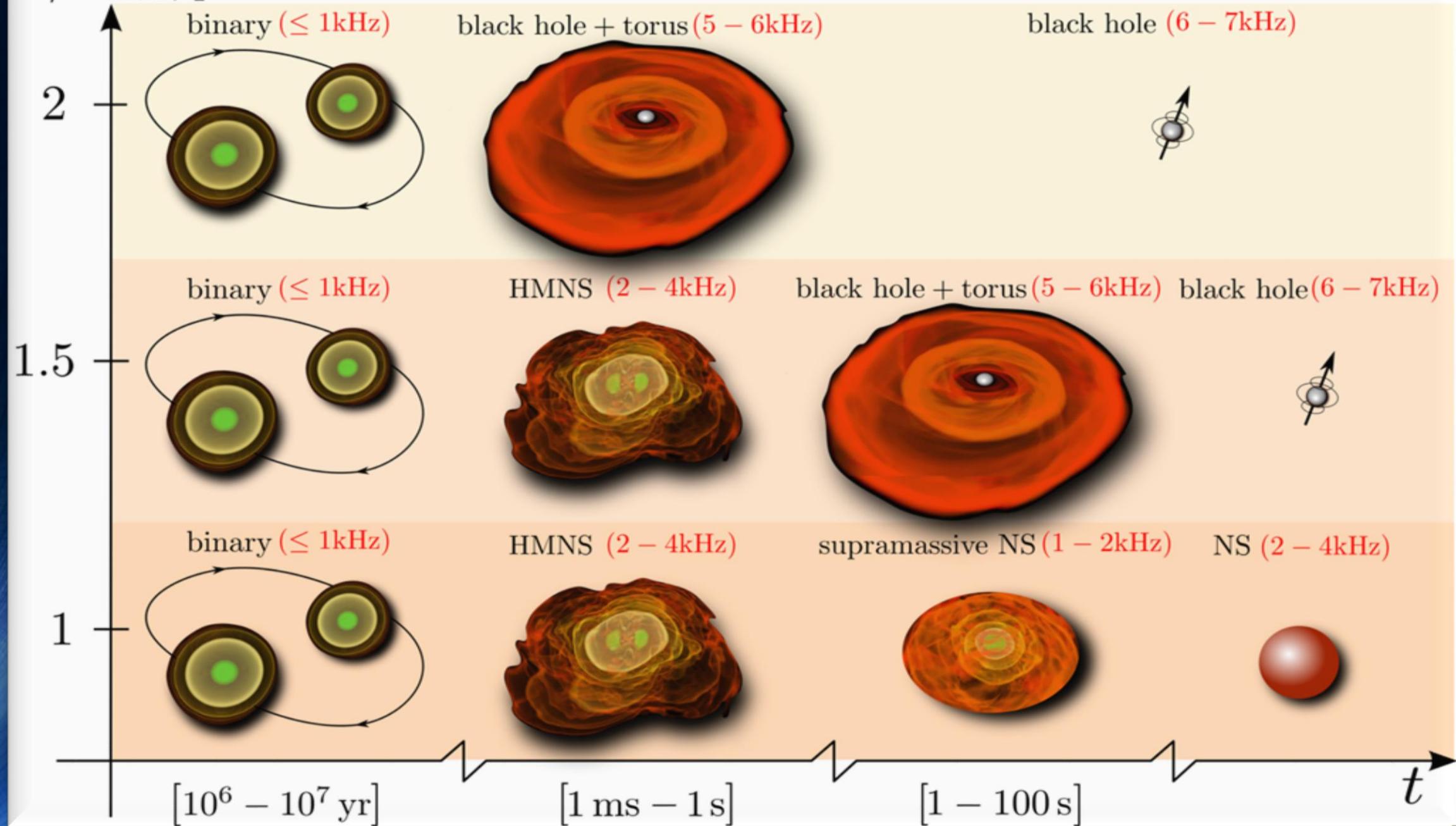
$$\text{where } f(\alpha) > 0 \text{ and } K_0 := K(t = 0)$$

“Gamma-Driver” shift condition:

$$\partial_t \beta^i - \beta^j \partial_j \beta^i = \frac{3}{4} B^i,$$

$$\partial_t B^i - \beta^j \partial_j B^i = \partial_t \tilde{\Gamma}^i - \beta^j \partial_j \tilde{\Gamma}^i - \eta B^i$$

$M/M_{\max}, q \simeq 1$



Simulations of Binary Neutron Star Mergers

Credits: Cosima Breu, David Radice
and Luciano Rezzolla



Density

8.5 14



$\lg(\rho)$ [g/cm³]

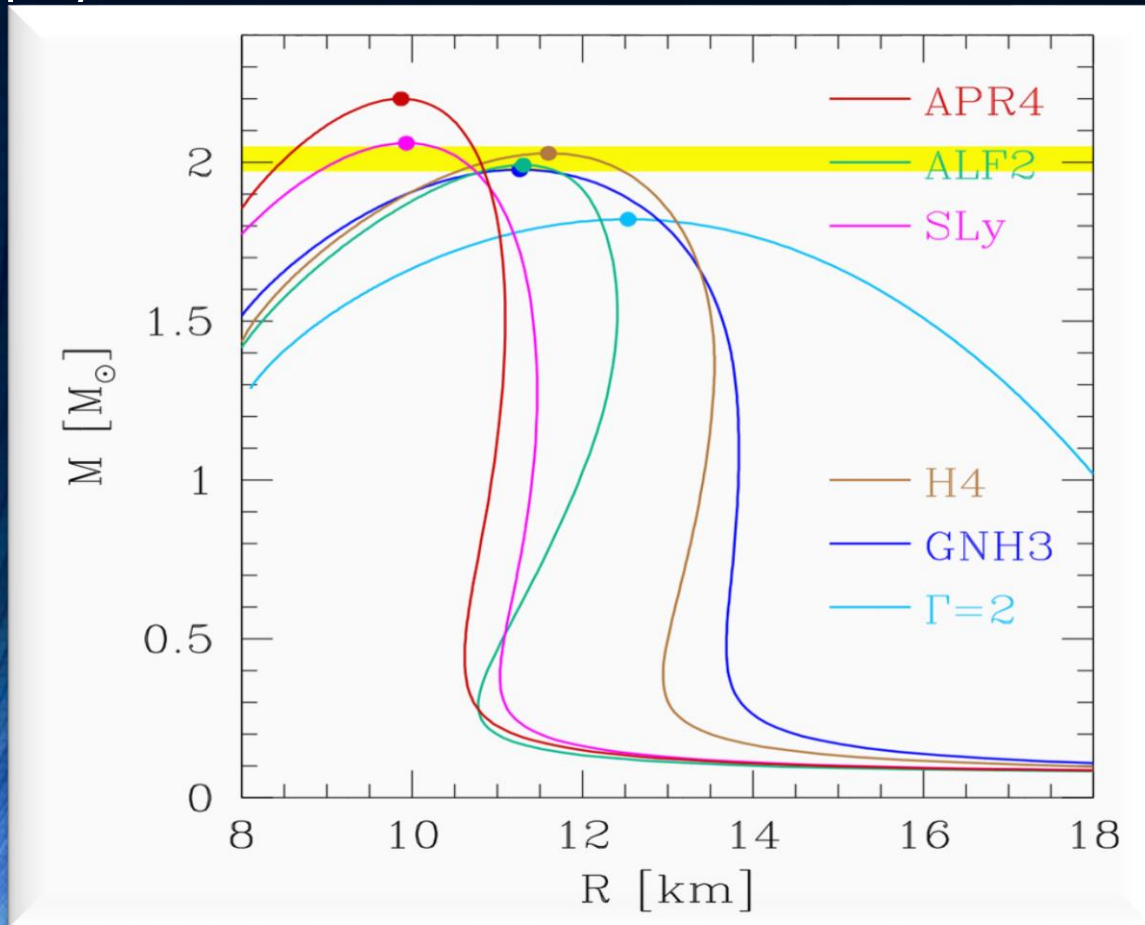
Temperature

0 50



T [MeV]

Several different EOSs : ALF₂, APR₄, GNH₃, H₄ and SLy, approximated by piecewise polytopes. Thermal ideal fluid component ($\Gamma=2$) added to the nuclear-physics EOSs.



EOSs

composed of a “cold” nuclear-physics part and of a “thermal” ideal-fluid component¹ [56]

$$p = p_c + p_{\text{th}}, \quad \epsilon = \epsilon_c + \epsilon_{\text{th}}, \quad (6)$$

where p and ϵ are the pressure and specific internal energy,

The “cold” nuclear-physics contribution to each EOS is obtained after expressing the pressure and specific internal energy ϵ_c in the rest-mass density range $\rho_{i-1} \leq \rho < \rho_i$ as (for details see [36, 64–66])

$$p_c = K_i \rho^{\Gamma_i}, \quad \epsilon_c = \epsilon_i + K_i \frac{\rho^{\Gamma_i-1}}{\Gamma_i - 1}. \quad (7)$$

($\Gamma_1 = 4.070$ and $\Gamma_2 = 2.411$). Finally, the “thermal” part of the EOS is given by

$$p_{\text{th}} = \rho \epsilon_{\text{th}} (\Gamma_{\text{th}} - 1), \quad \epsilon_{\text{th}} = \epsilon - \epsilon_c. \quad (8)$$

where the last equality in (8) is really a definition, since ϵ refers to the computed value of the specific internal energy. In all of the simulations reported hereafter we use $\Gamma_{\text{th}} = 2.0$

Additionally LS220-EOS used: Density and Temperature dependent EOS-table (Lattimer-Swesty)

Numerical Setup

BSSNOK conformal traceless formulation of the ADM equations.
3+1 Valencia formulation and high resolution shock capturing methods for the hydrodynamic evolution. Full general relativity using the **Einstein-Toolkit** and the **WHISKY/WhiskyTHC code** for the general-relativistic hydrodynamic equations.

Grid Structure:

Adaptive mesh refinement (six ref. levels)

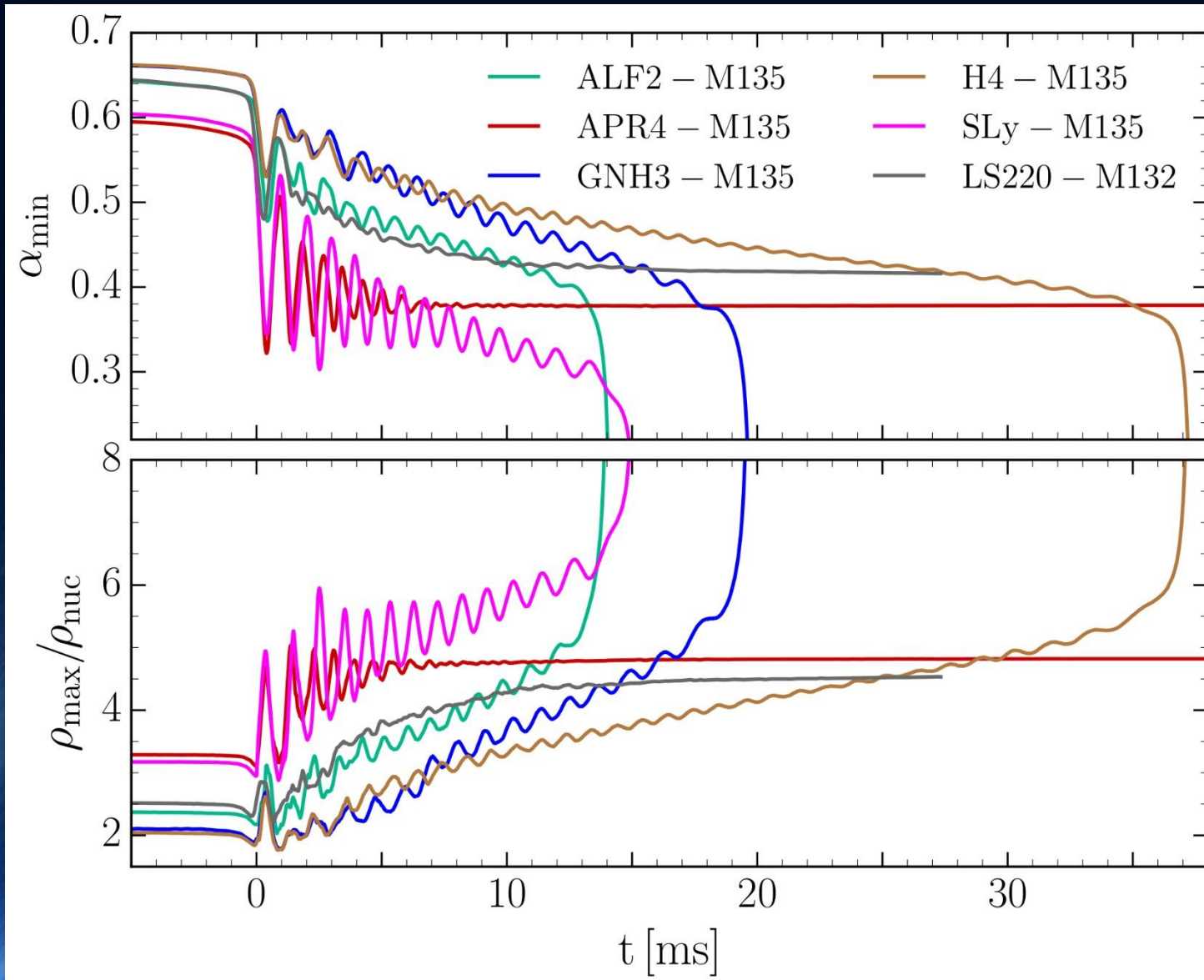
Grid resolution: (from 221 m to 7.1 km)

Outer Boundary: 759 km

Initial separation of stellar cores: 45 km

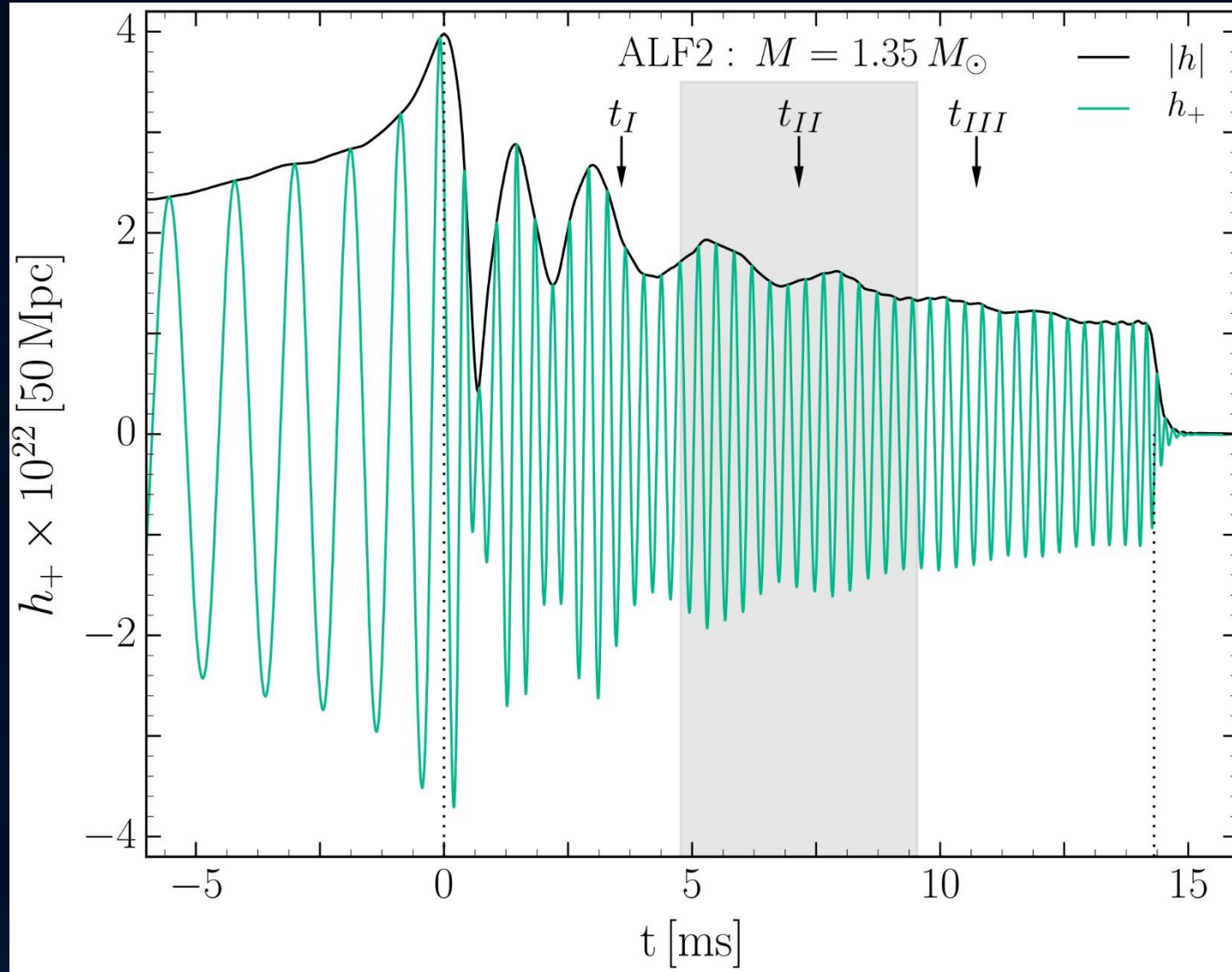
HMNS Evolution for different EoSs

High mass simulations ($M=1.35 M_{\text{solar}}$)



Central value of the lapse function α_c (upper panel) and maximum of the rest mass density ρ_{max} in units of ρ_0 (lower panel) versus time for the high mass simulations.

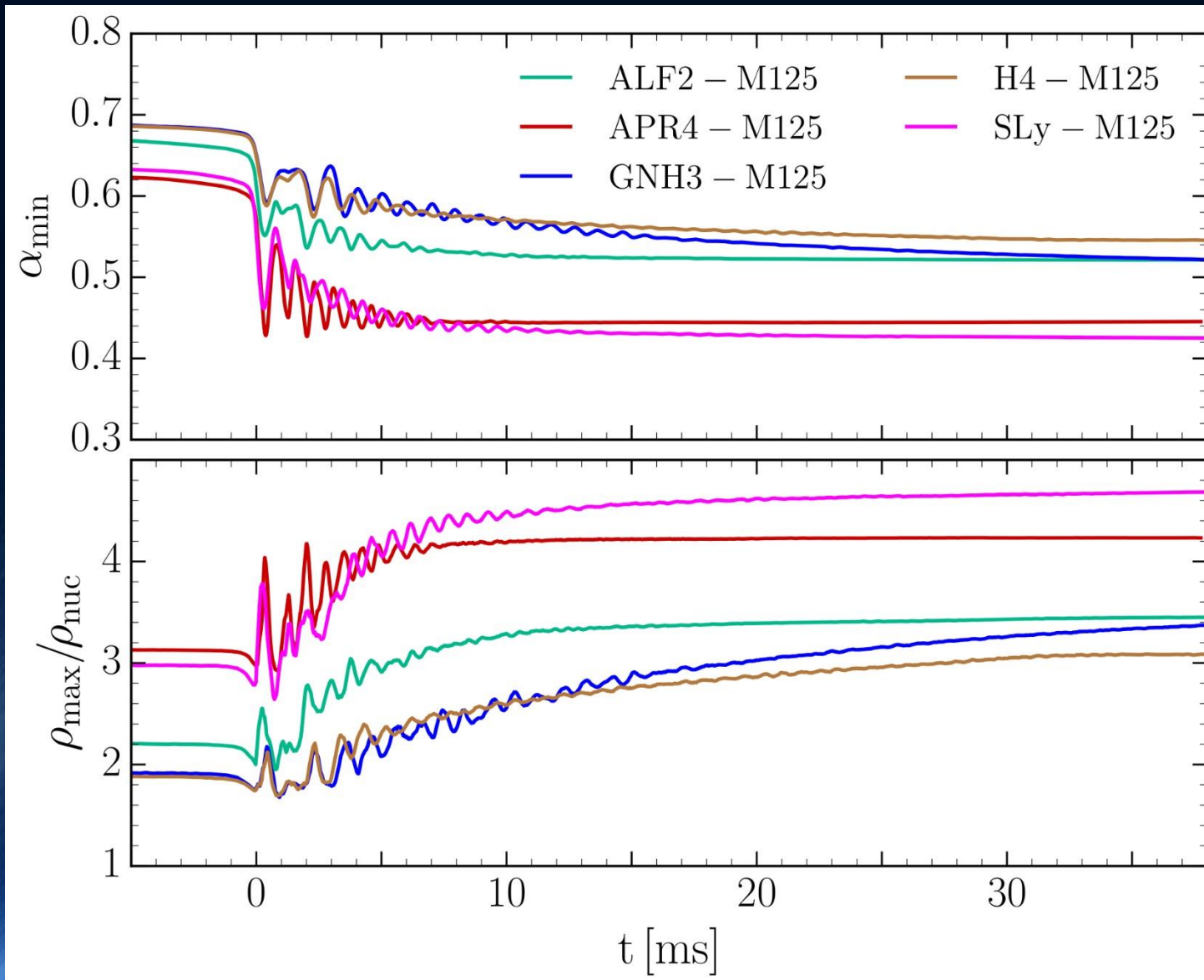
Gravitational Waves



Gravitational-wave amplitude for the ALF2-M135 binary at a distance of 50 Mpc.

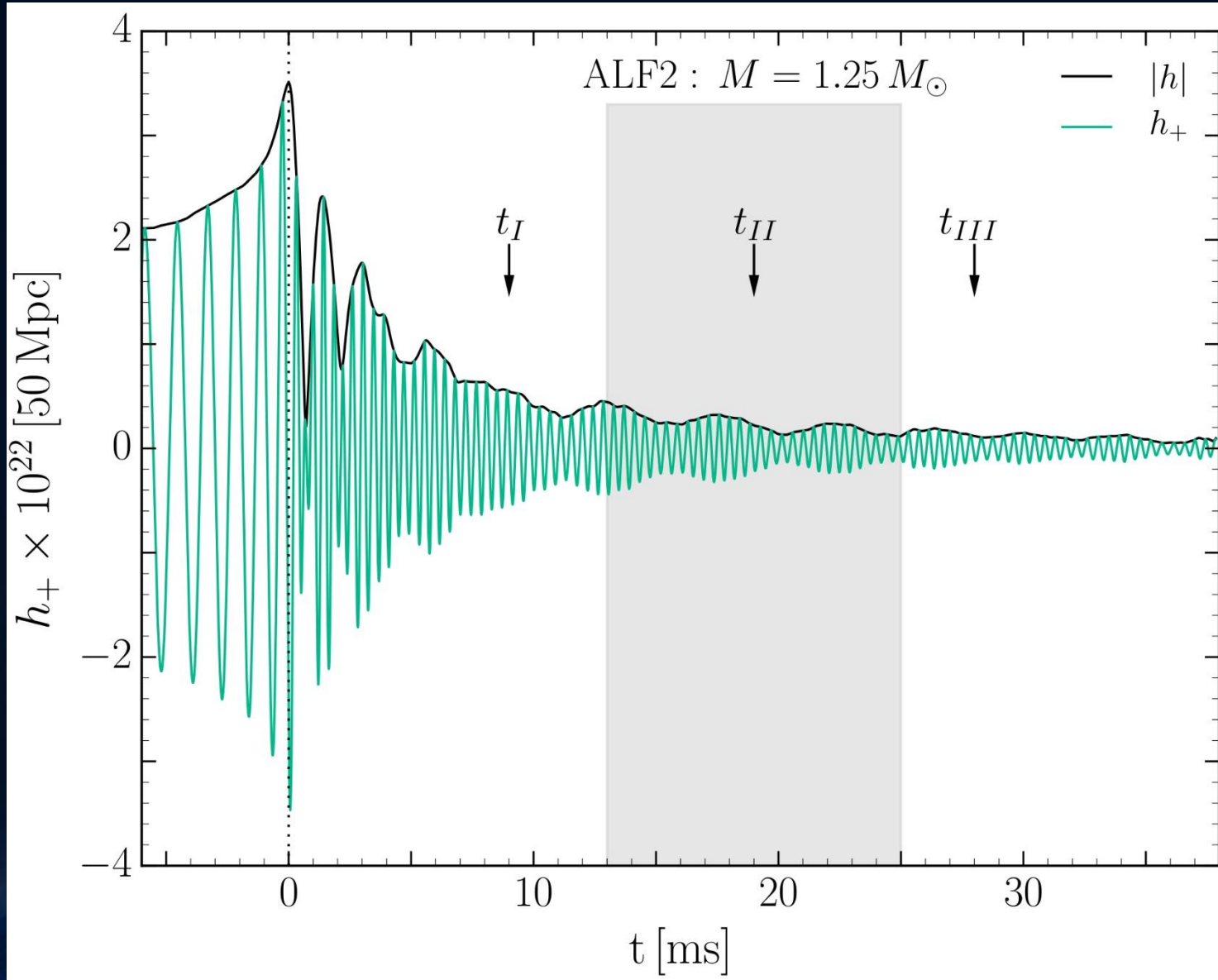
HMNS Evolution for different EoSs

Low mass simulations ($M=1.32 M_{\text{solar}}$)



Central value of the lapse function α_c (upper panel) and maximum of the rest mass density ρ_{max} in units of ρ_0 (lower panel) versus time for the low mass simulations.

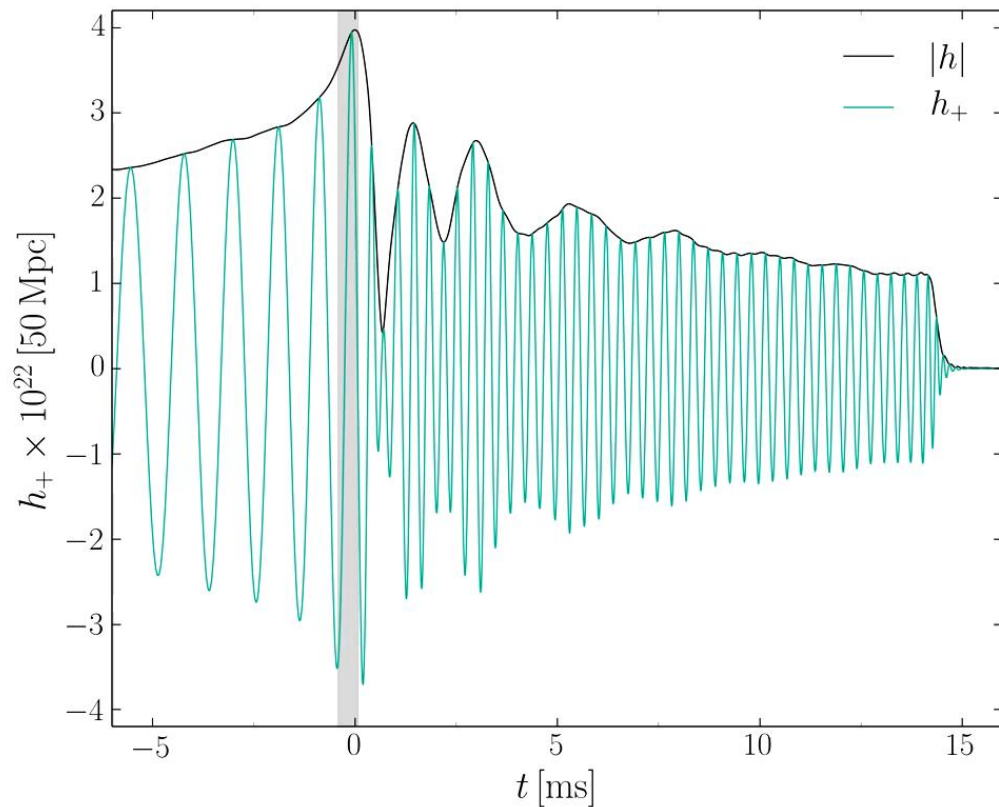
Gravitational Waves



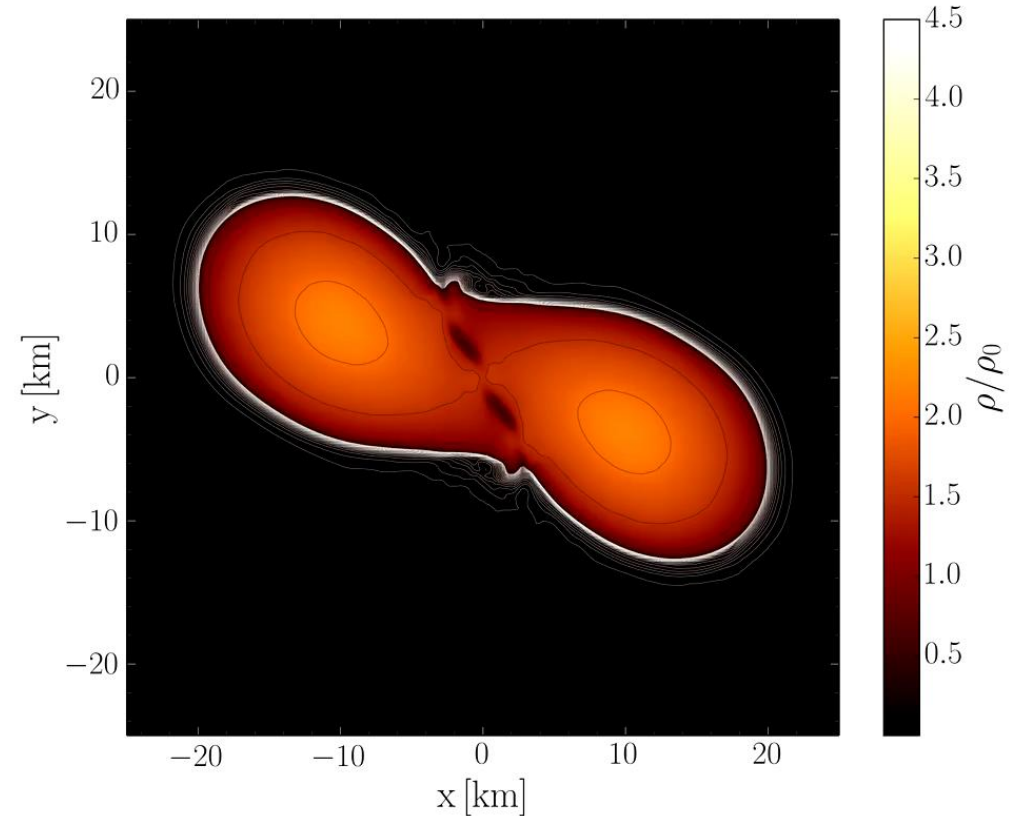
Gravitational-wave amplitude for the ALF2-M125 binary at a distance of 50 Mpc.

Evolution of the rest-mass density distribution

ALF2, High mass model: Mixed phase region starts at $3\rho_0$, initial NS mass: $1.35 M_{\text{solar}}$



Gravitational wave amplitude
at a distance of 50 Mpc

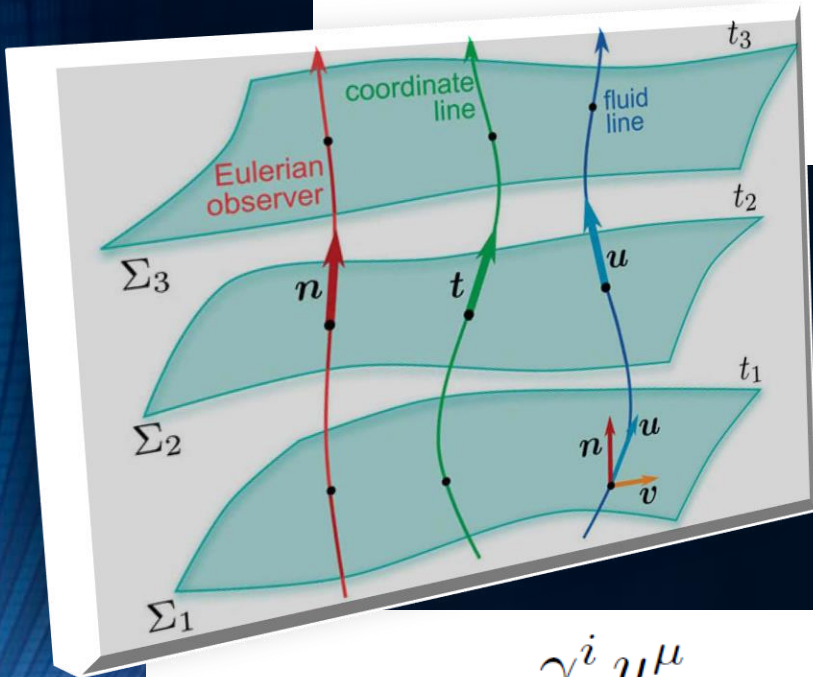


Rest mass density distribution $\rho(x,y)$
in the equatorial plane
in units of the nuclear matter density ρ_0

The Angular Velocity in the (3+1)-Split

$$\Omega(x, y, z, t) = \Omega = \frac{d\phi}{dt} = \frac{dx^\phi}{dt} = \quad \text{with: } x^\mu = (t, r, \phi, \theta) \quad (1)$$

$$= \frac{dx^\phi}{dt} = \frac{\frac{dx^\phi}{d\tau}}{\frac{dt}{d\tau}} = \frac{u^\phi}{u^t} \quad \text{with: } u^\mu = \frac{dx^\mu}{d\tau}$$



The angular velocity Ω in the (3+1)-Split is a combination of the lapse function α , the ϕ -component of the shift vector β^ϕ and the 3-velocity v^ϕ of the fluid (spatial projection of the 4-velocity \mathbf{u}):

$$v^i = \frac{\gamma^i_\mu u^\mu}{-n_\mu u^\mu} = \frac{1}{\alpha} \left(\frac{u^i}{u^t} - \beta^i \right) \quad \text{with: } i = 1, 2, 3 \text{ and } \mu = 0, 1, 2, 3$$

$$\Leftrightarrow \frac{u^i}{u^t} = \alpha v^i - \beta^i \quad \text{Insert in (1)} \Rightarrow \quad \Omega = \frac{d\phi}{dt} = \frac{u^\phi}{u^t} = \alpha v^\phi - \beta^\phi$$

The Angular Velocity in the (3+1)-Split

The angular velocity Ω in the (3+1)-Split is a combination of the lapse function α , the ϕ -component of the shift vector β^ϕ and the 3-velocity v^ϕ of the fluid (spatial projection of the 4-velocity \mathbf{u}):

**(3+1)-decomposition
of spacetime:**

$$\Omega(x, y, z, t) = \frac{u^\phi}{u^t} = \alpha v^\phi - \beta^\phi$$

$$g_{\mu\nu} = \begin{pmatrix} -\alpha^2 + \beta_i \beta^i & \beta_i \\ \beta_i & \gamma_{ij} \end{pmatrix}$$

Angular velocity
 Ω

Lapse function
 α

Φ -component of
3-velocity v^ϕ

Frame-dragging
 β^ϕ

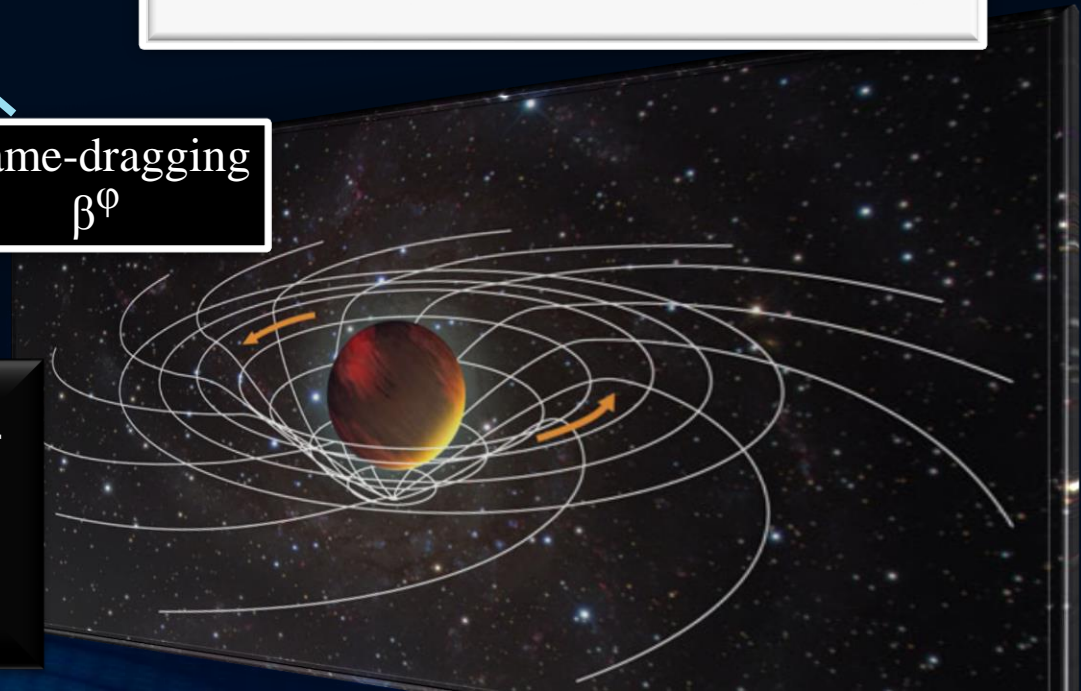
Focus: Inner core of the differentially rotating HMNS

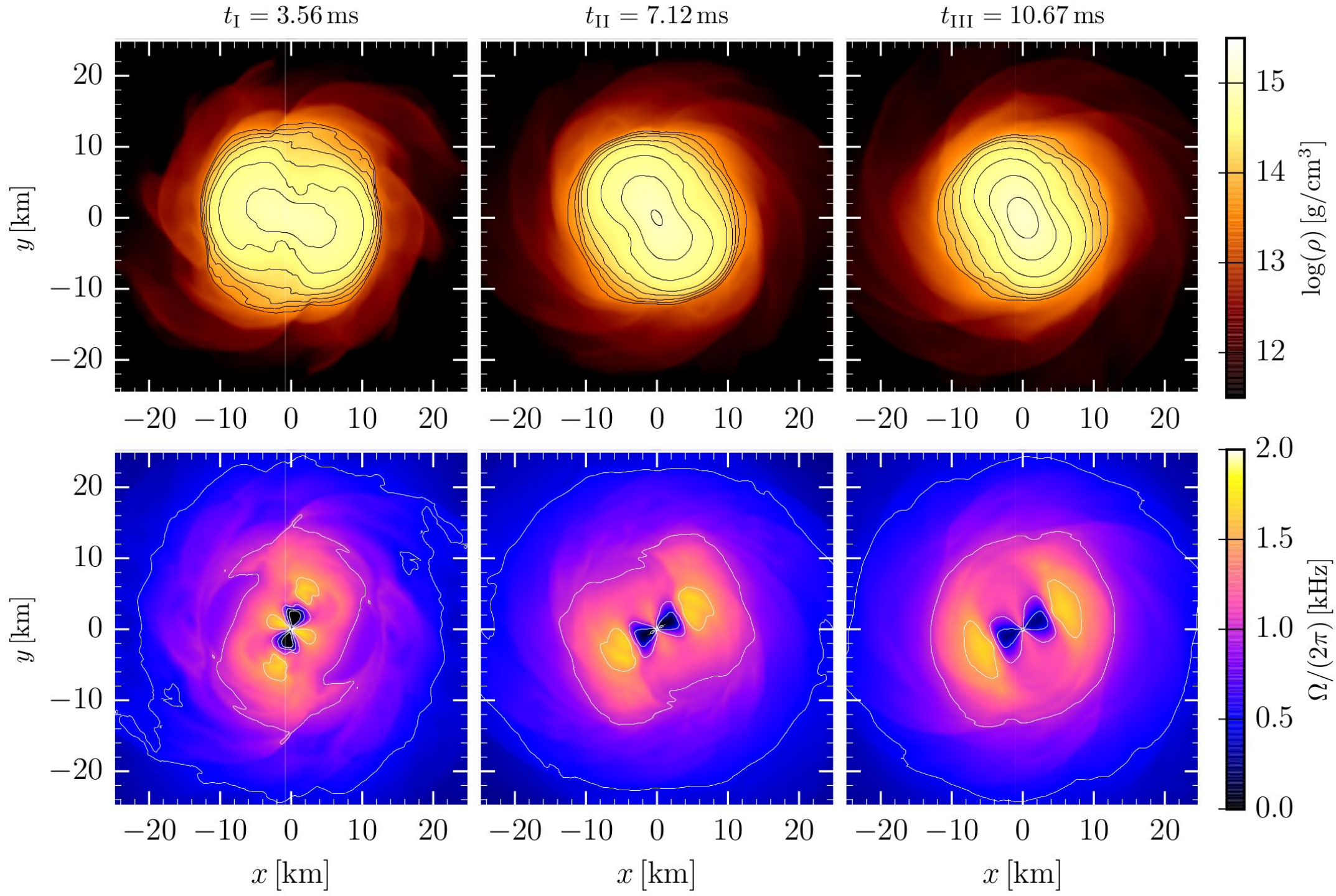
M. Shibata, K. Taniguchi, and K. Uryu, Phys. Rev. D 71, 084021 (2005)

M. Shibata and K. Taniguchi, Phys. Rev. D 73, 064027 (2006)

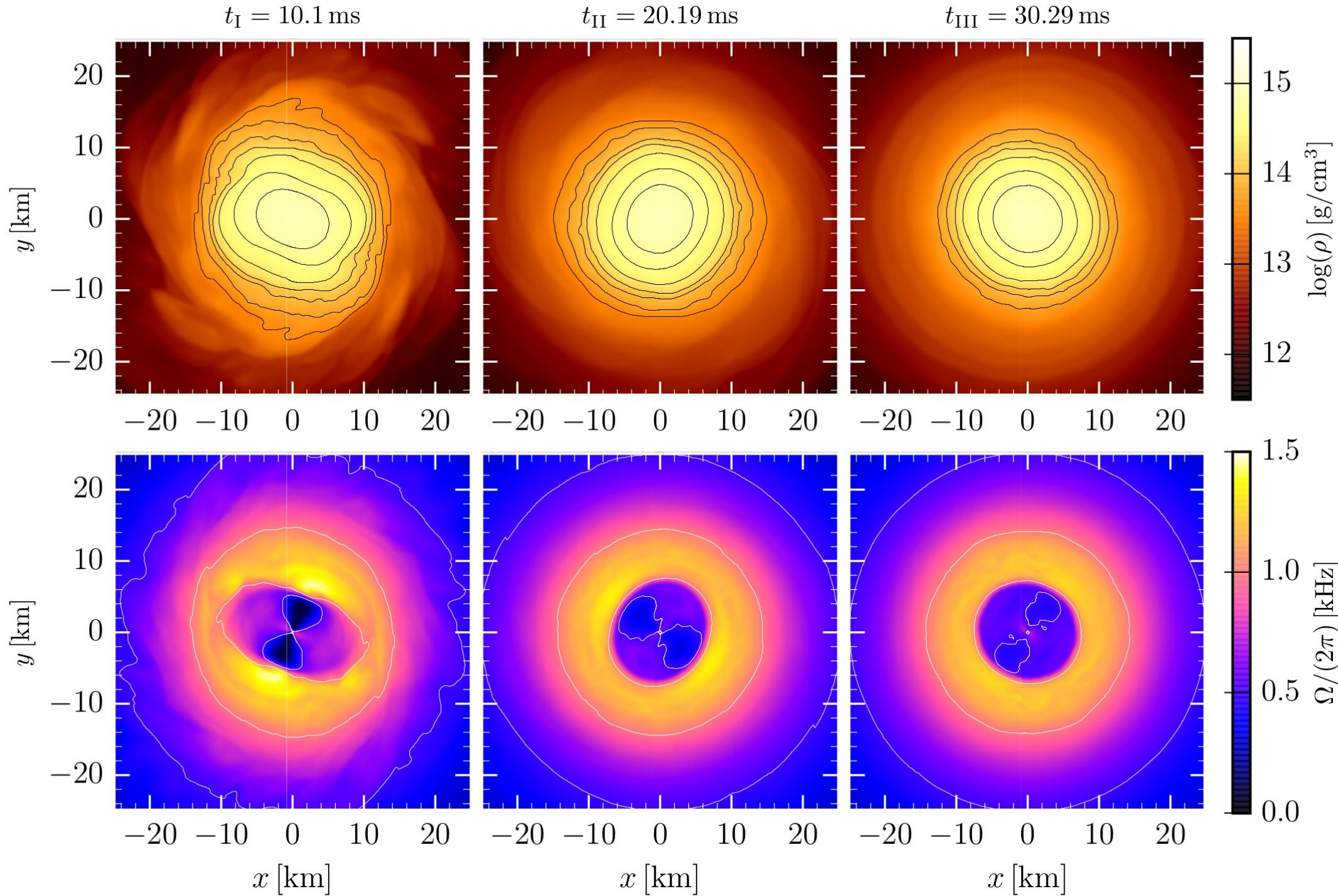
F. Galeazzi, S. Yoshida and Y. Eriguchi, A&A 541, p. A156 (2012)

W. Kastaun and F. Galeazzi, Phys. Rev. D 91, p. 064027 (2015)





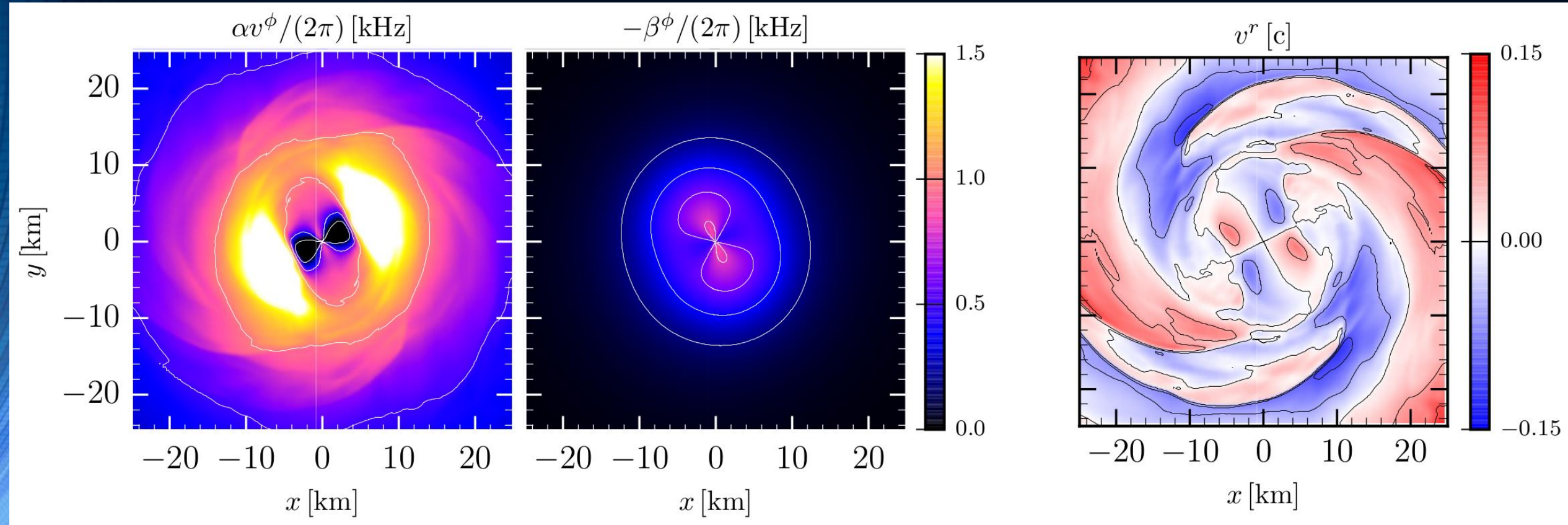
ALF2-M135
binary



ALF2-M125
binary

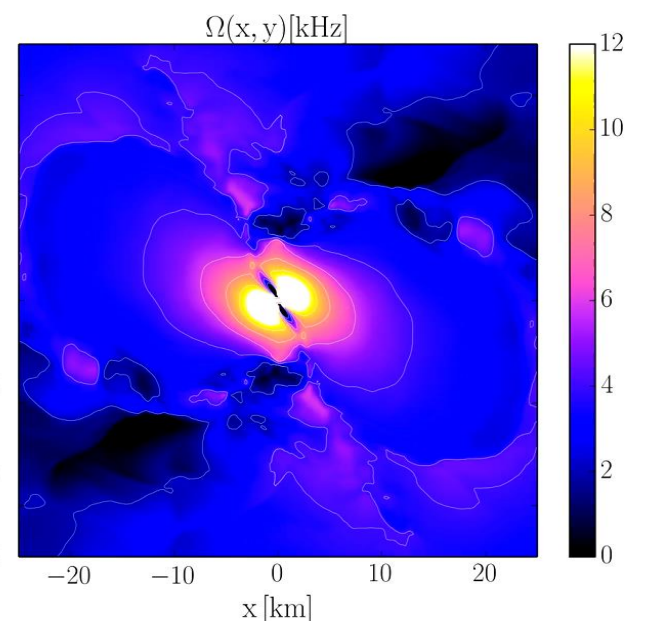
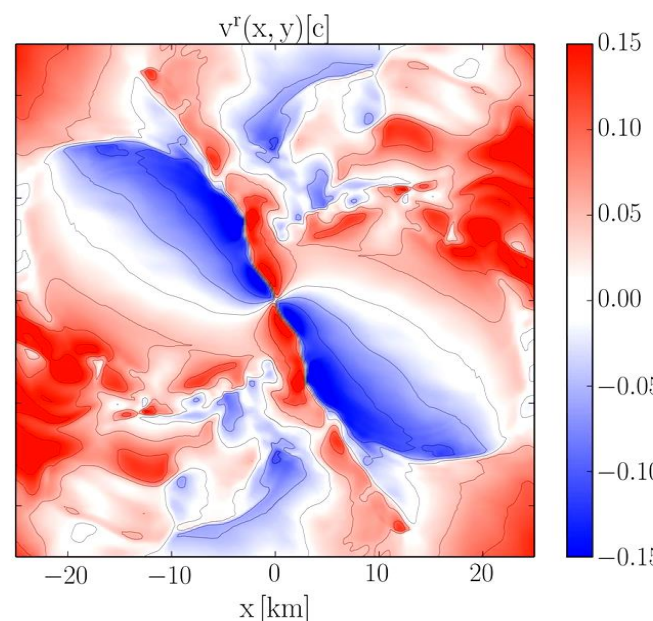
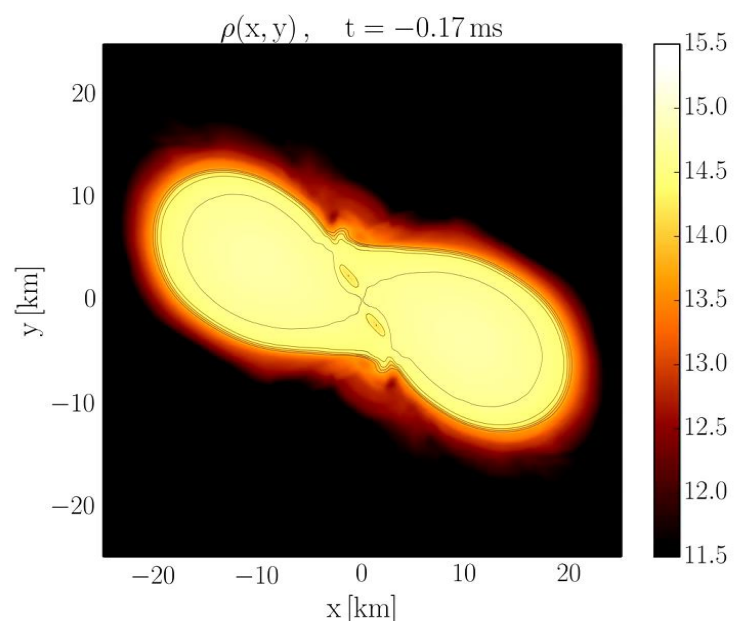
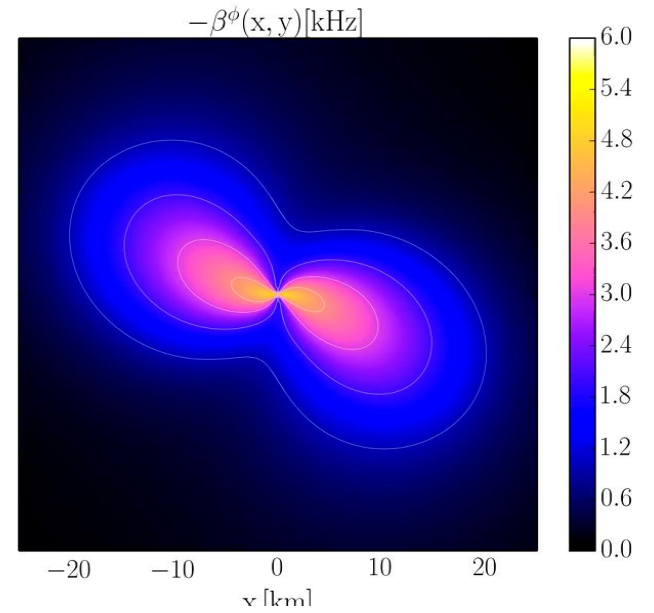
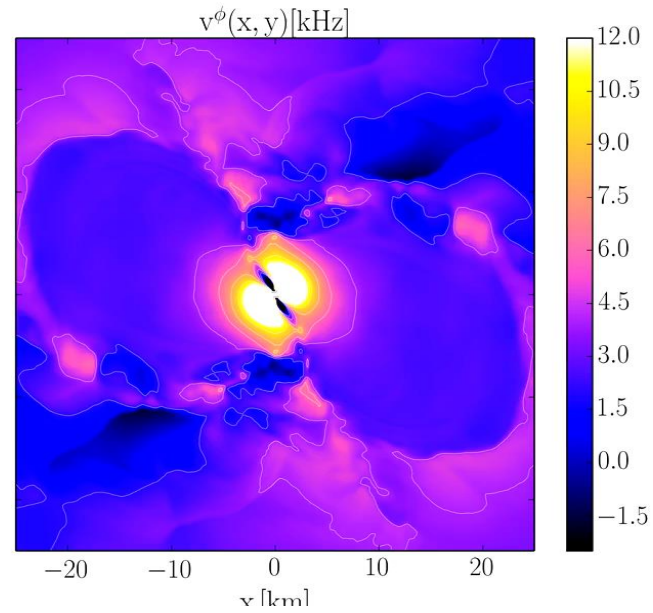
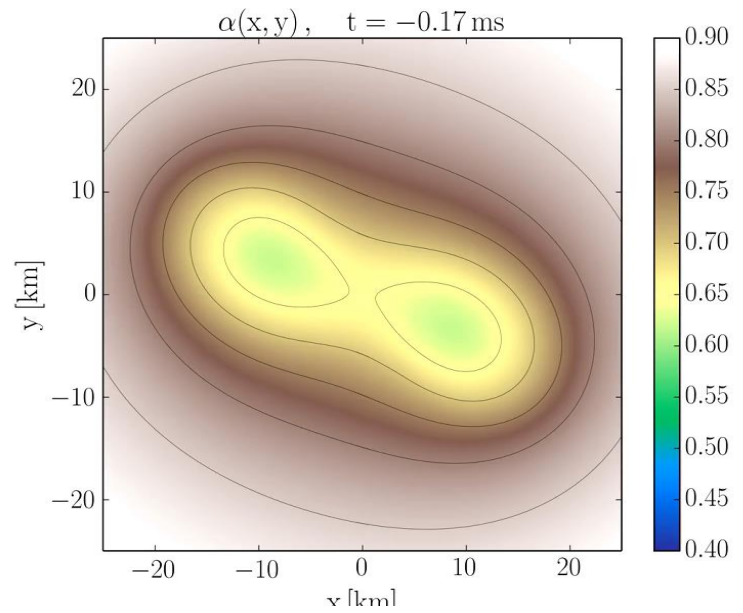
The Structure of the Angular Velocity Ω

$$\Omega(x, y, z, t) = \frac{u^\phi}{u^t} = \alpha v^\phi - \beta \phi$$

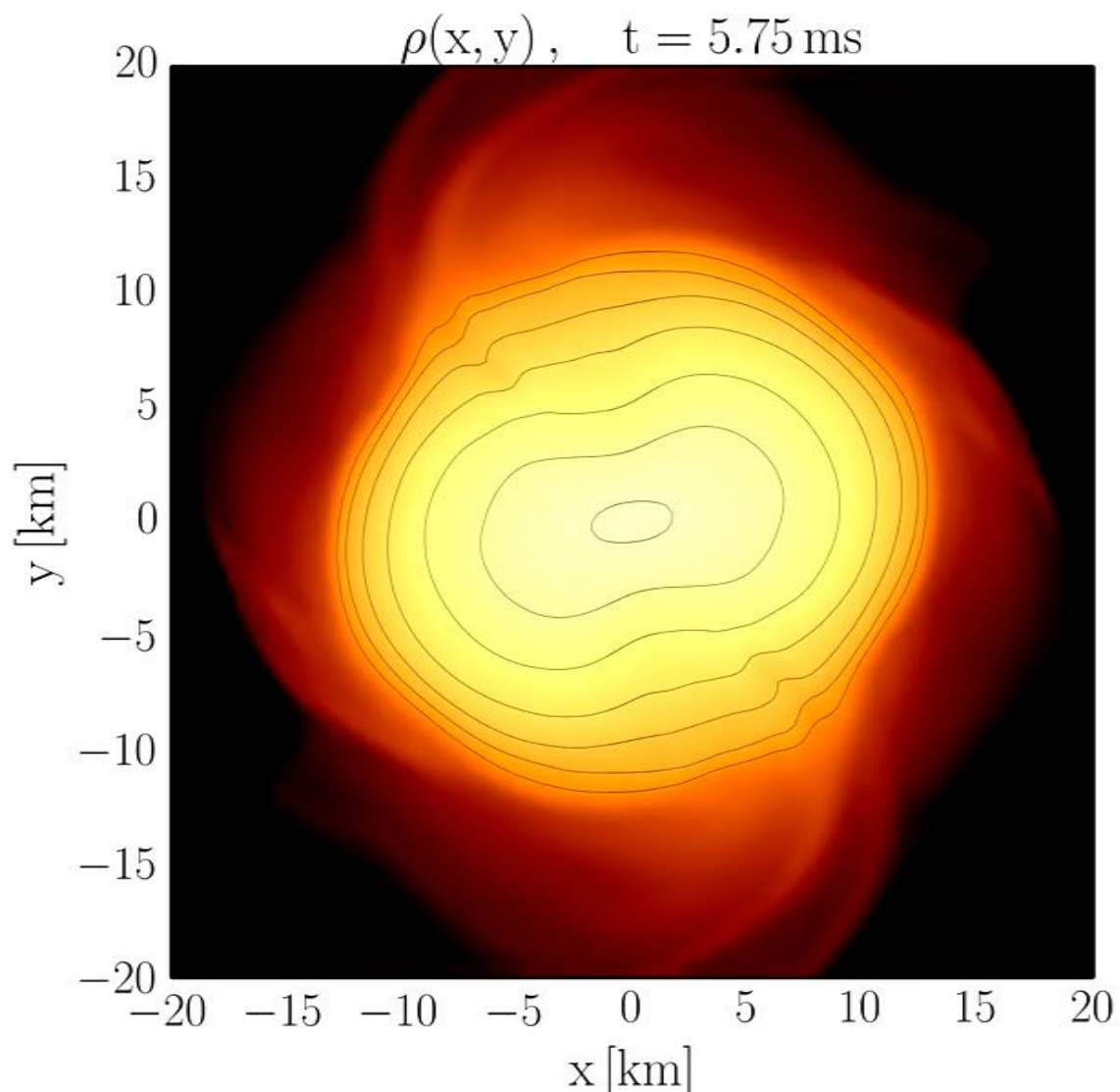


The Structure of Ω

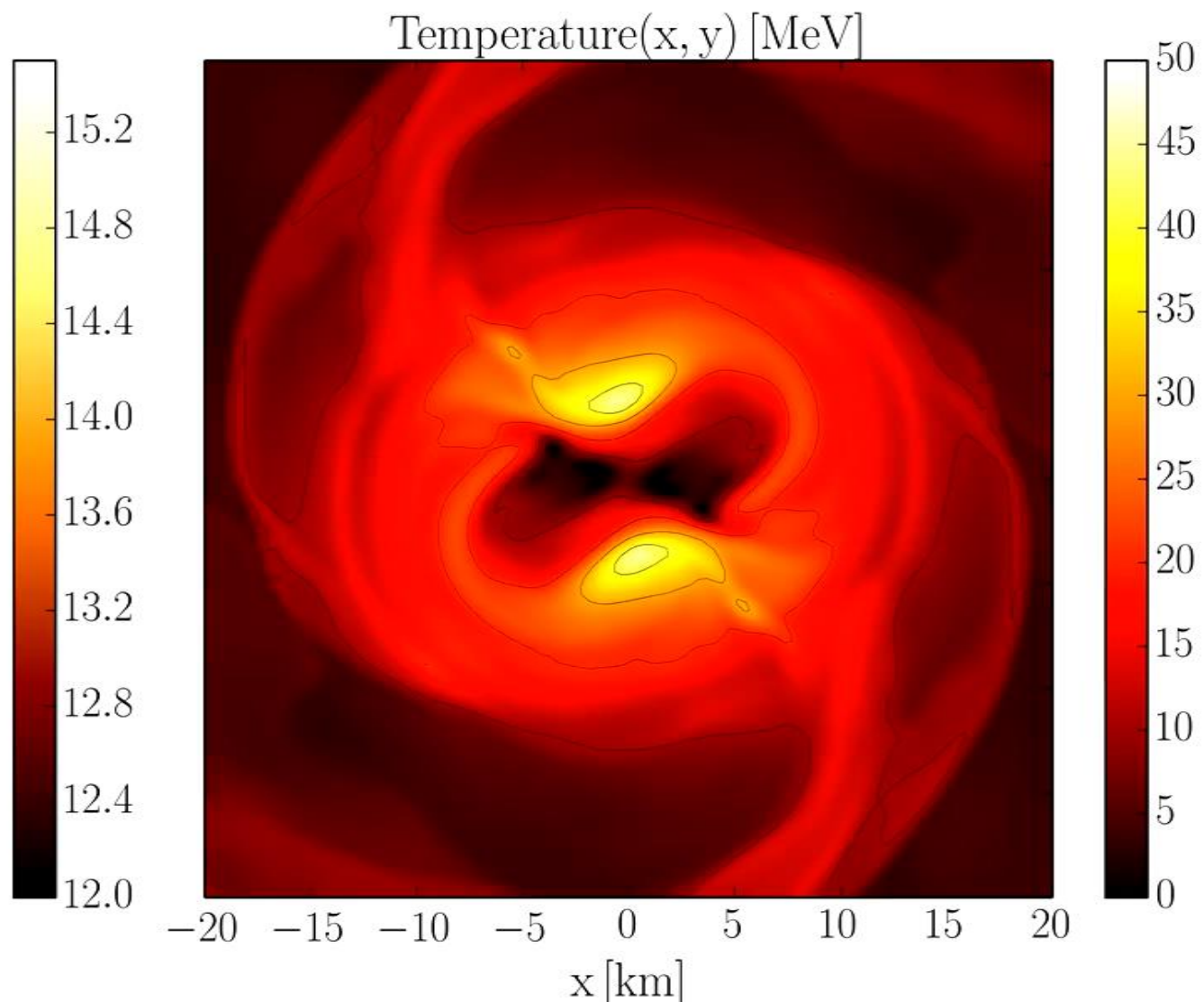
$$\Omega(x, y, z, t) = \frac{u^\phi}{u^t} = \alpha v^\phi - \beta^\phi$$



Logarithm of the density

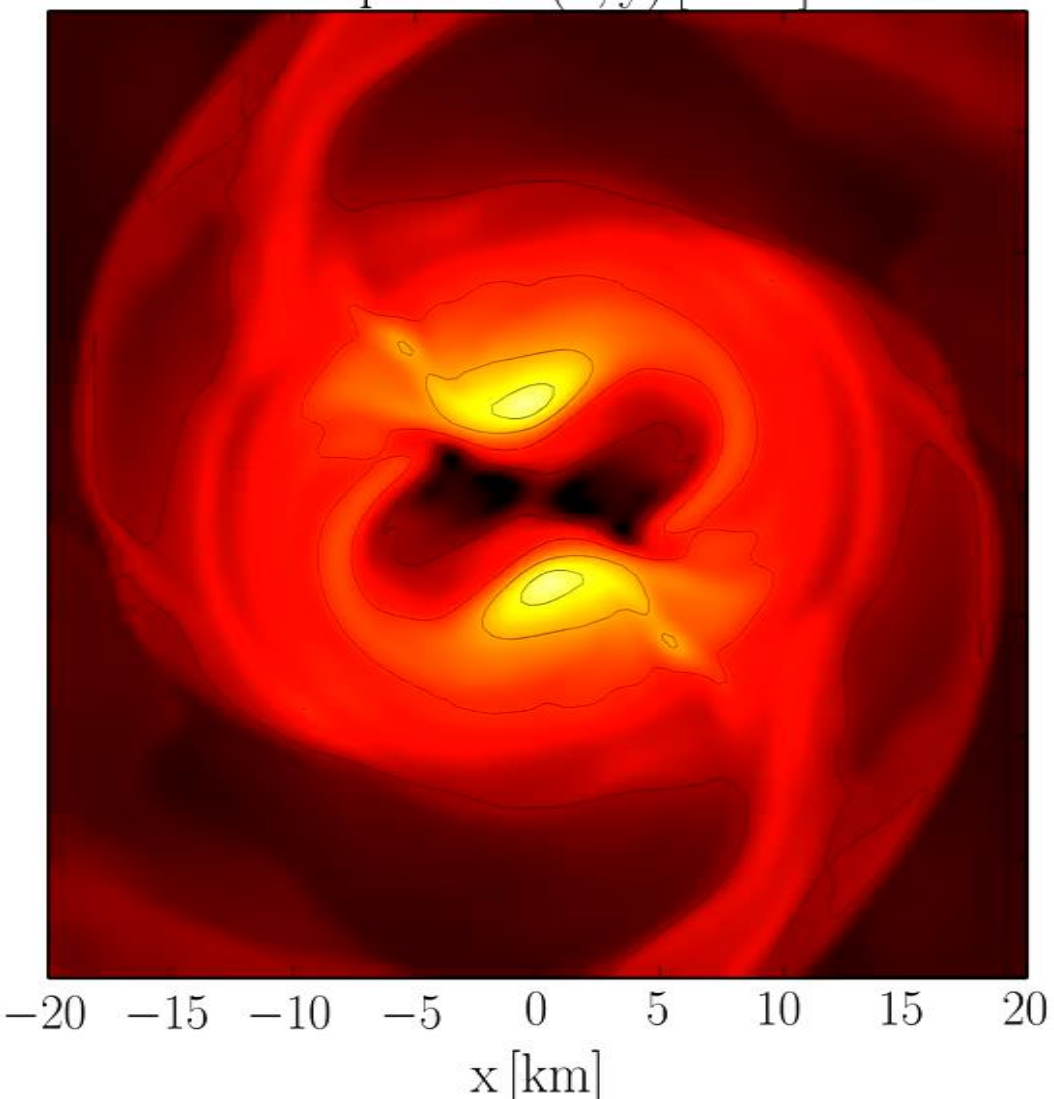


Temperature



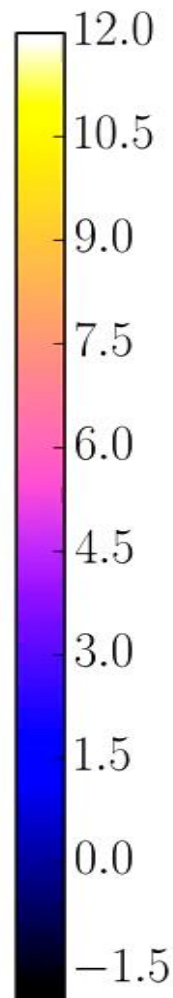
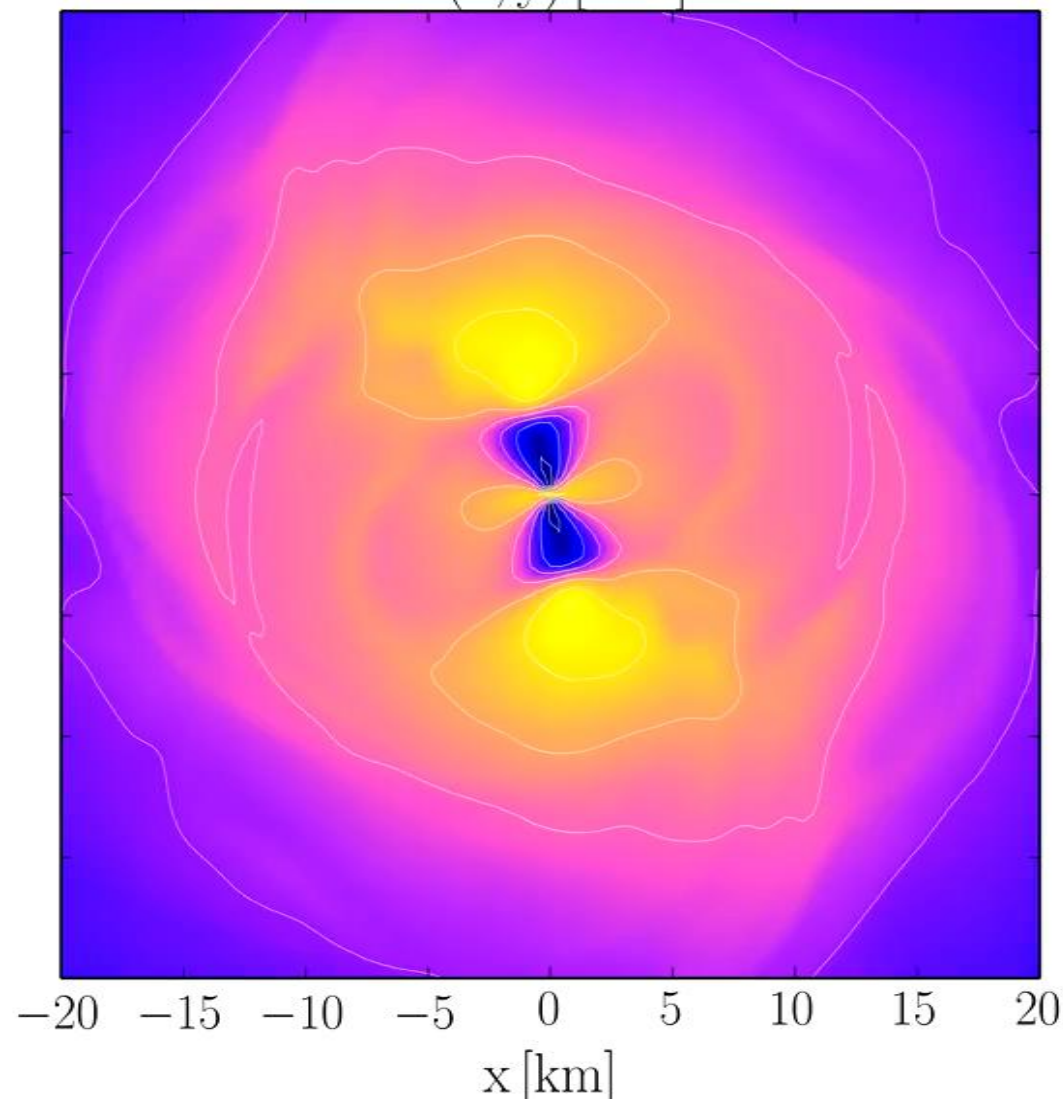
Temperature

Temperature(x, y) [MeV]

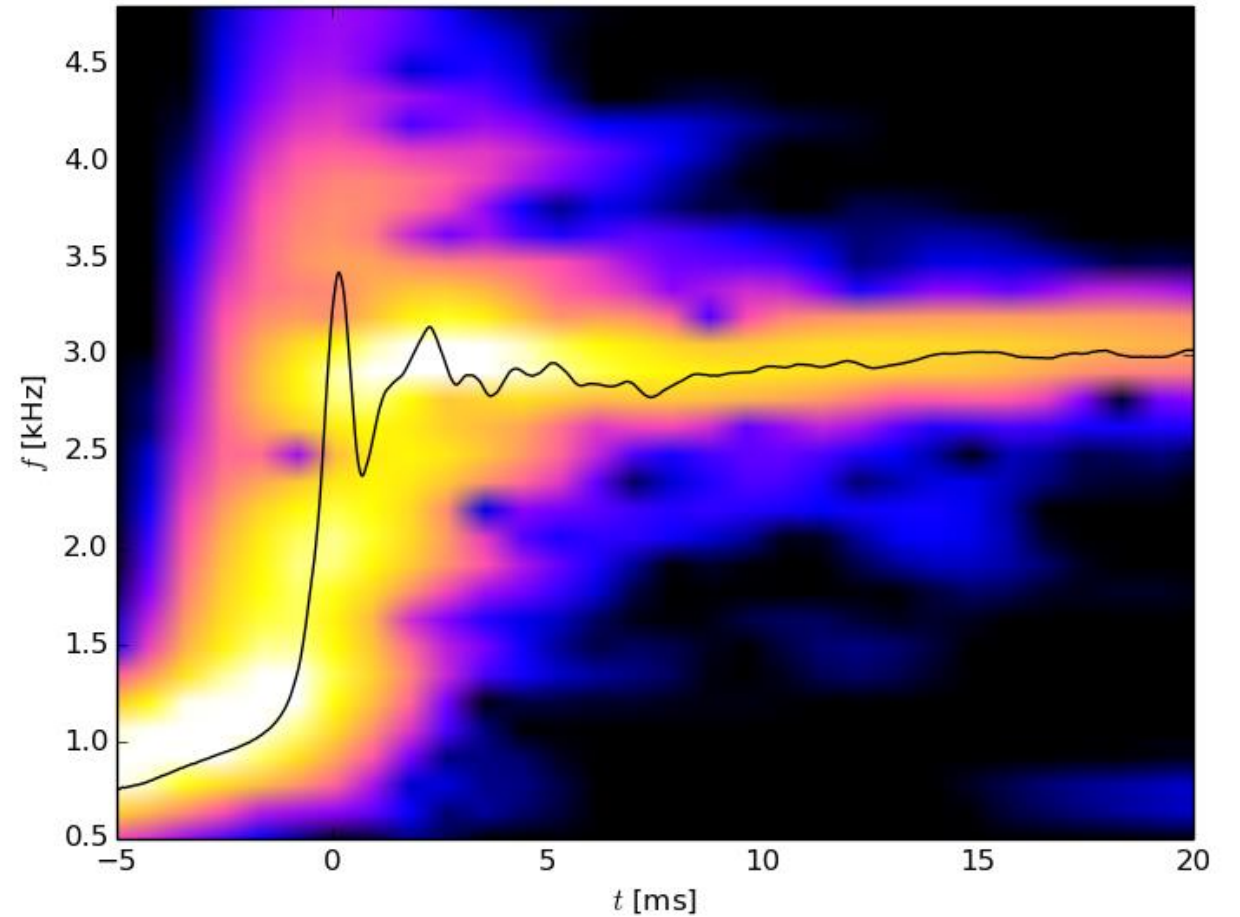
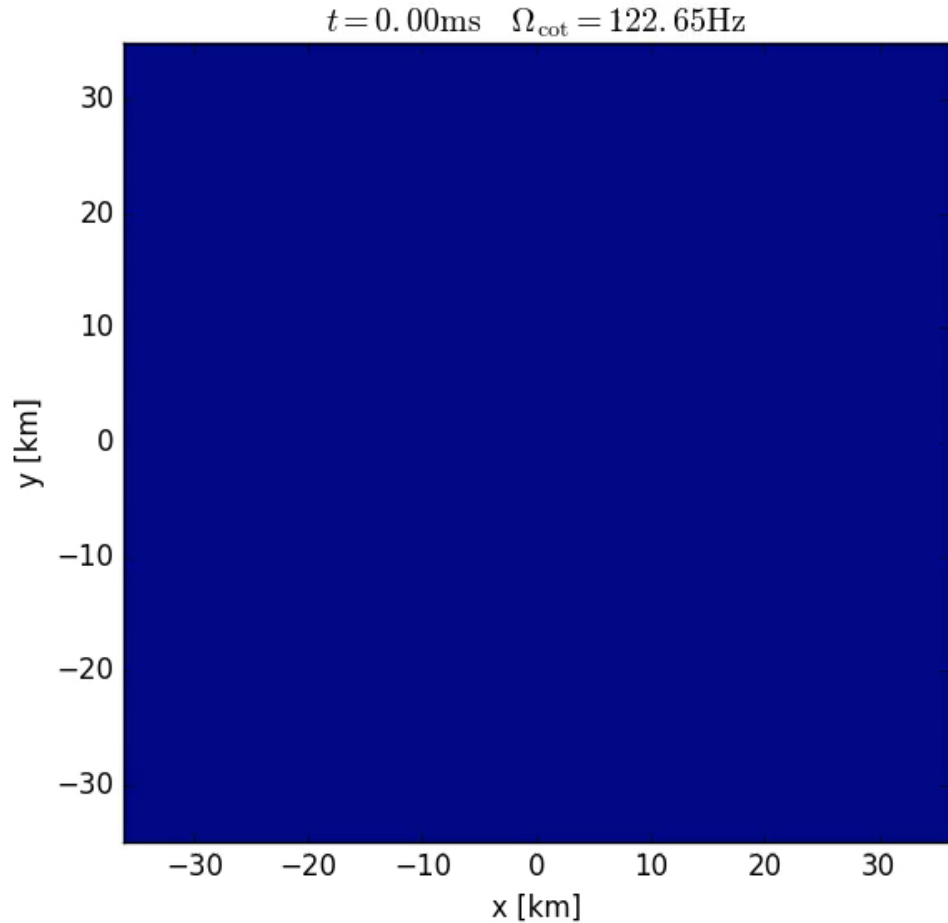


Angular Velocity

$\Omega(x, y)$ [kHz]

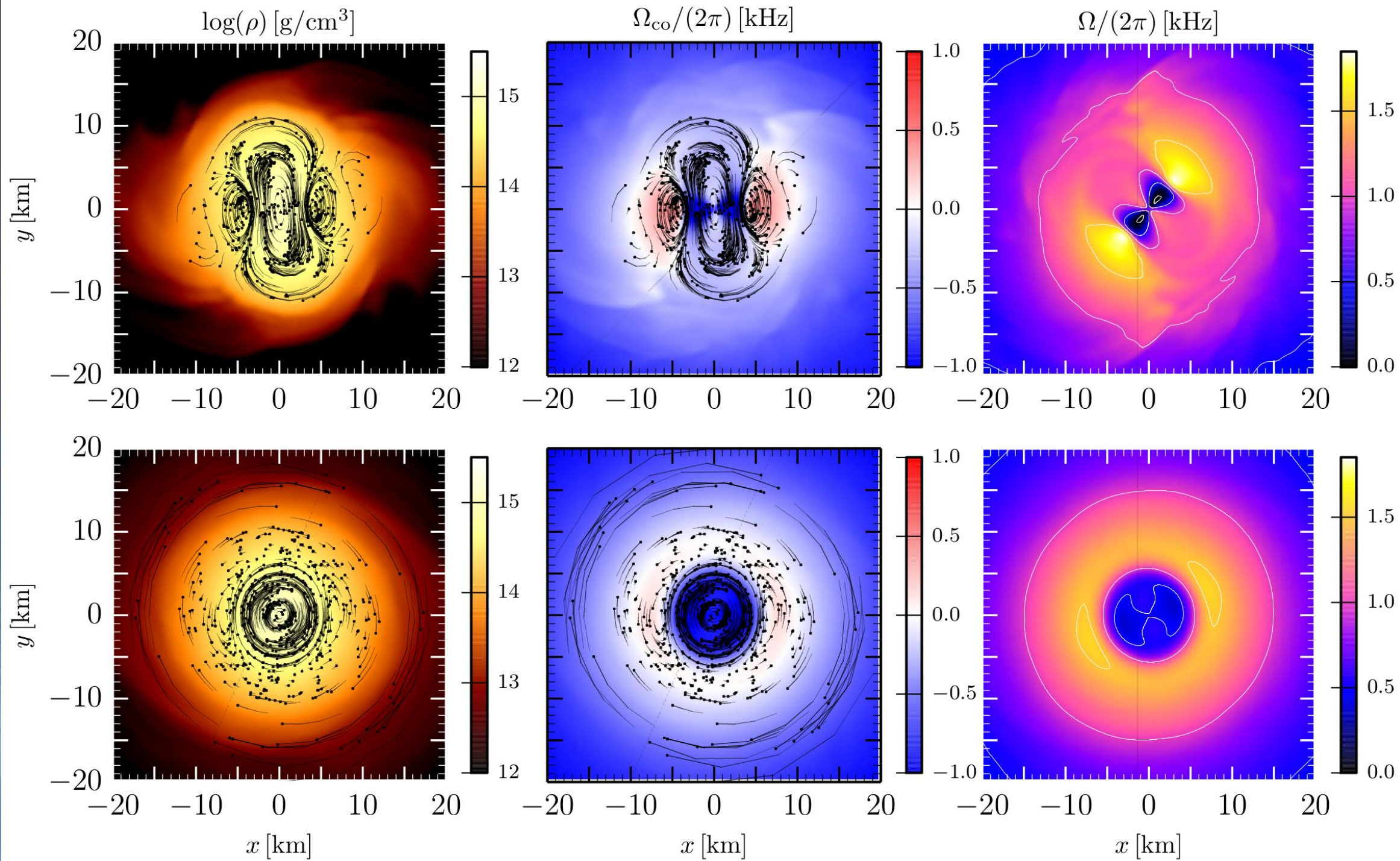


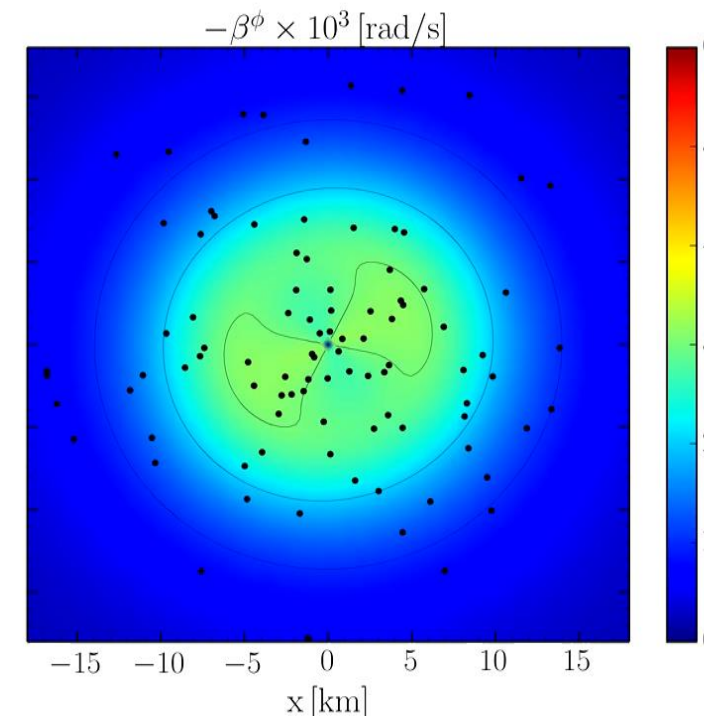
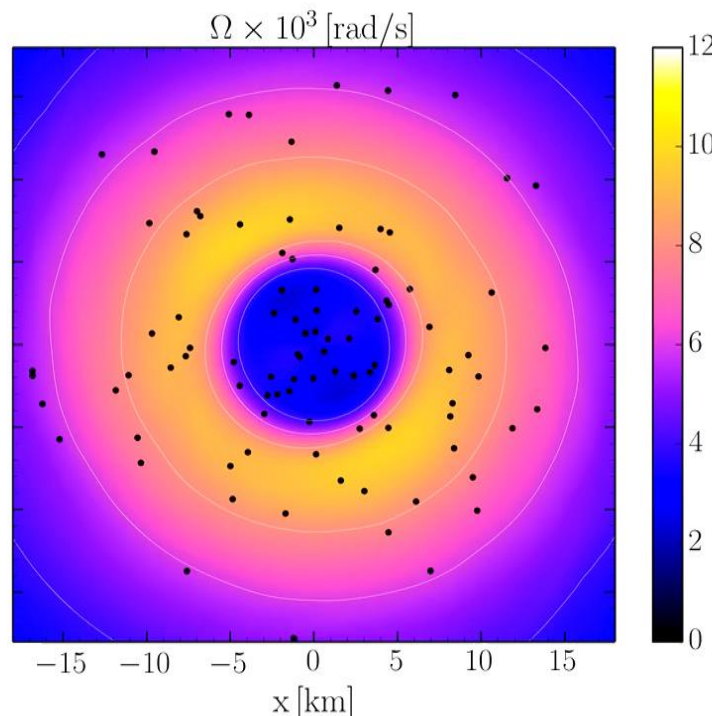
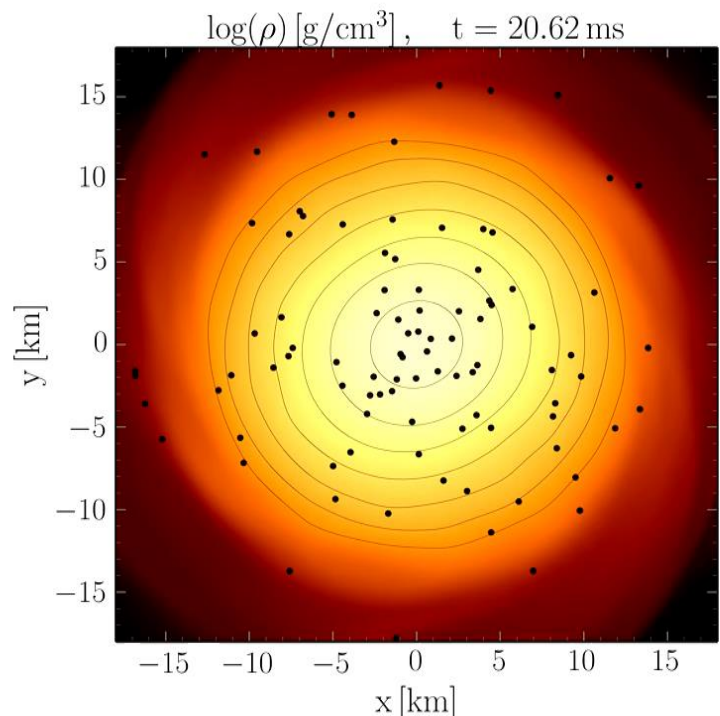
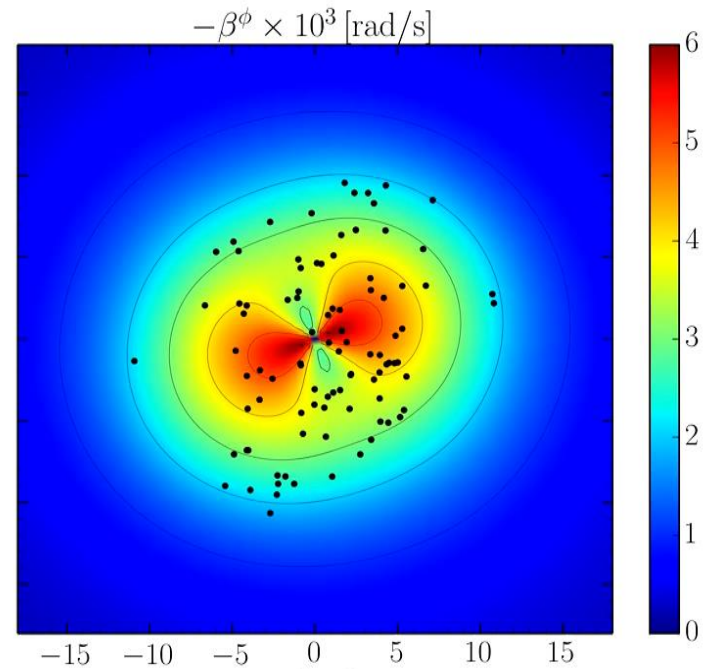
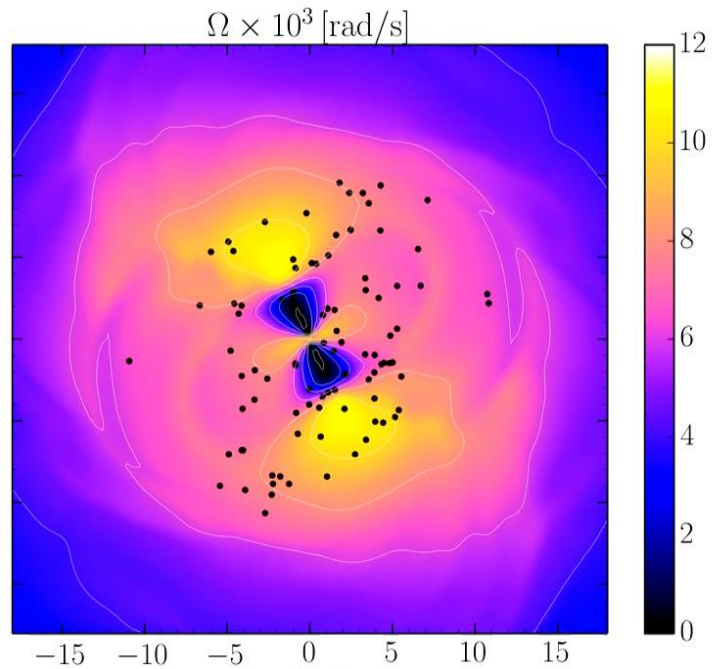
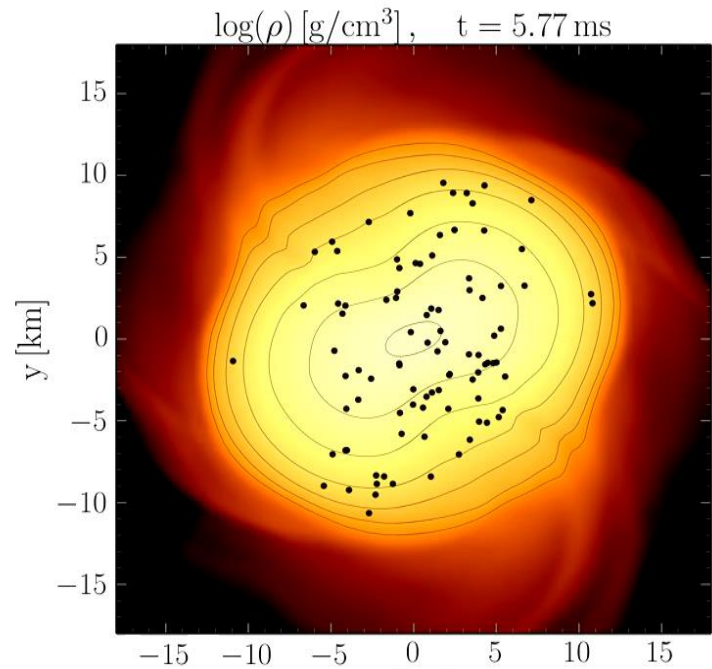
The Co-Rotating Frame

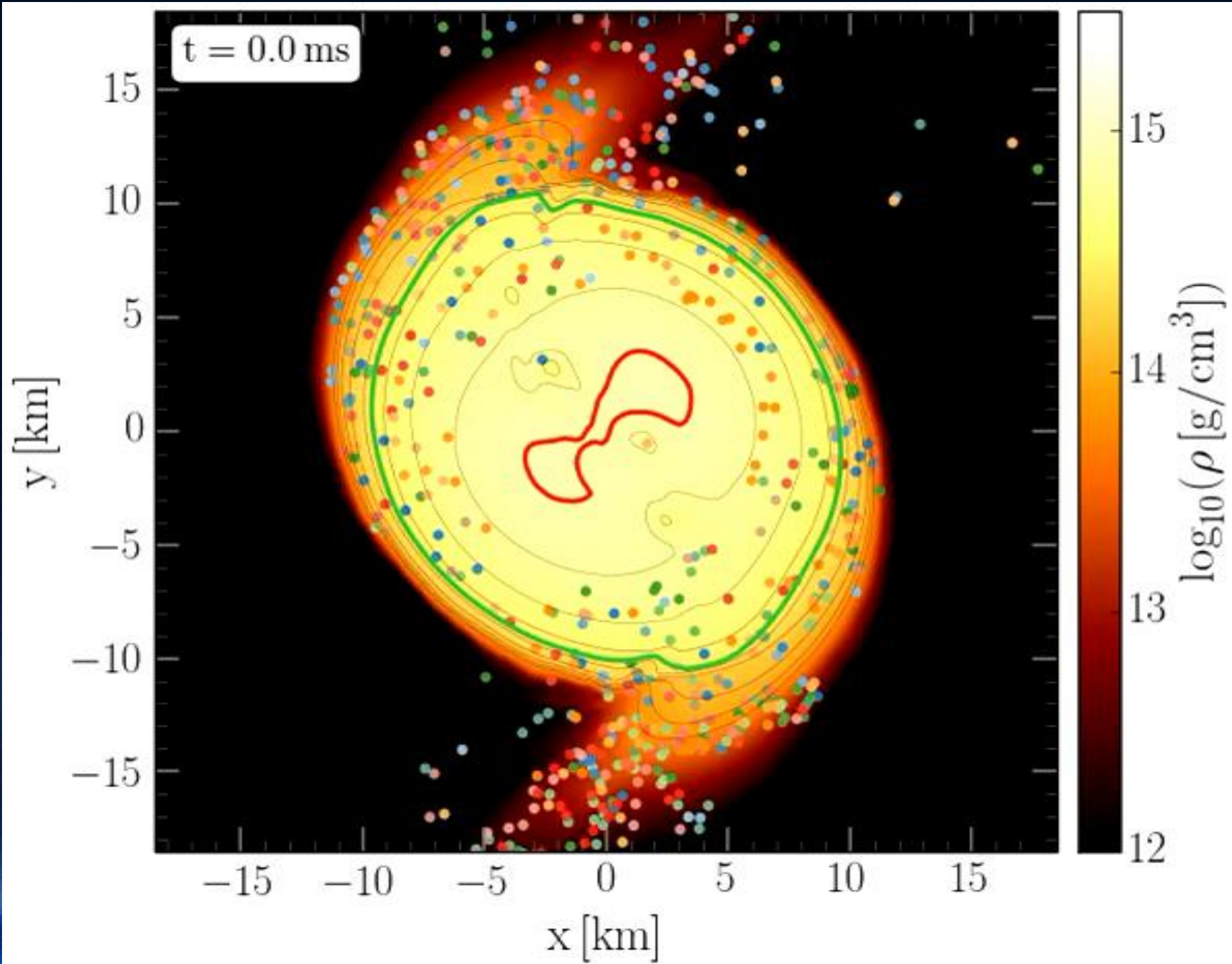


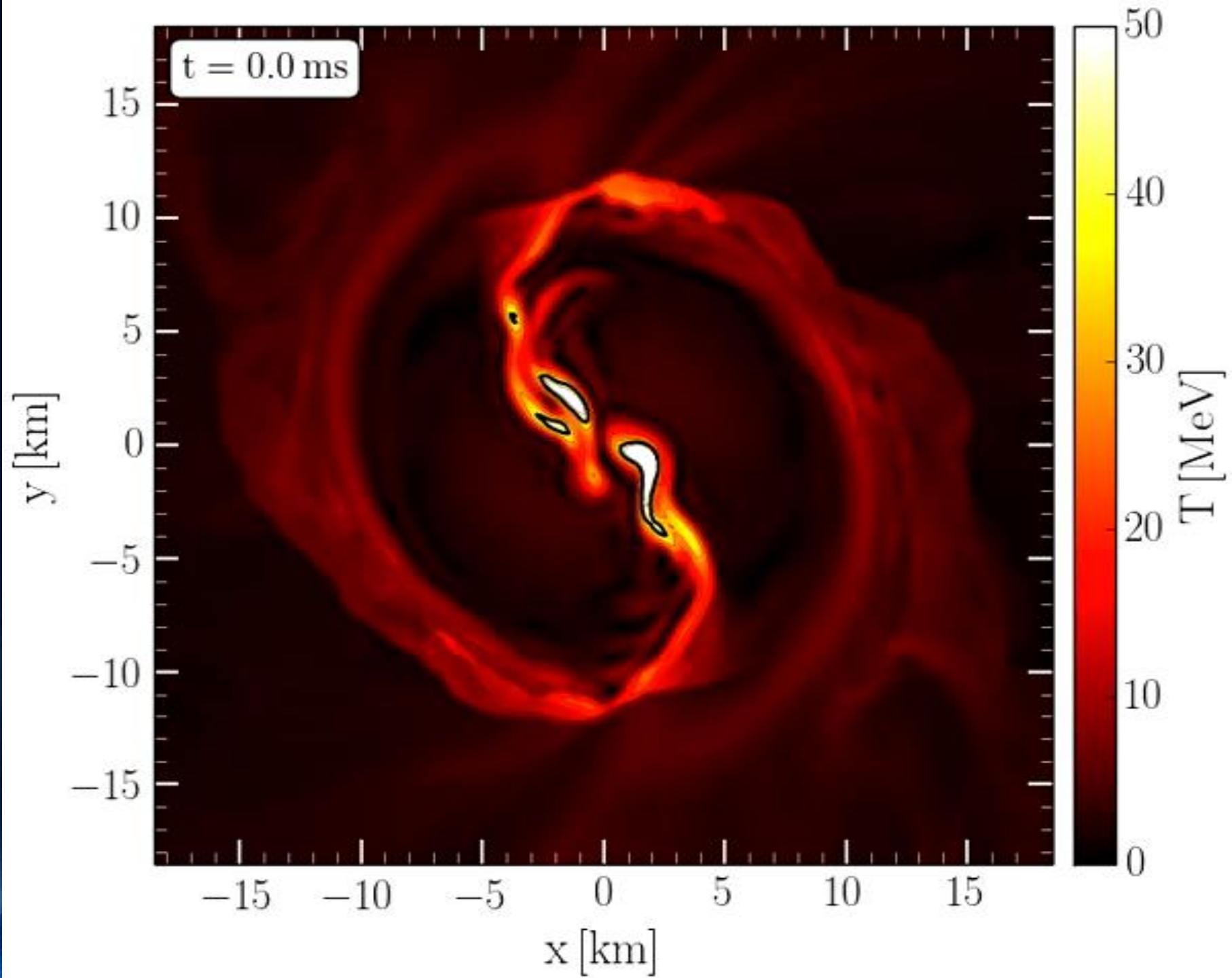
- ² Note that the angular-velocity distribution in the lower central panel of Fig. 10 refers to the corotating frame and that this frame is rotating at half the angular frequency of the emitted gravitational waves, Ω_{GW} . Because the maximum of the angular velocity Ω_{max} is of the order of $\Omega_{\text{GW}}/2$ (cf. left panel of Fig. 12), the ring structure in this panel is approximately at zero angular velocity.

Simulation and movie has been produced by Luke Bovard









Averaging Procedure for Ω

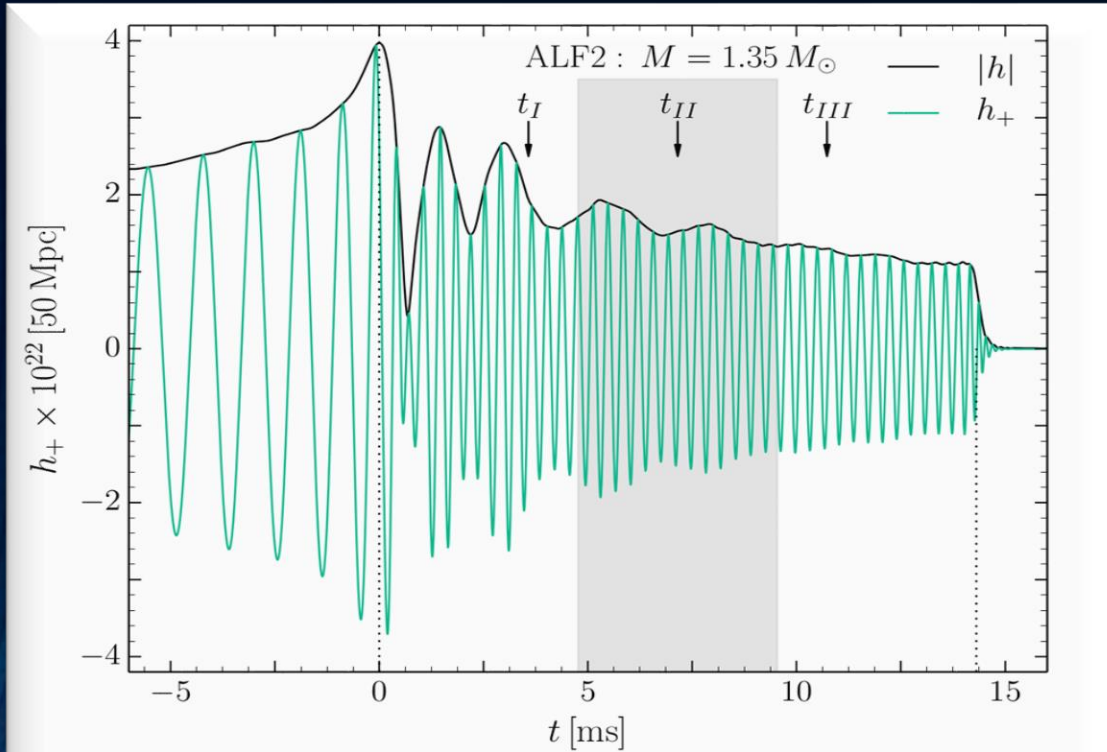


FIG. 2. Gravitational wave amplitude $|h|$ and h_+ at a distance of 50 Mpc for the ALF2-M135 model.

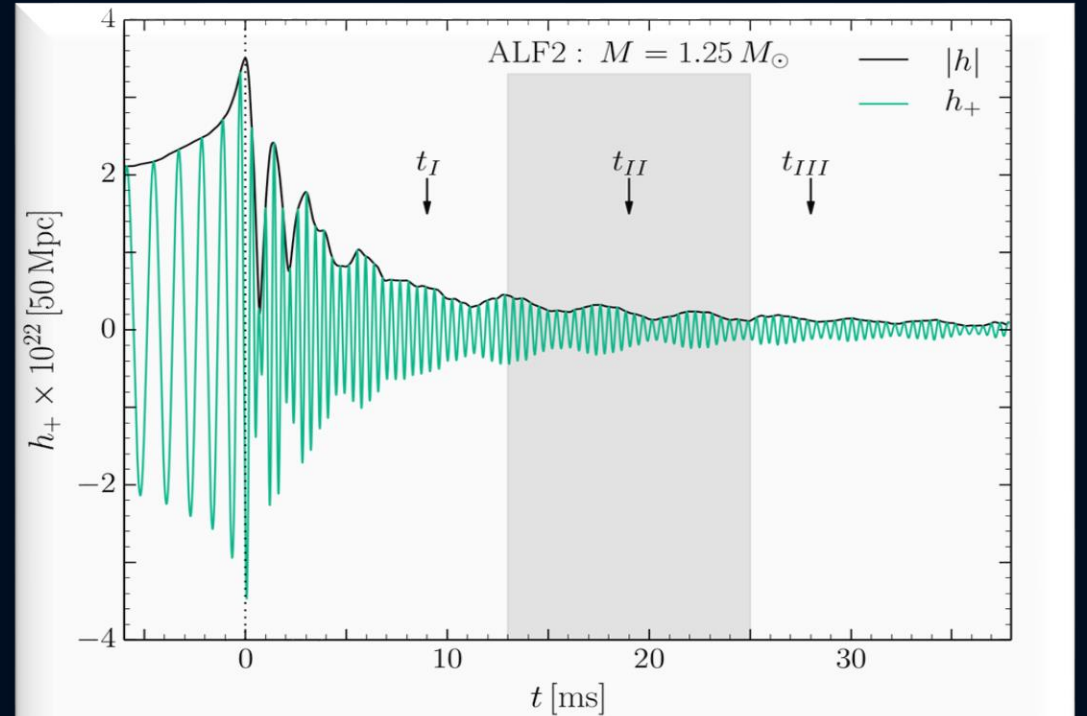
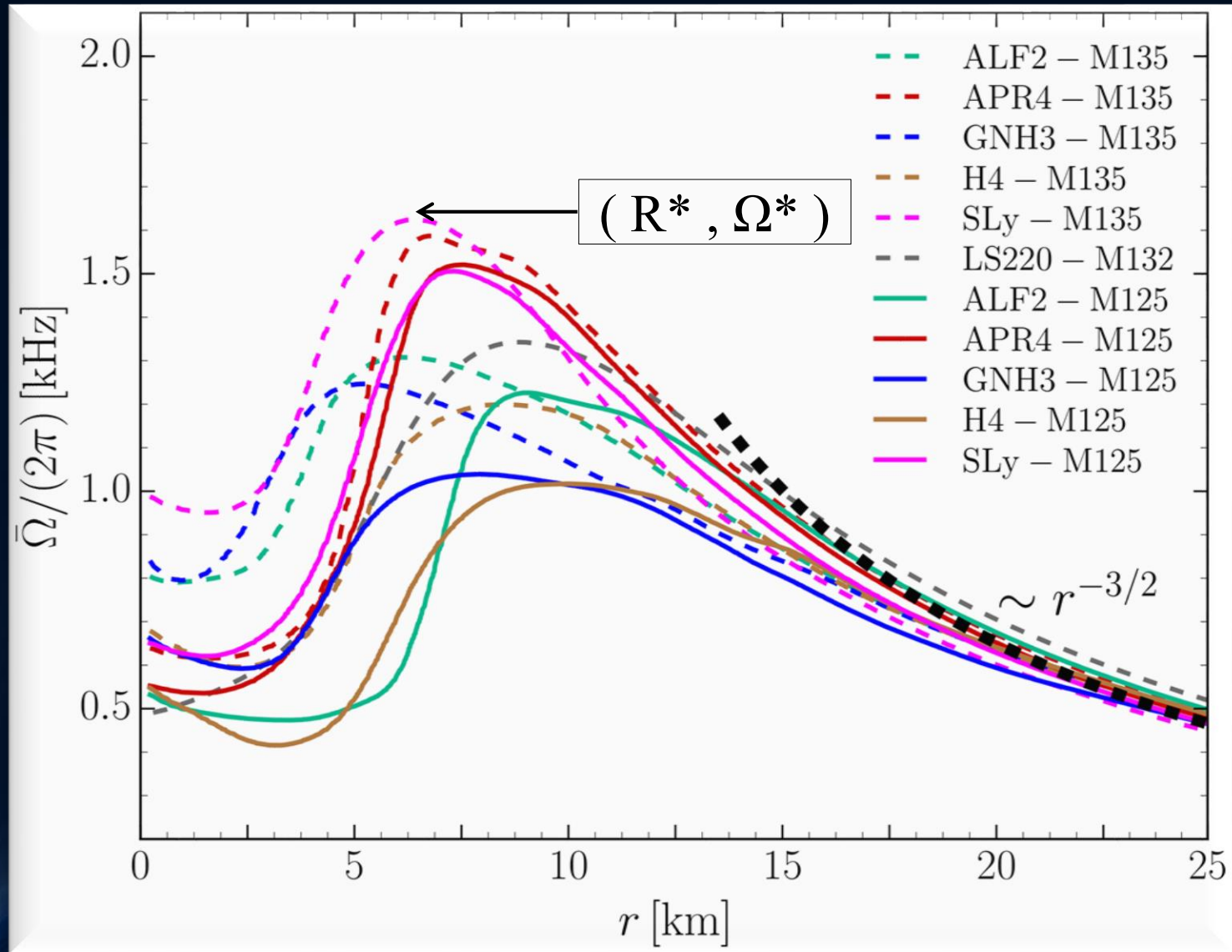


FIG. 10. Gravitational wave amplitude h_+ and $|h|$ at a distance of 50 Mpc for the ALF2-M125 model.

$$\bar{\Omega}(r, t_c) = \int_{t_c - \Delta t/2}^{t_c + \Delta t/2} \int_{-\pi}^{\pi} \Omega(r, \phi, t') d\phi dt'$$

In order to compare the structure of the rotation profiles between the different EOSs, a certain time averaging procedure has been used:

Time-averaged Rotation Profiles



Soft EoSs:

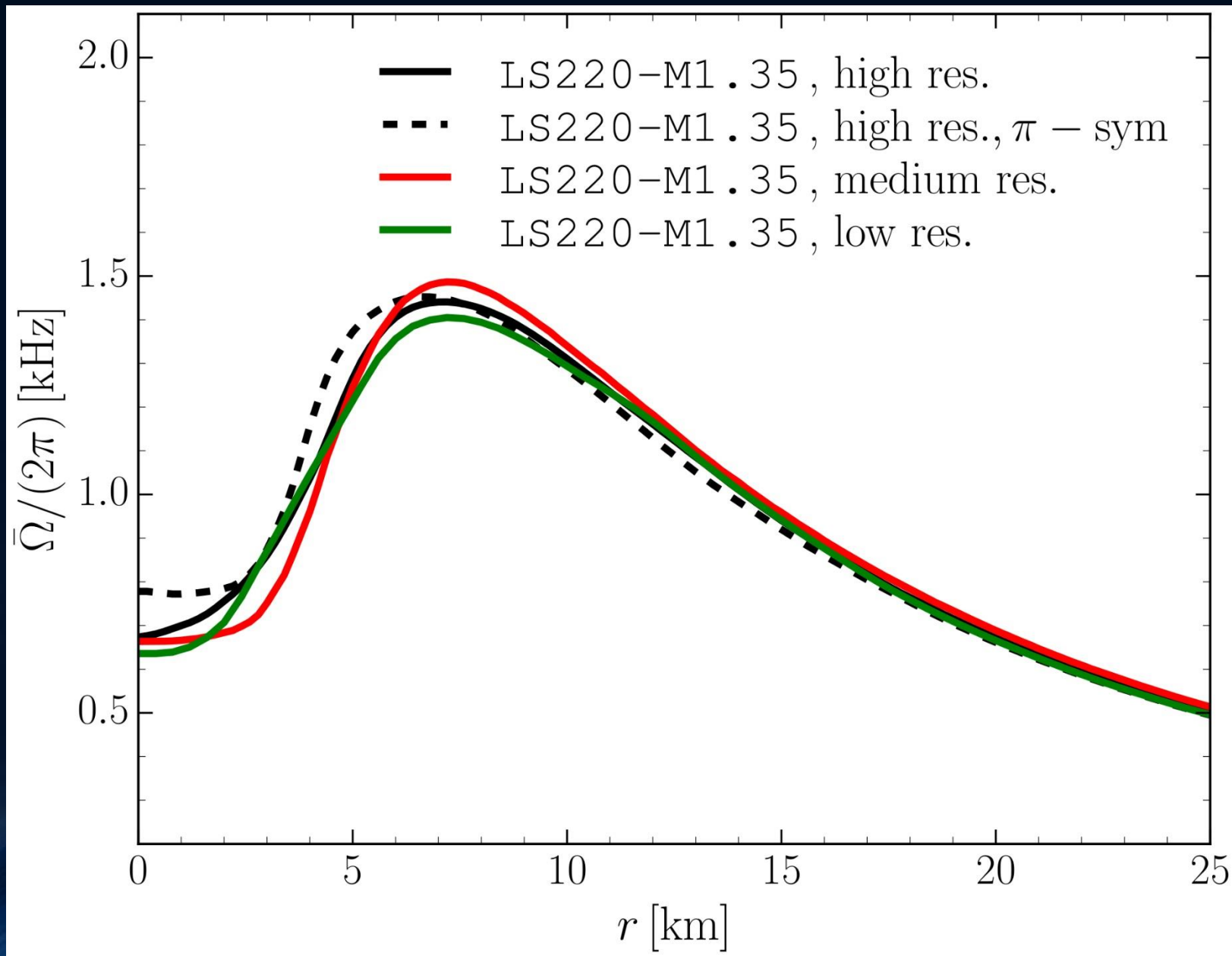
Sly
APR4

Stiff EoSs:

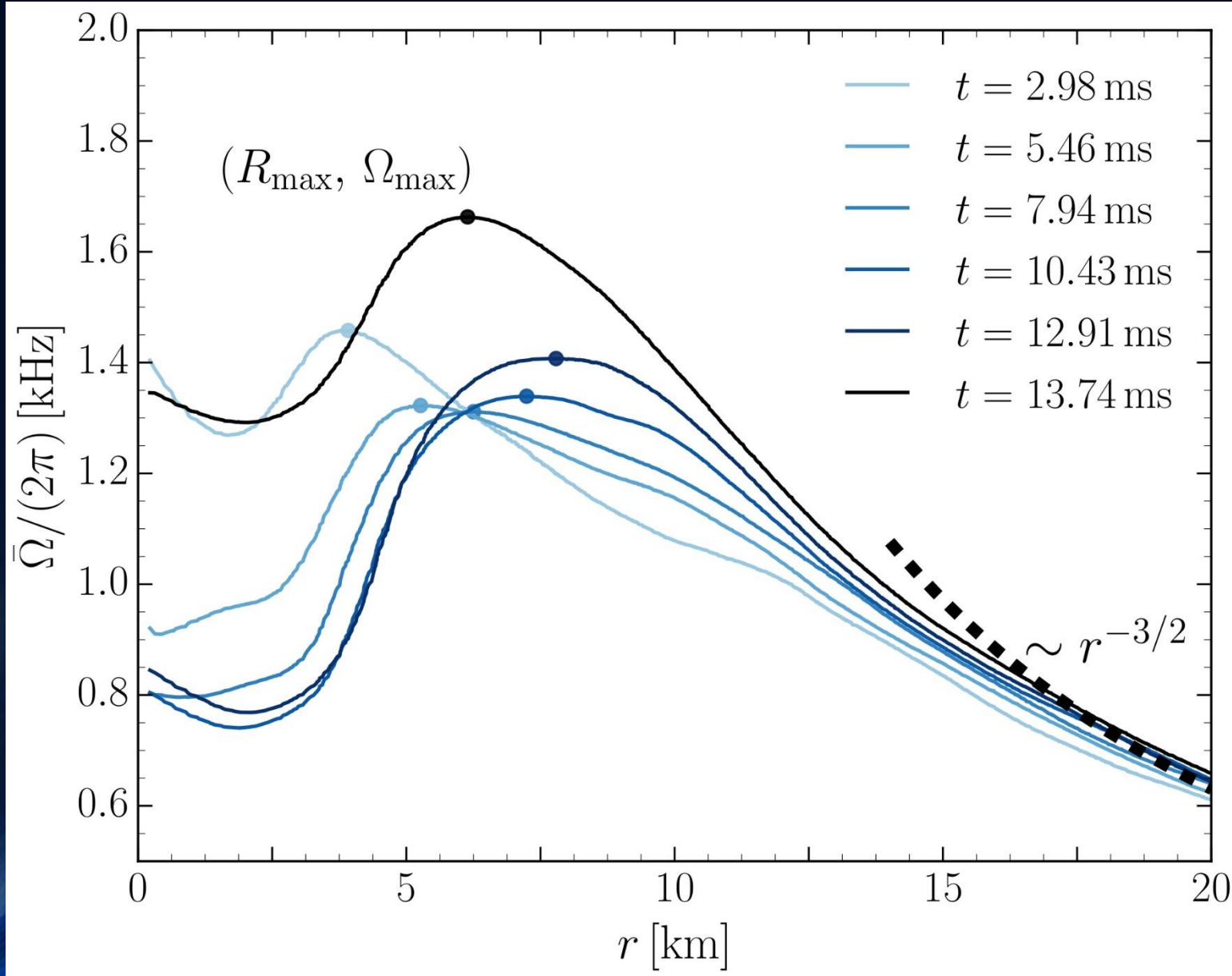
GNH3
H4

Time-averaged rotation profiles for different EoS
Low mass runs (solid curves), high mass runs (dashed curves).

Dependence on Pi-Symmetry and Grid Resolution

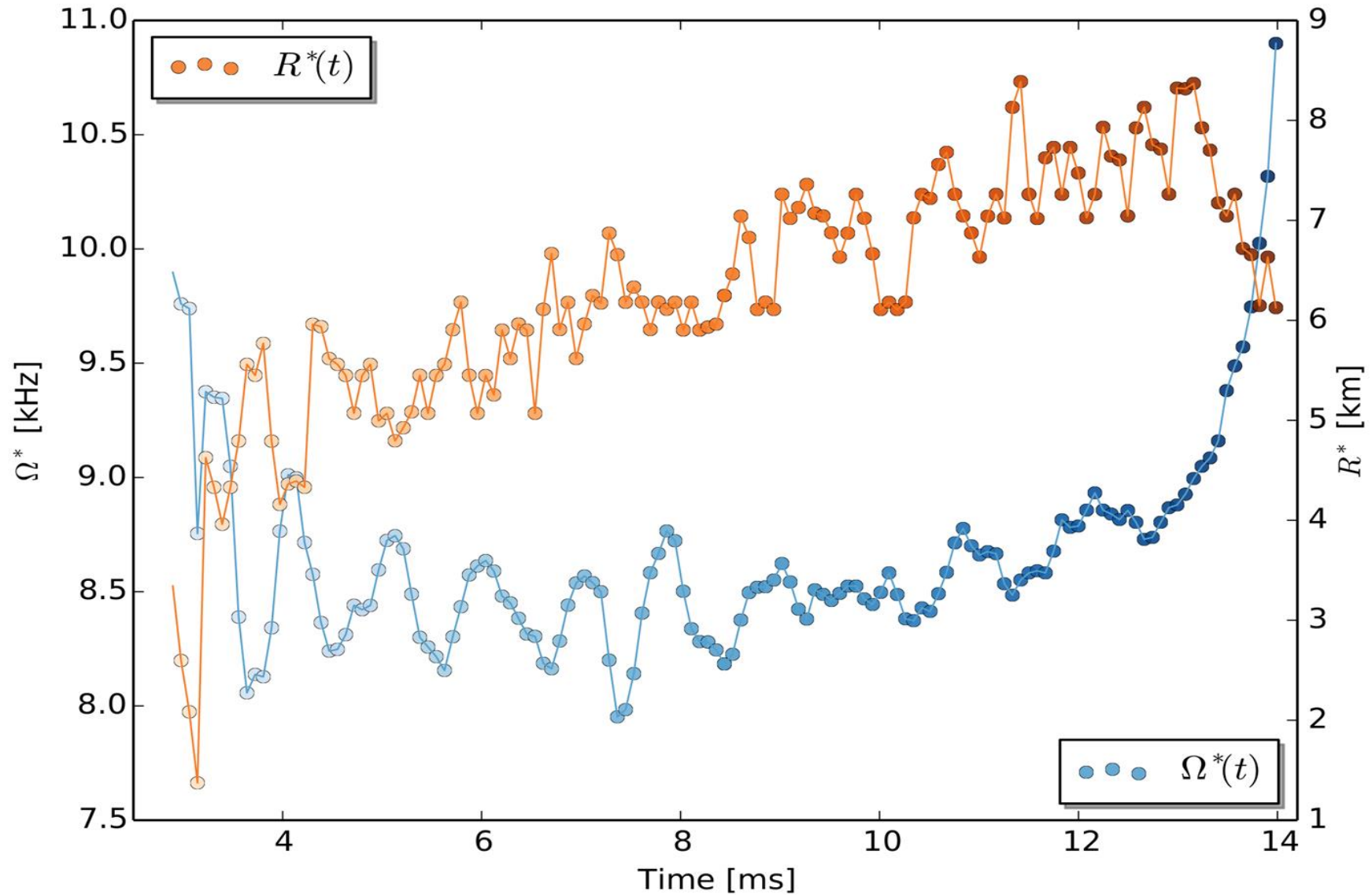


Time dependence of the Rotation Profile

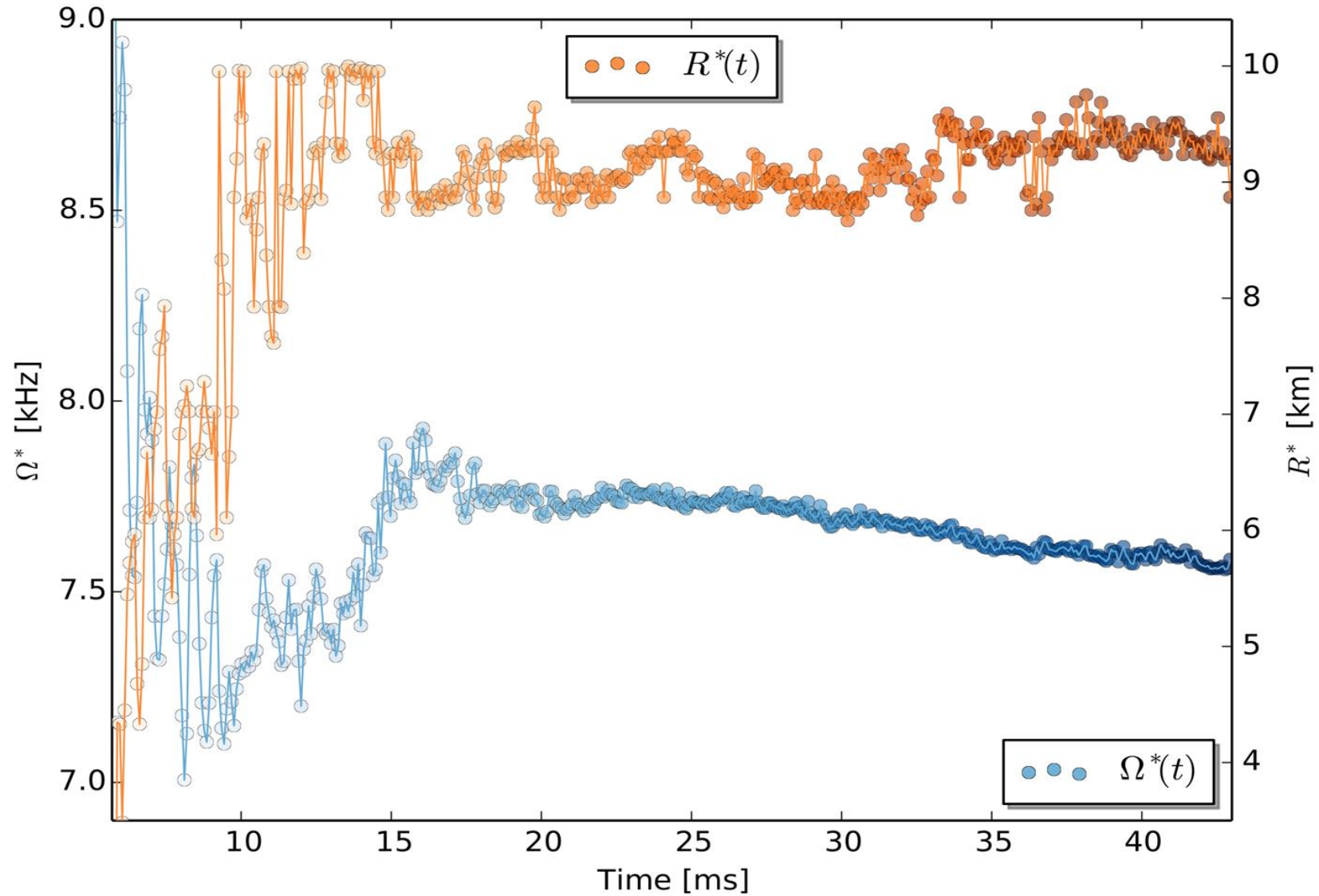


Averaged fluid angular velocity on the equatorial plane for the ALF2-M135 binary as averaged at different times and with intervals of length $t = 1$ ms.

$\Omega^*(t)$ [rad/s] and $R^*(t)$ for ALF2, $M=1.35$

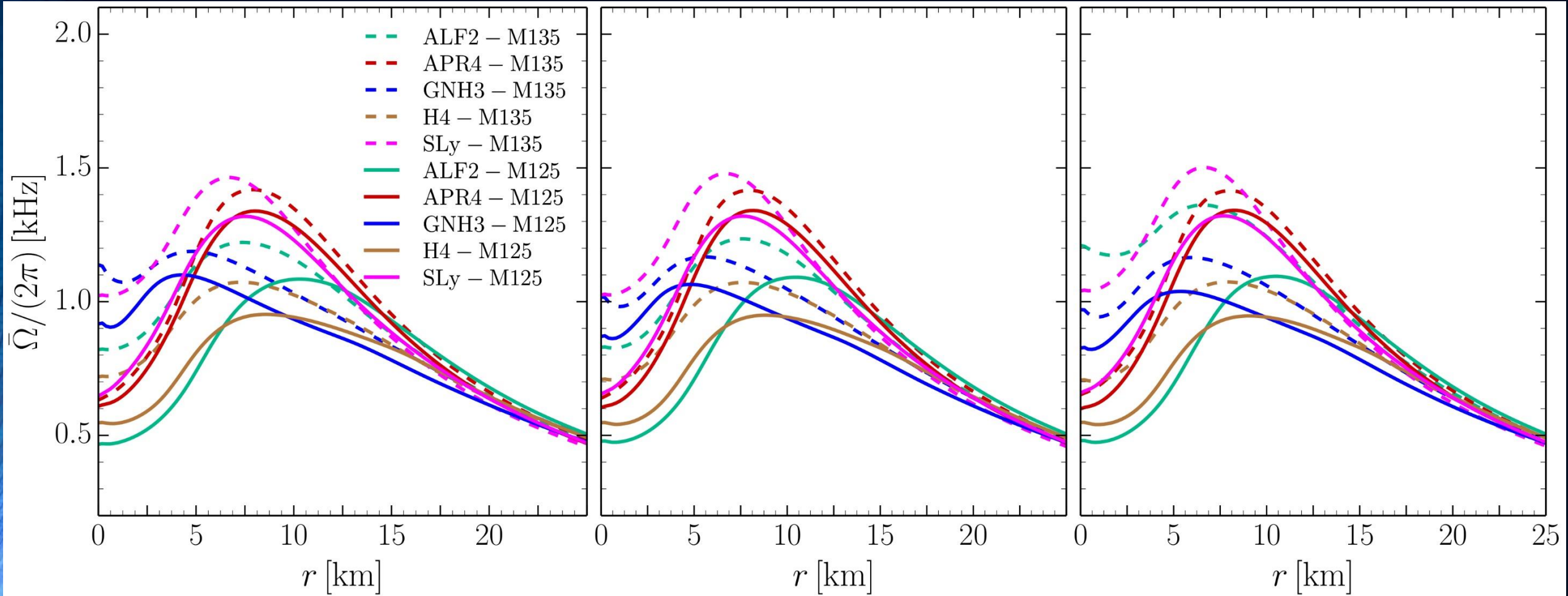


$\Omega^*(t)$ [rad/s] and $R^*(t)$ for ALF2, $M=1.25$



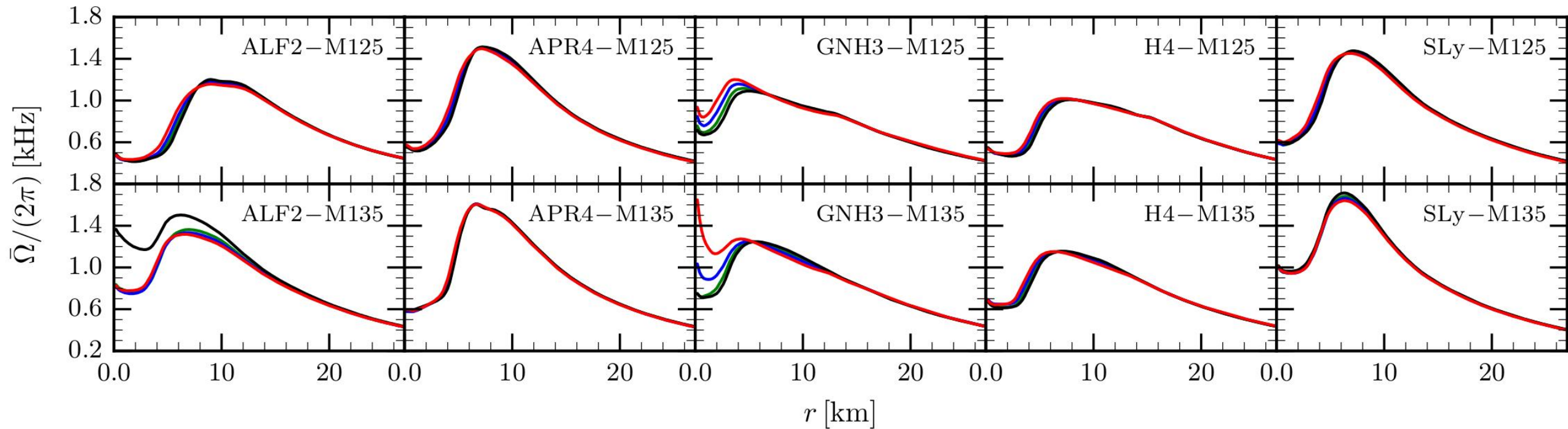
Dependence on the time averaging window

For all EOS the same time averaging window. From the left to right the data refer to time windows [6 ; 11]; [6 ; 13] and [6 ; 15] ms, respectively.

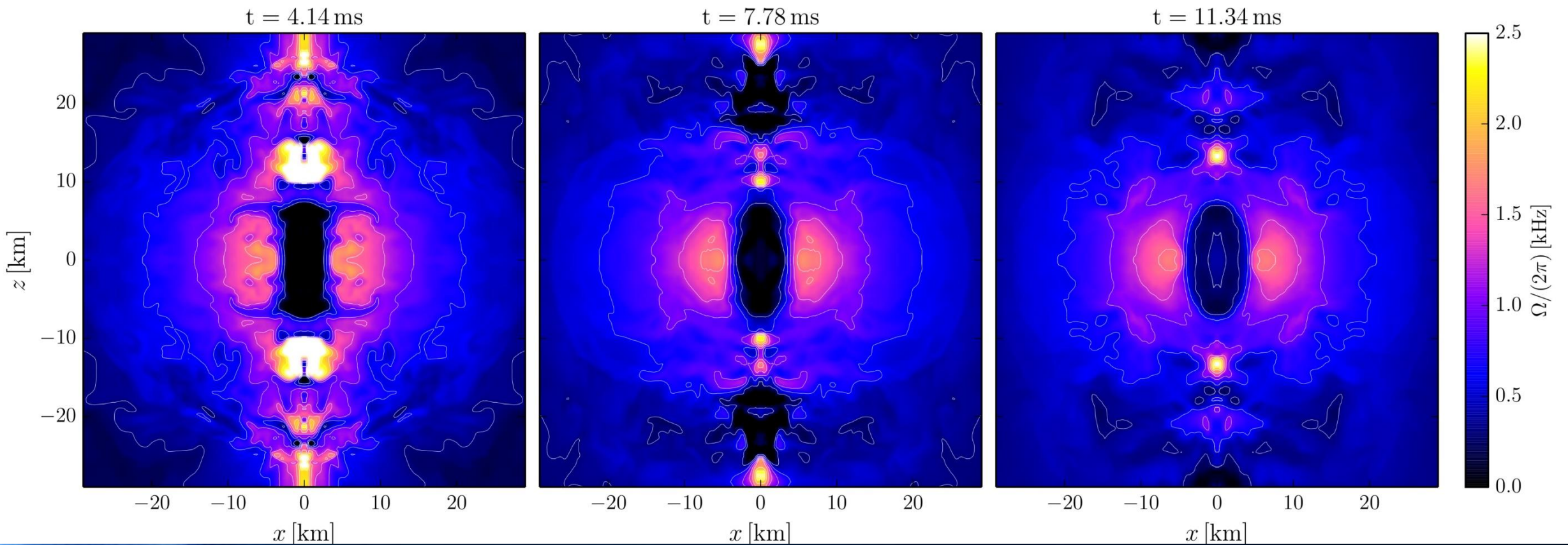


Dependence on the time averaging window

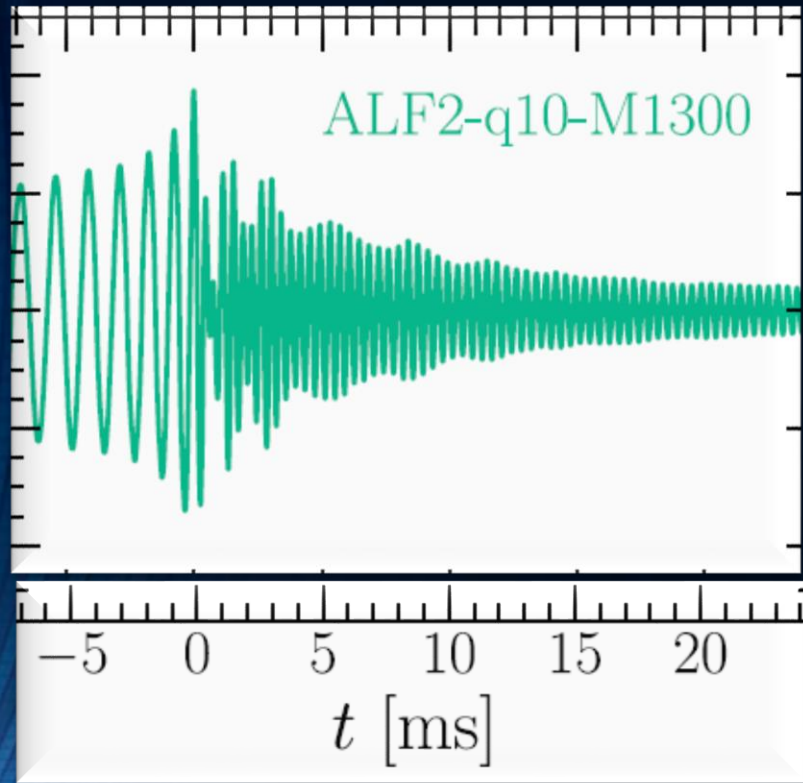
Averaged angular-velocity profiles when the averaging window is set to be 7 ms for all EOSs and masses, but where the initial averaging time is varied and set to be 5 (red line), 6 (blue line), 7 (green line), and 8 ms (black line), respectively. The four lines refer to averaging windows given by [5; 12], [6; 13], [7; 14], and [8; 15] ms, respectively; note that the top part of each panel refers to the low-mass binary, while the bottom one to the high-mass one.



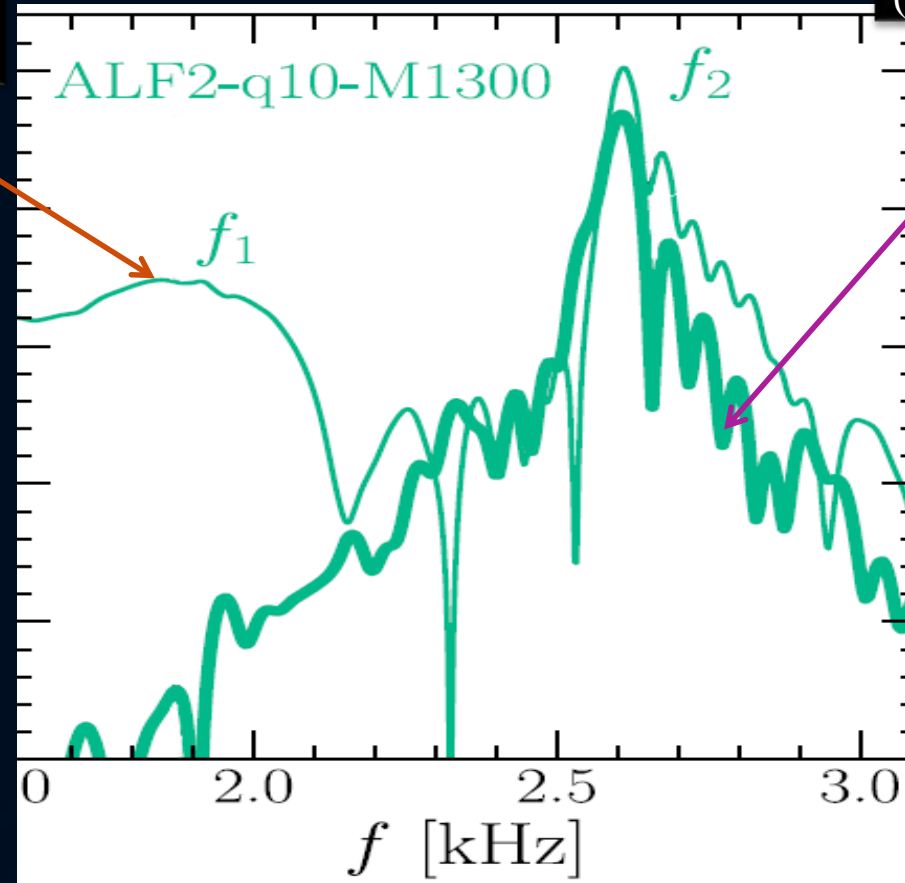
Angular Velocity away from the equatorial plane



Spectral Properties of GWs



Full spectral profile
(thin curve)

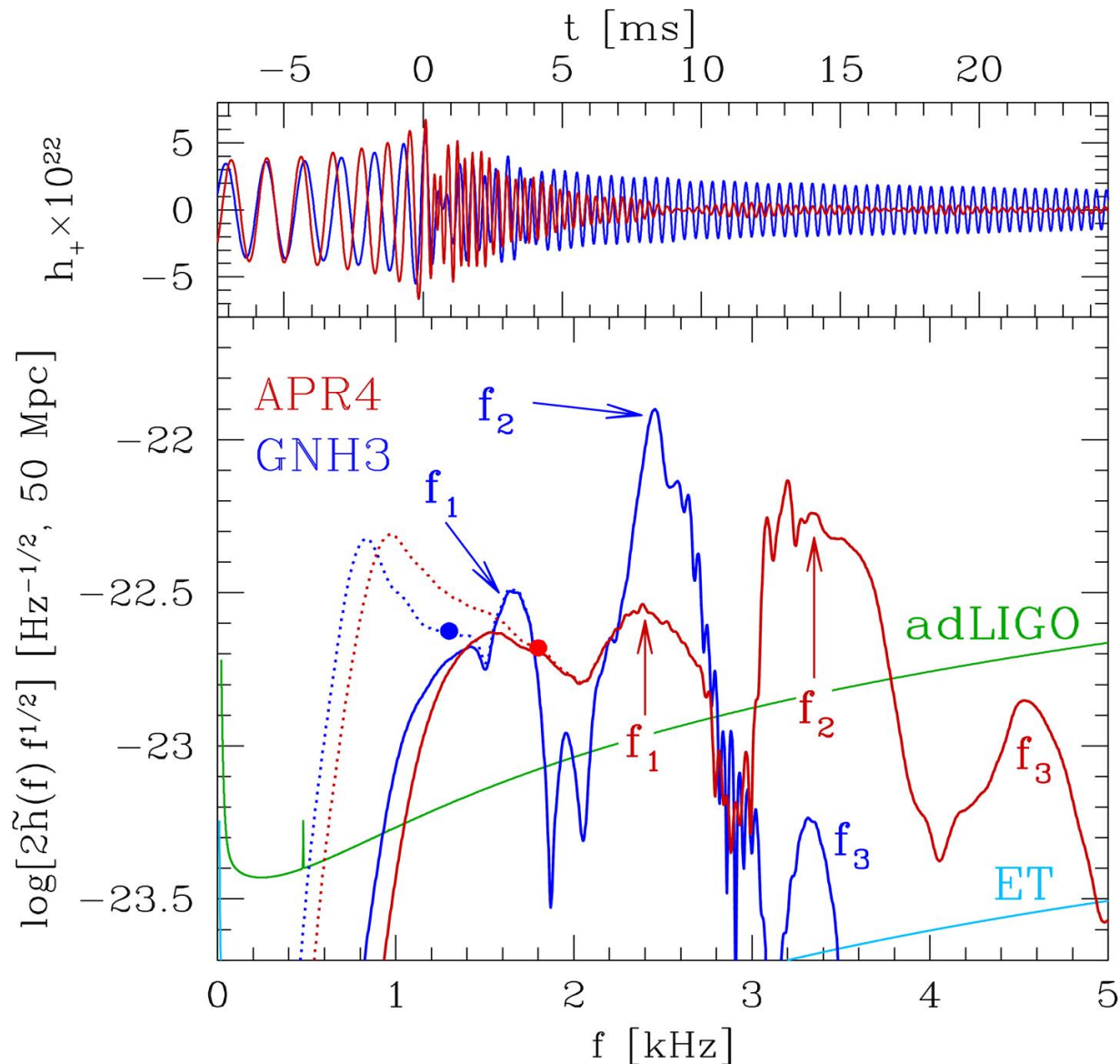


Spectral profile
($t > 3$ ms)
(thick curve)

Two characteristic GW frequency peaks (f_1 and f_2);

the origin of f_1 comes from $t < 3$ ms. By measuring M , f_1 and f_2 one can set high constraints on the EoS.

GW-Spectrum for different EOSs



See:

Kentaro Takami, Luciano Rezzolla, and Luca Baiotti, *Physical Review D* 91, 064001 (2015)

Hotokezaka, K., Kiuchi, K., Kyutoku, K., Muranushi, T., Sekiguchi, Y. I., Shibata, M., & Taniguchi, K. (2013). *Physical Review D*, 88(4), 044026.

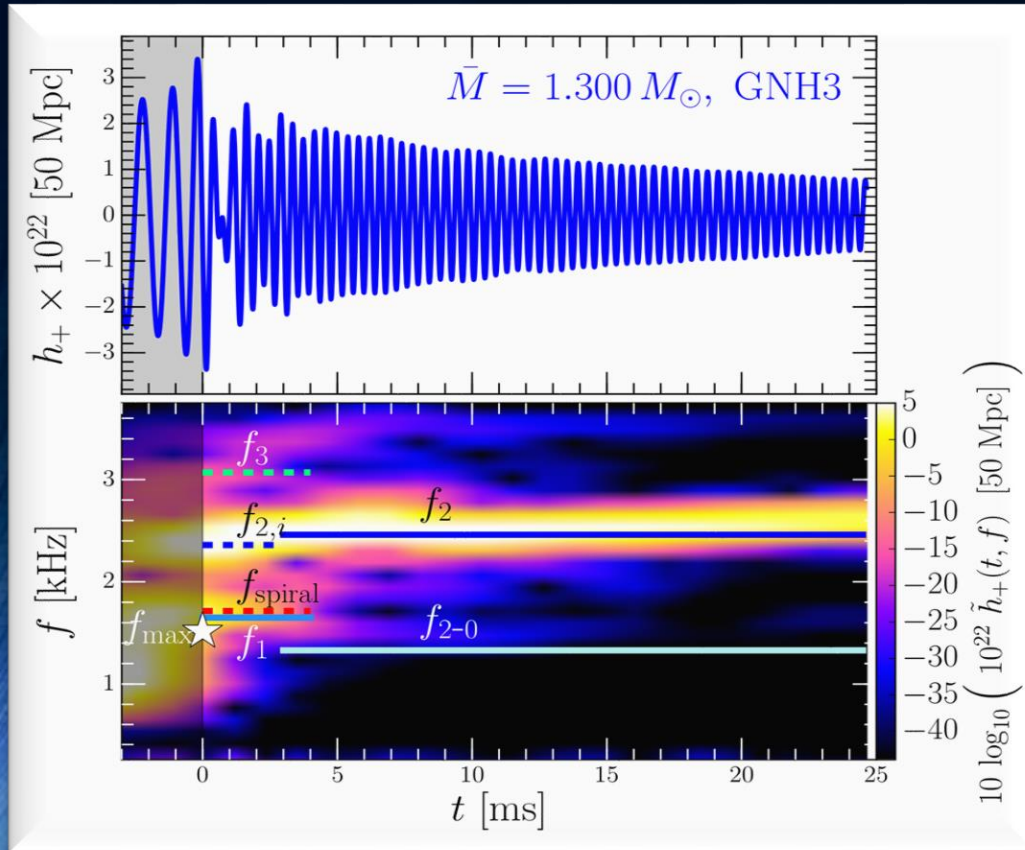
Bauswein, A., & Janka, H. T. (2012). *Physical review letters*, 108(1), 011101.

Clark, J. A., Bauswein, A., Stergioulas, N., & Shoemaker, D. (2015). *arXiv:1509.08522*.

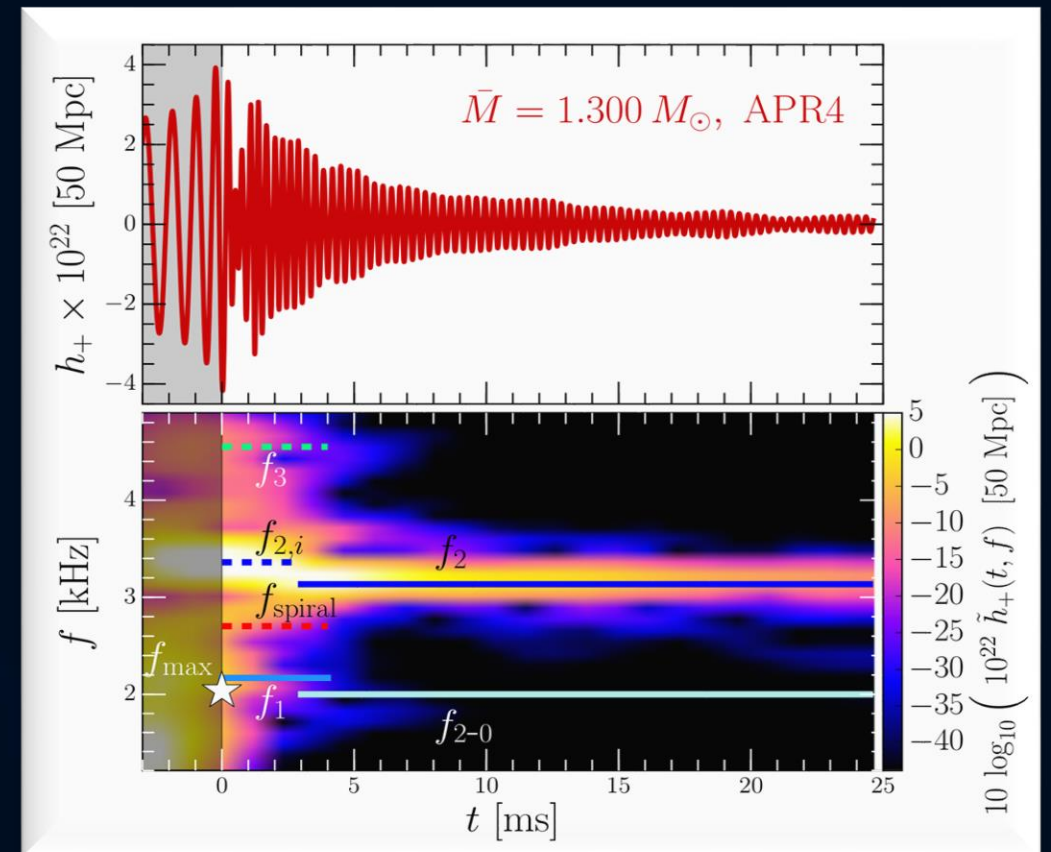
Bernuzzi, S., Dietrich, T., & Nagar, A. (2015). *Physical review letters*, 115(9), 091101.

Time Evolution of the GW-Spectrum

The power spectral density profile of the post-merger emission is characterized by several distinct frequencies f_{\max} , f_1 , f_2 , f_3 and f_{2-0} . After approximately 5 ms after merger, the only remaining dominant frequency is the f_2 -frequency (See L.Rezzolla and K.Takami, arXiv:1604.00246)



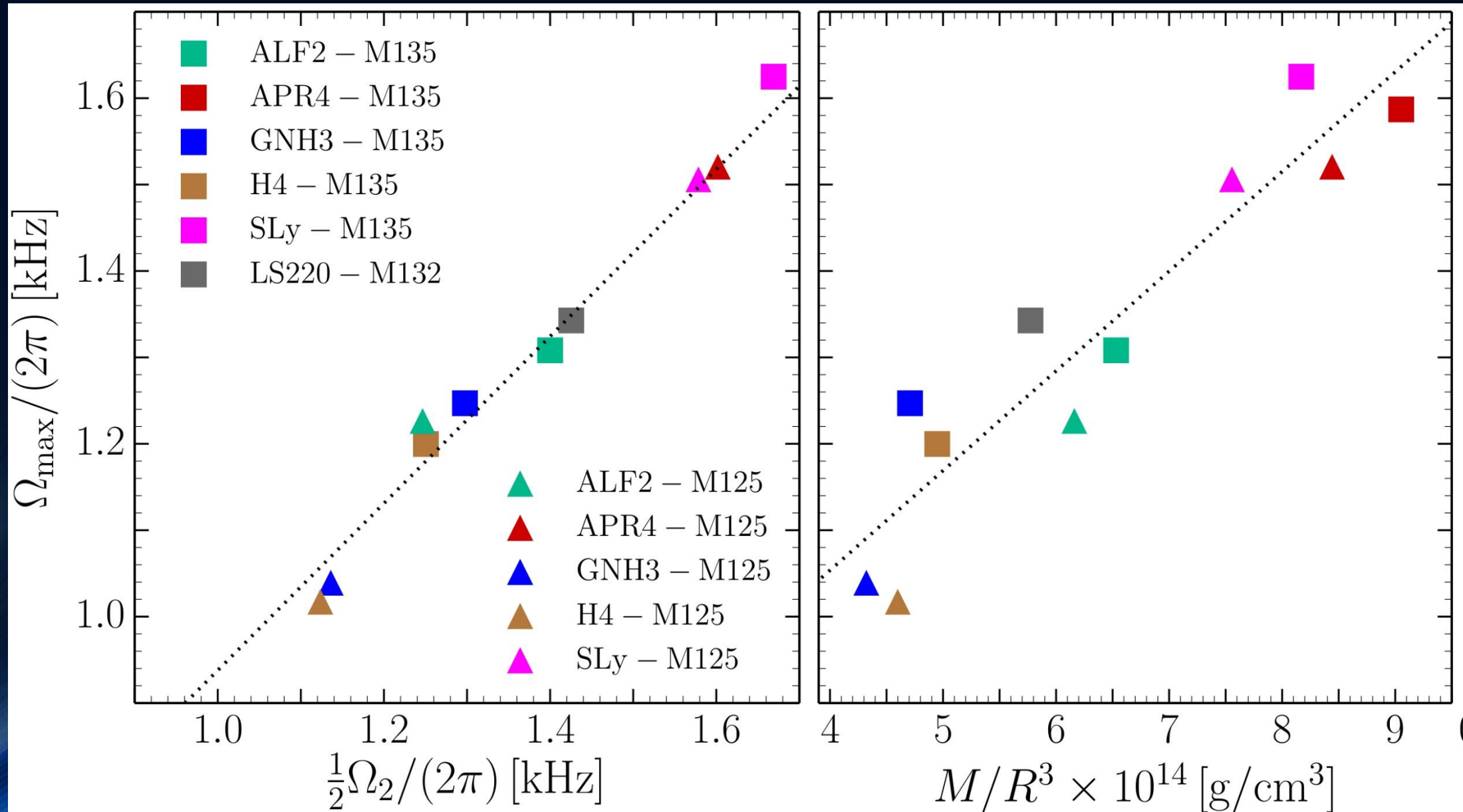
Stiff EOS



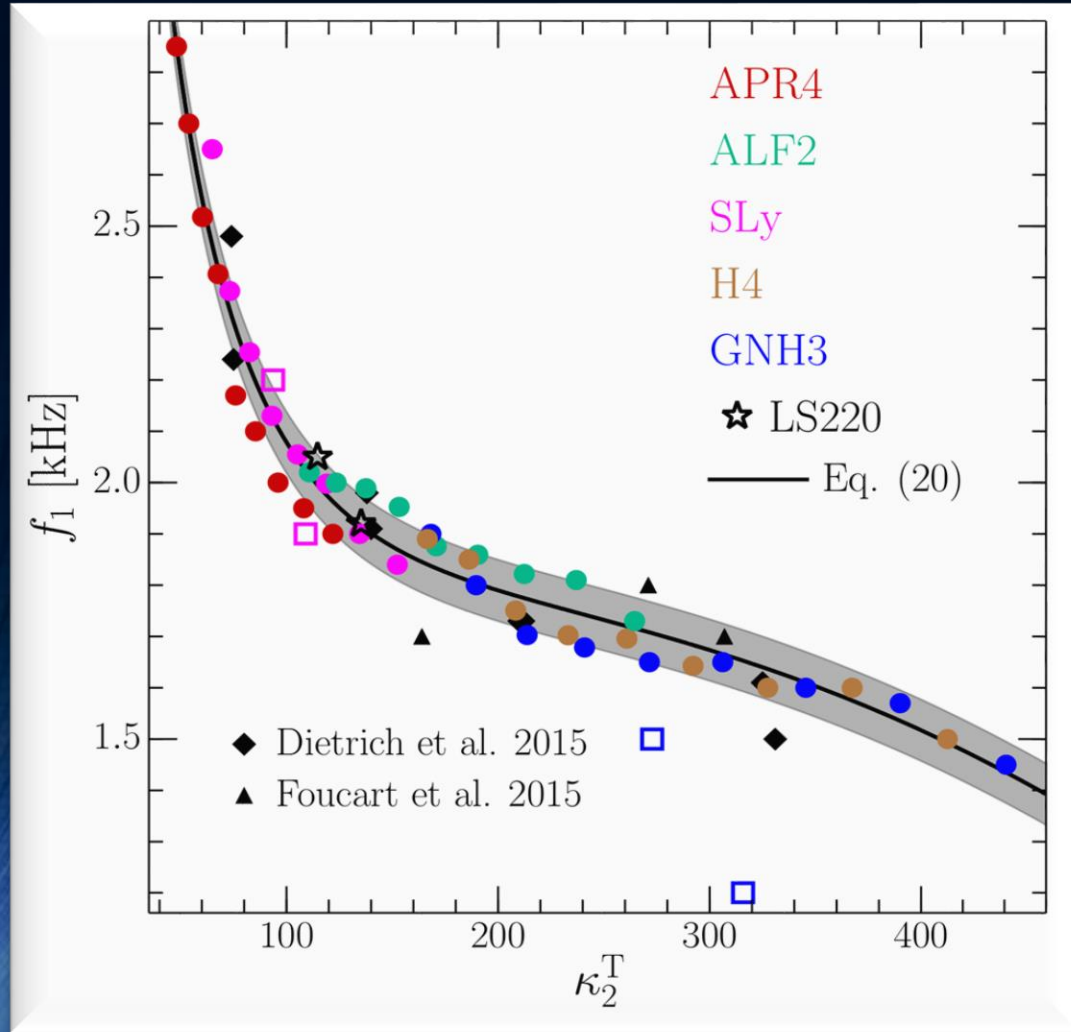
Soft EOS

Evolution of the frequency spectrum of the emitted gravitational waves for the stiff GNH3 (left) and soft APR4 (right) EOS.

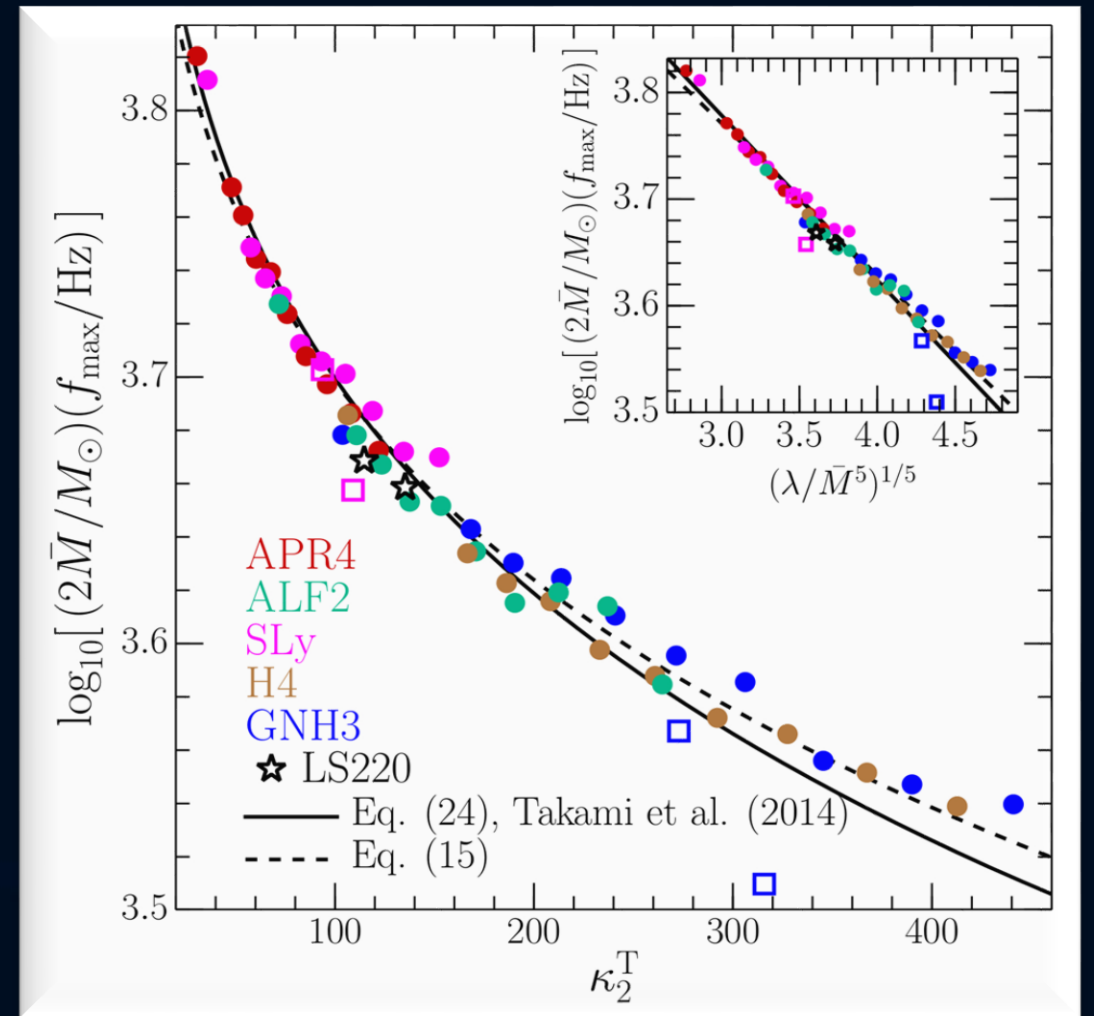
Gravitational Waves and the Maximum of the Rotation Profile



Universal Behavior of f_1 and f_{\max}



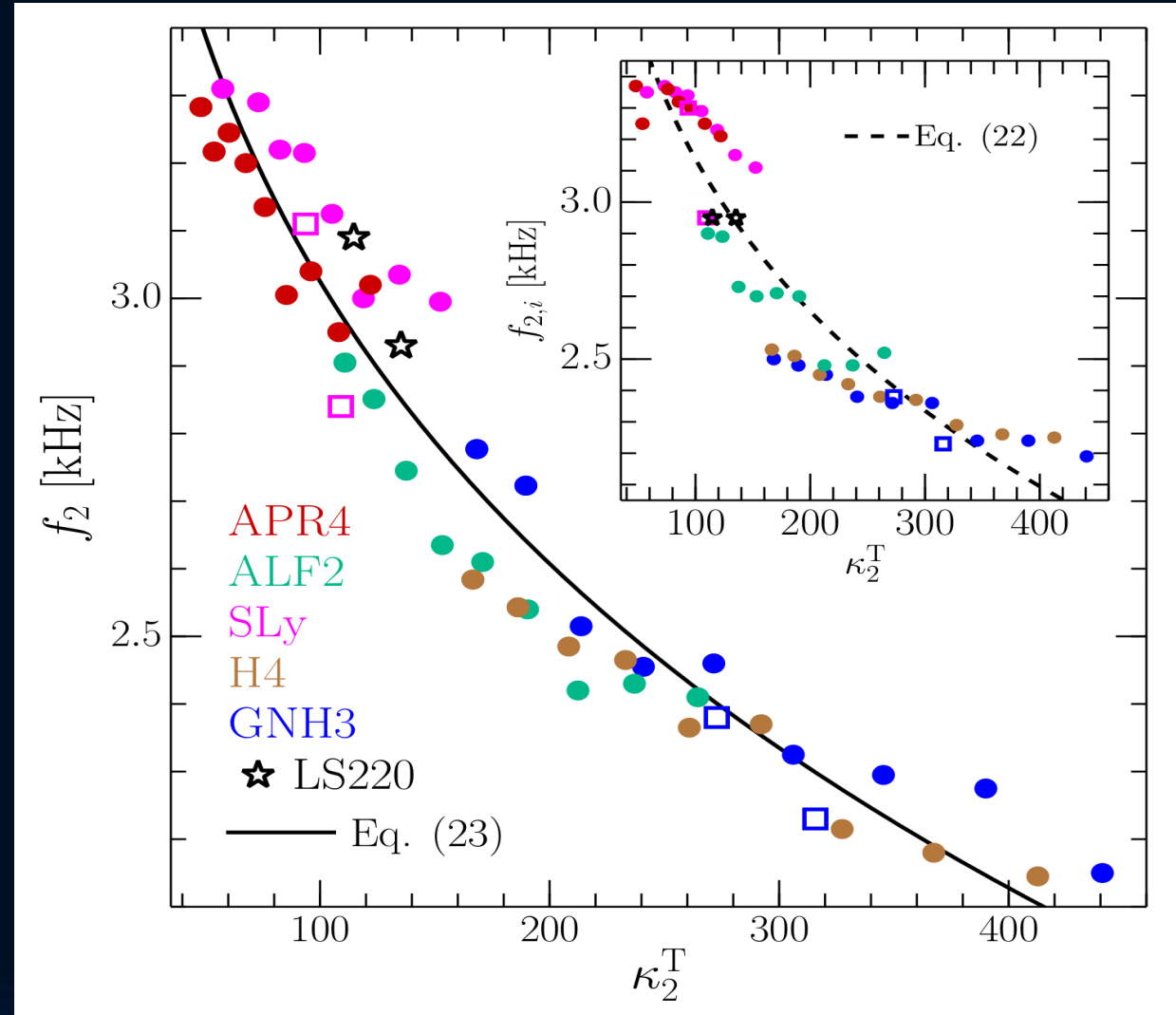
Values of the low-frequency peaks f_1 shown as a function of the tidal deformability parameter κ_2^T .



Mass-weighted frequencies at amplitude maximum f_{\max} shown as a function of the tidal deformability parameter κ_2^T .

Universal behavior of the f_2 -peak

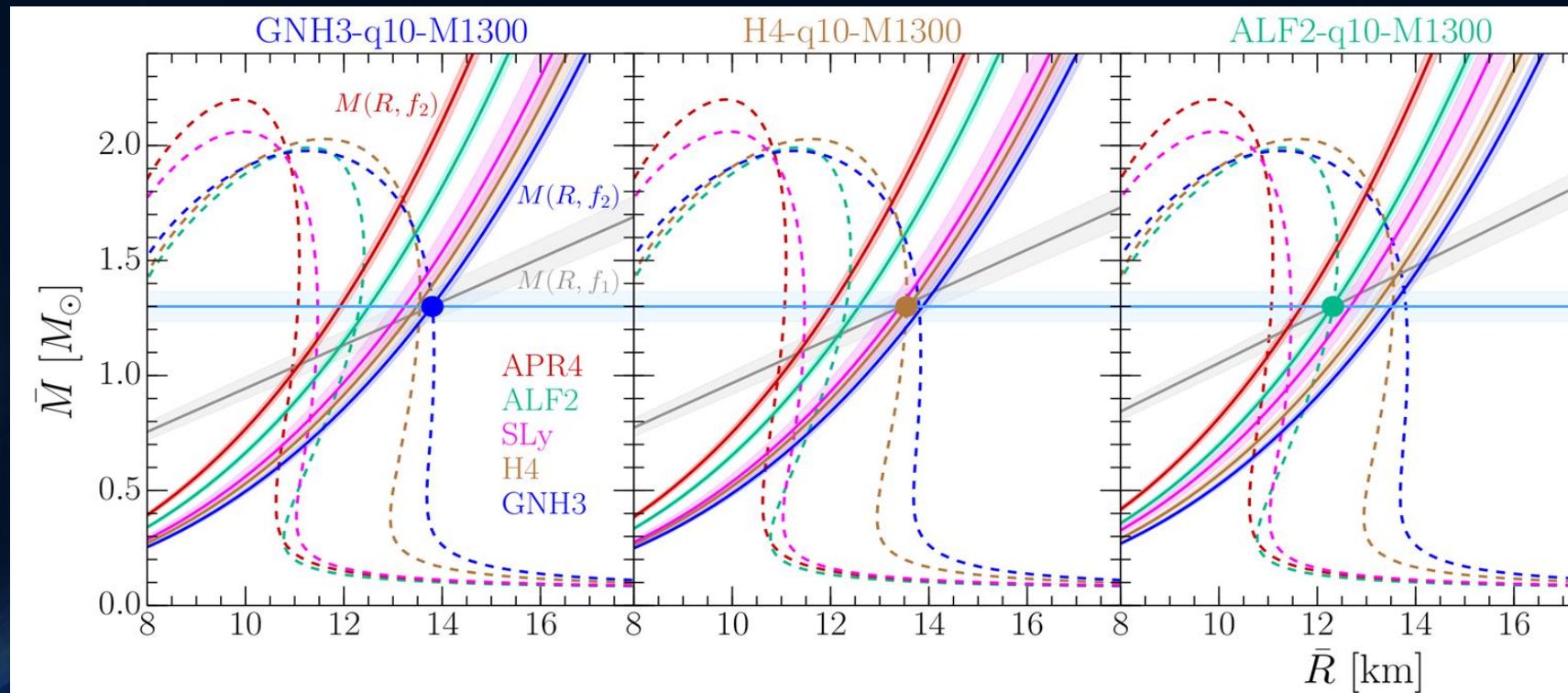
Values of the high-frequency peaks f_2
Shown as a function of the
tidal deformability
parameter κ_2^T .



Gravitational Waves → Equation of State

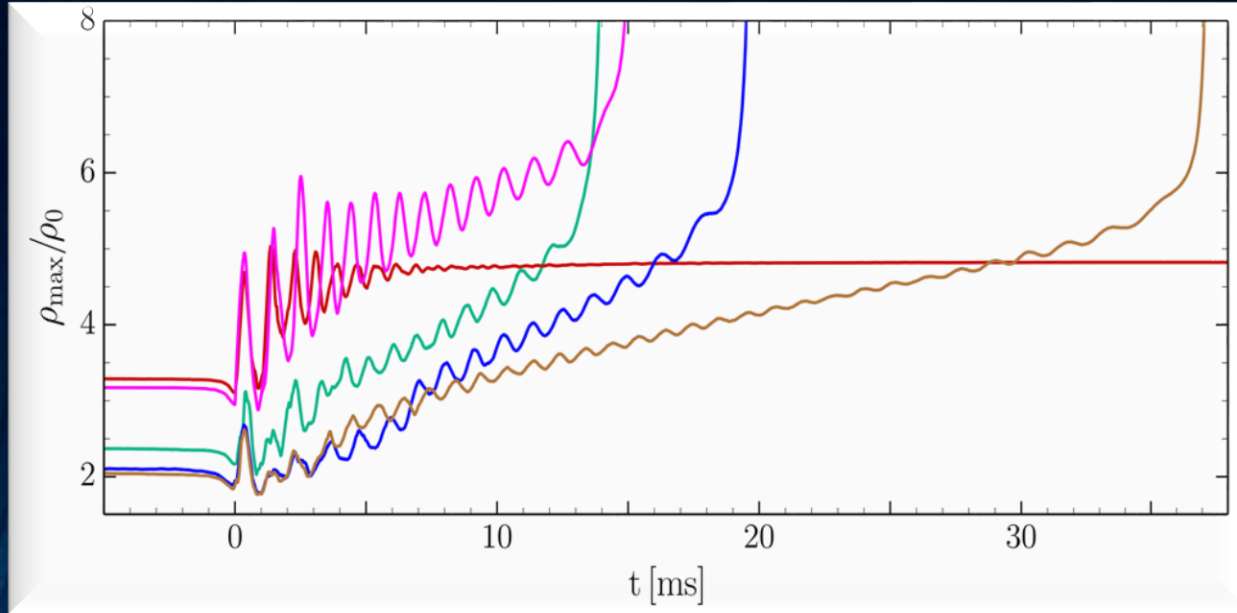
The detection of GWs from merging neutron star binaries can be used to determine the high density regime of the EOS.

With the knowledge of f_1 , f_2 and the total mass the system, the GW signal can set tight constraints on the EOS.



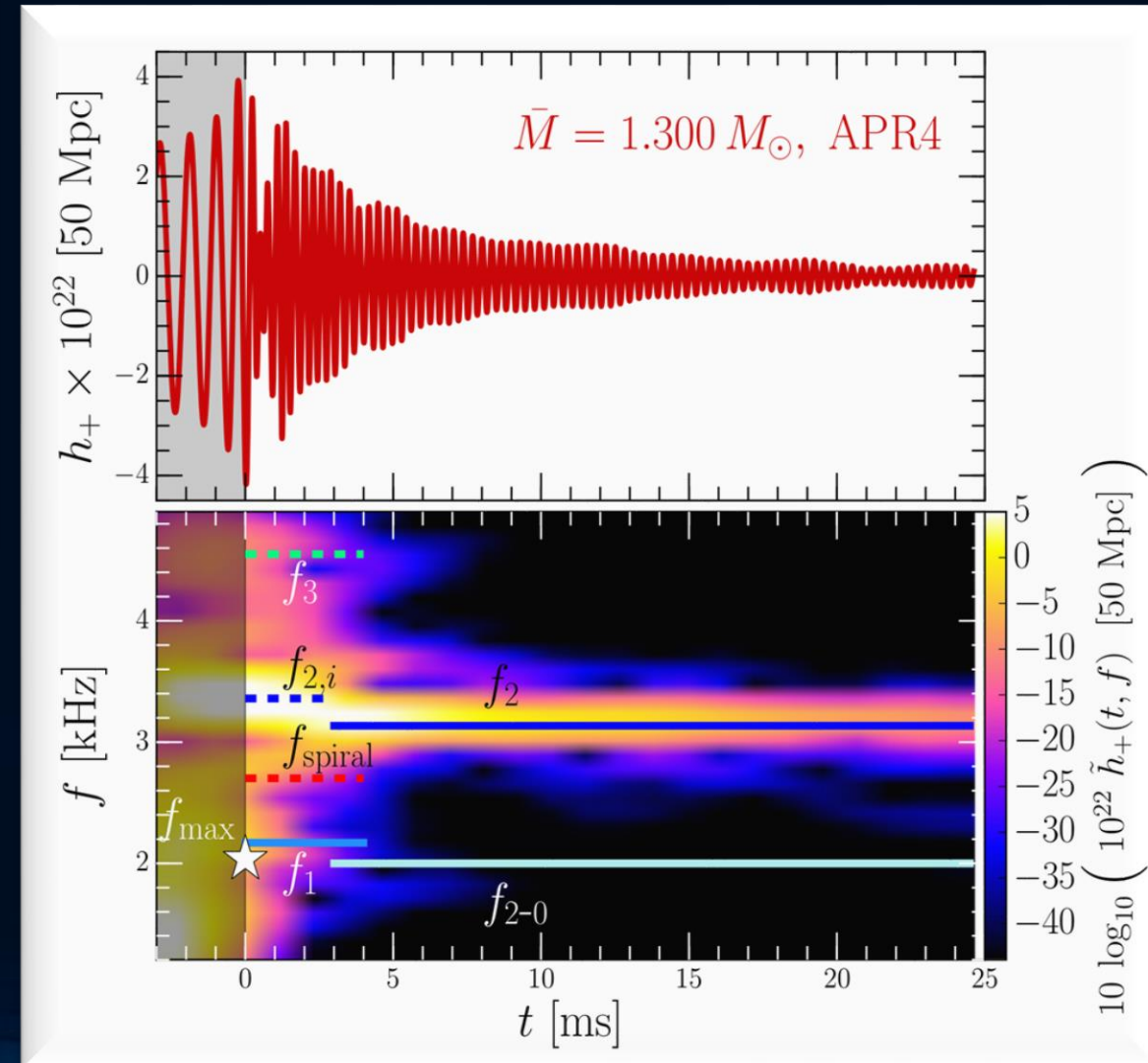
How to observe the QGP with gravitational waves from NS mergers?

Outlook



Maximum of the rest mass density ρ_{\max} in units of ρ_0 versus time for the high mass simulations.

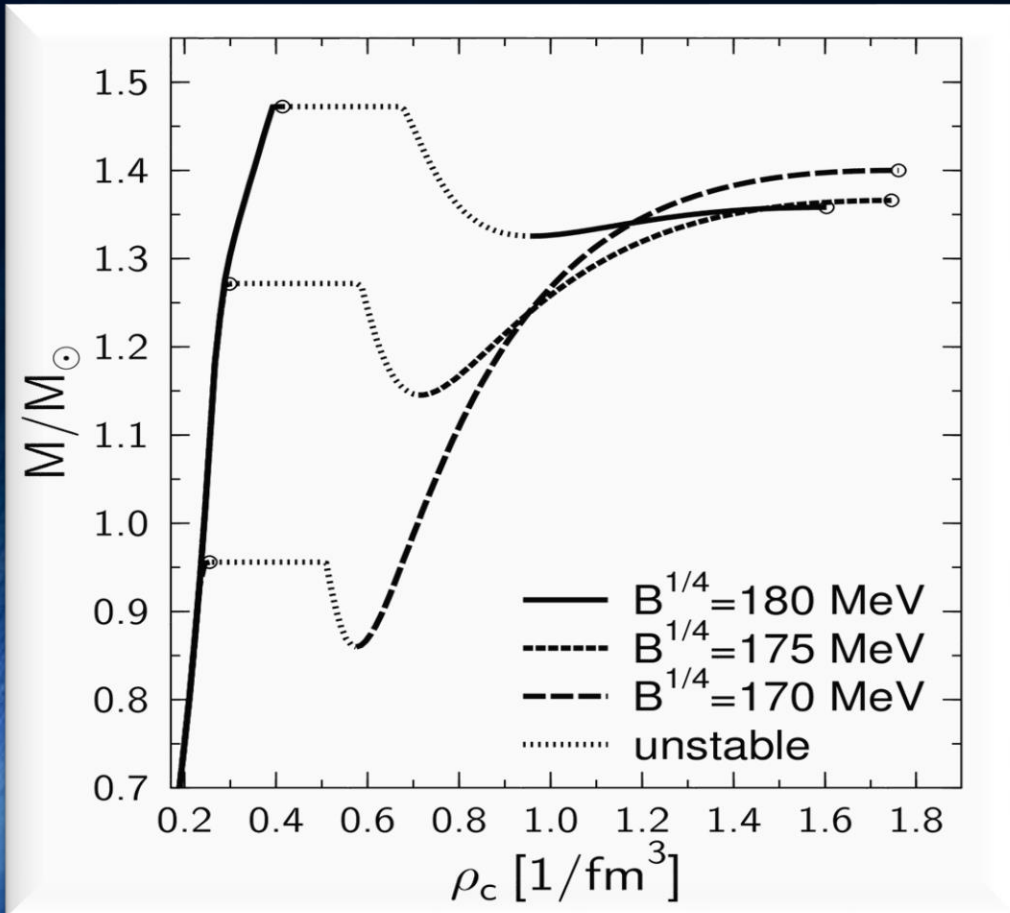
The power spectral density profile of the post-merger emission is characterized by several distinct frequencies f_{\max} , f_1 , f_2 , \dots , $f_{2\text{-PT}}$



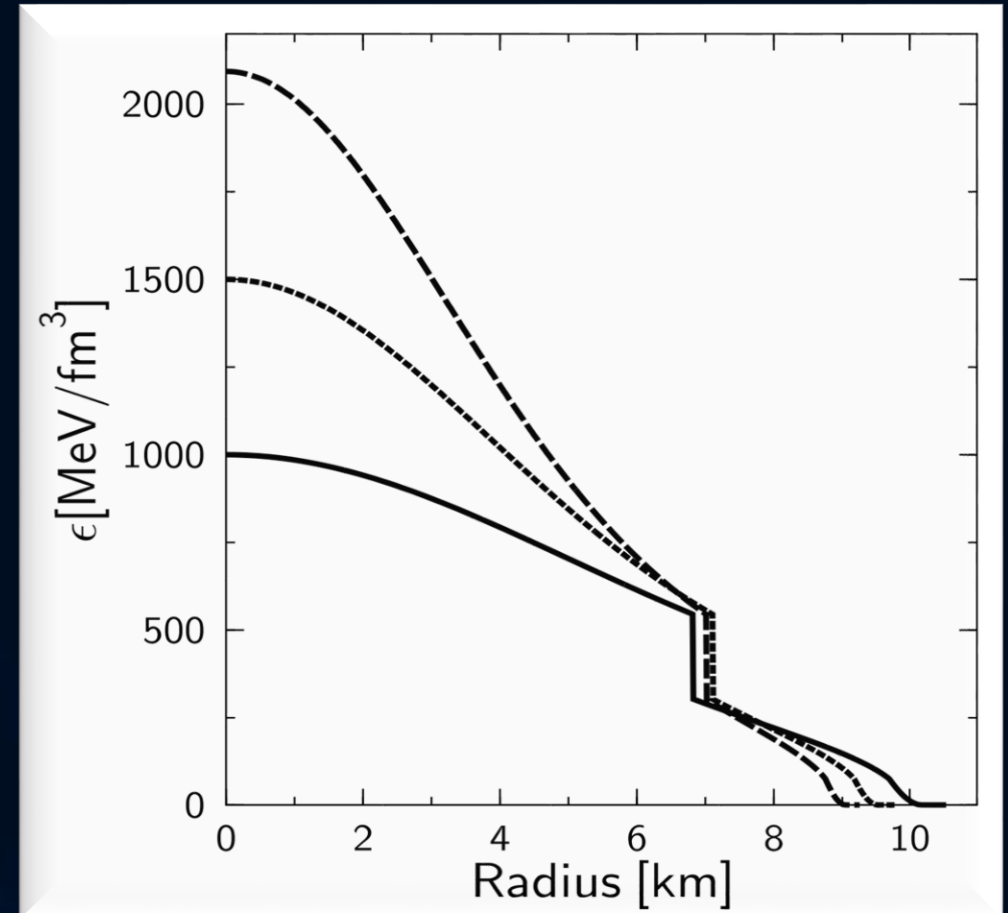
Hybrid Star Properties

In contrast to the Gibbs construction, the star's density profile within the Maxwell construction (see right figure) will have a huge density jump at the phase transition boundary. Twin star properties can be found more easily when using a Maxwell construction.

Mass-Density relation

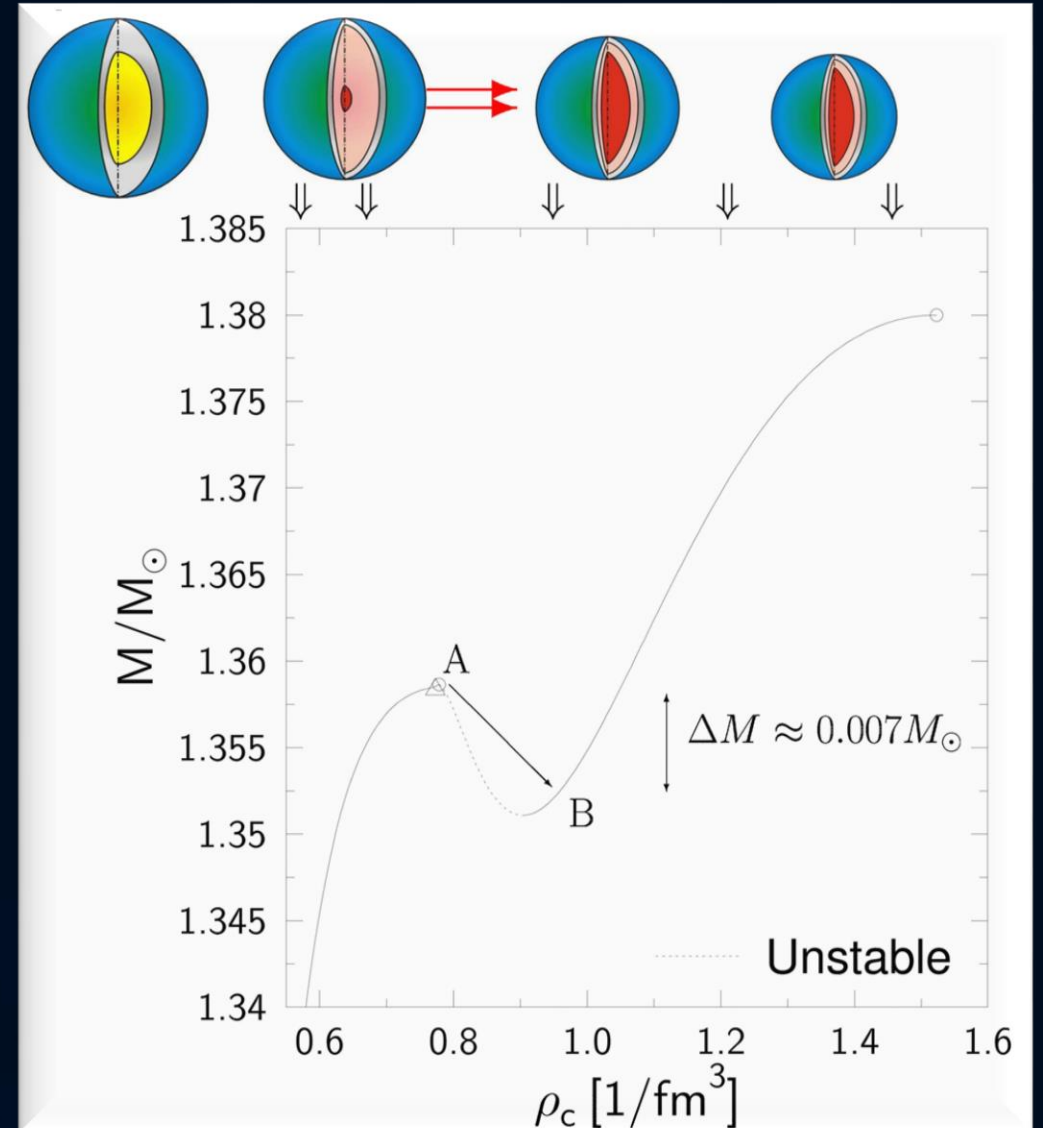
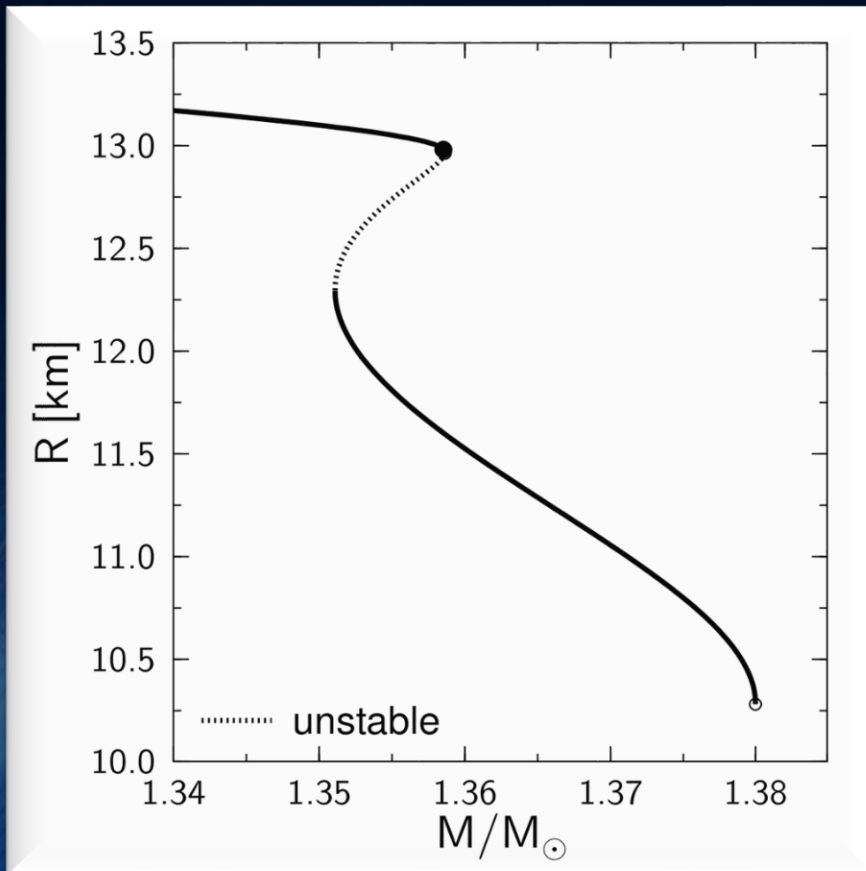


Energy-density profiles



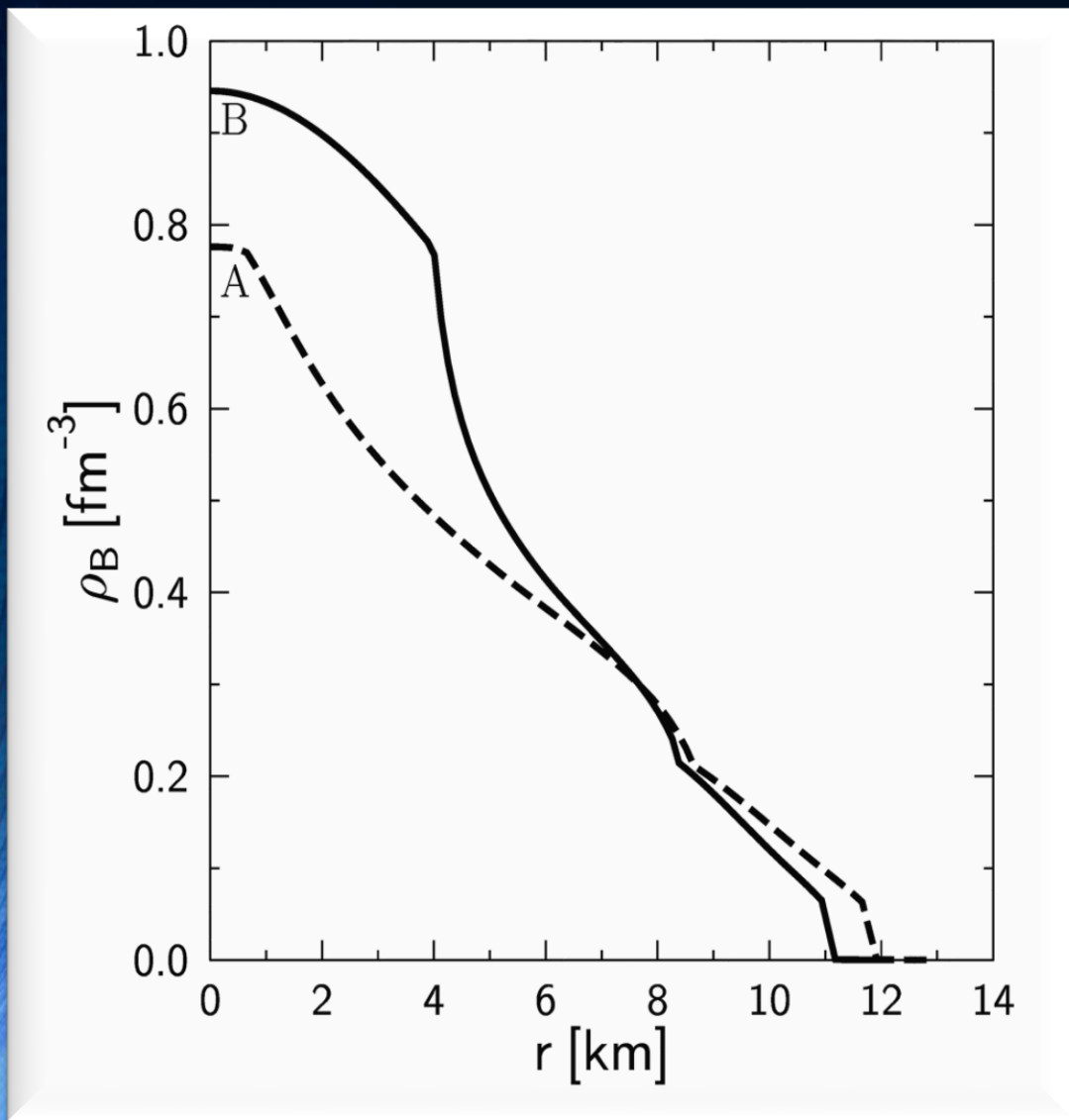
Twin Stars

Usually it is assumed that this loss of stability leads to the collapse into a black hole. However, realistic calculations open another possibility: the collapse into the twin star on the second sequence.

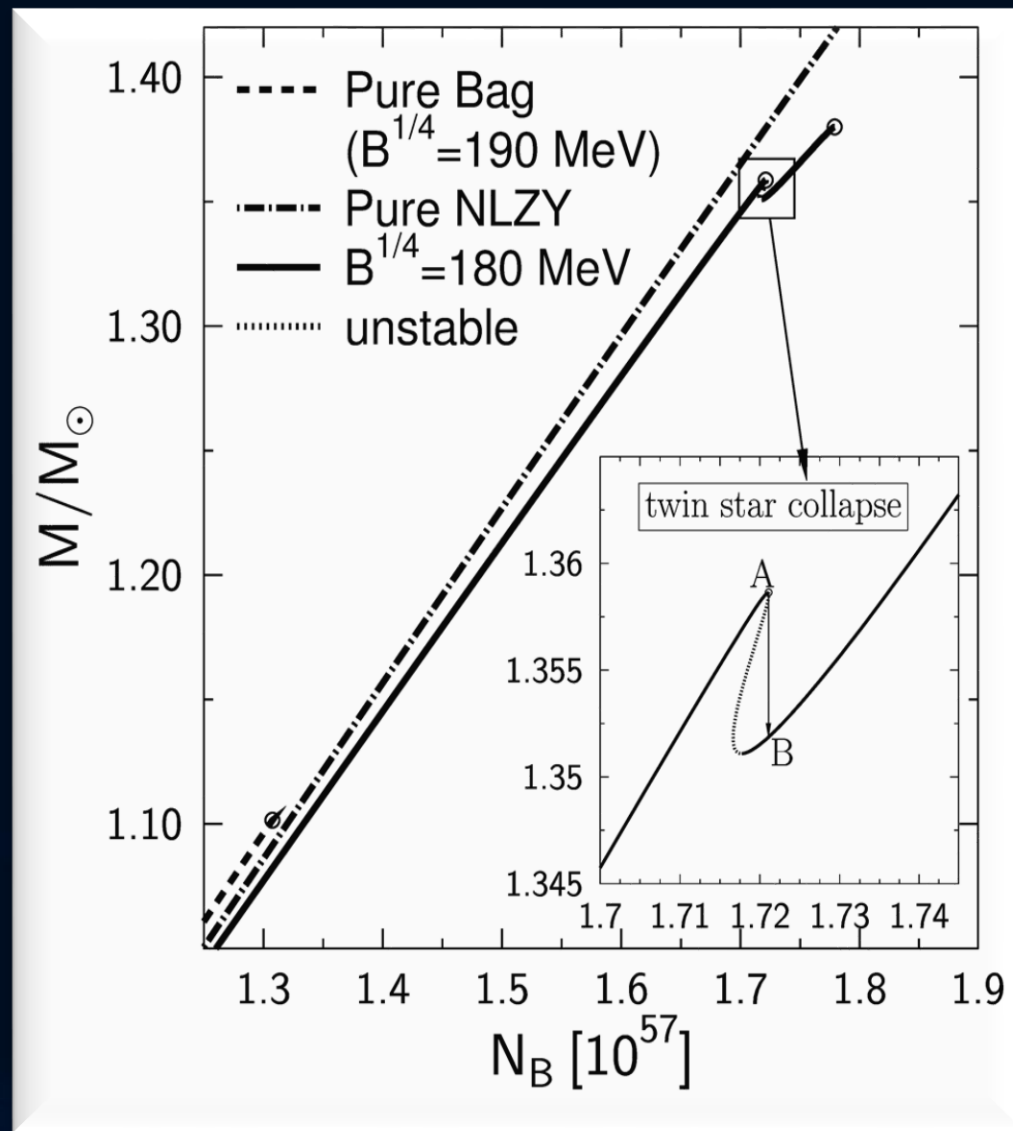


The Twin Star Collapse

Density profiles of the two twins



Conservation of total baryonic mass

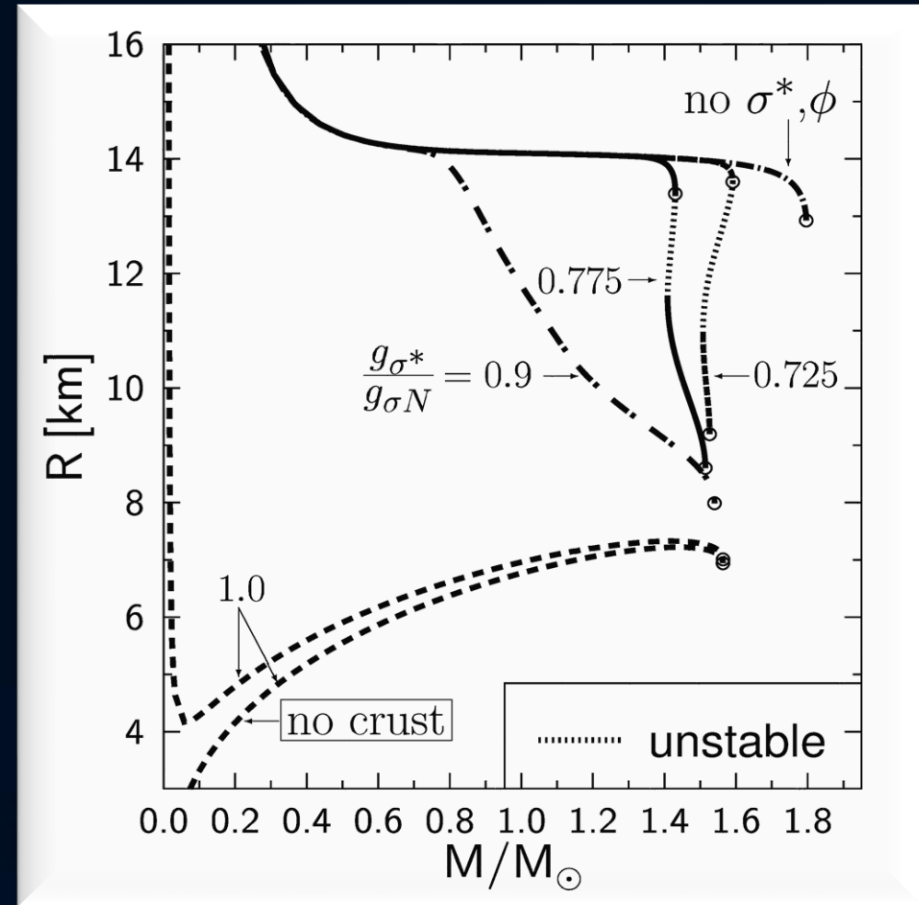
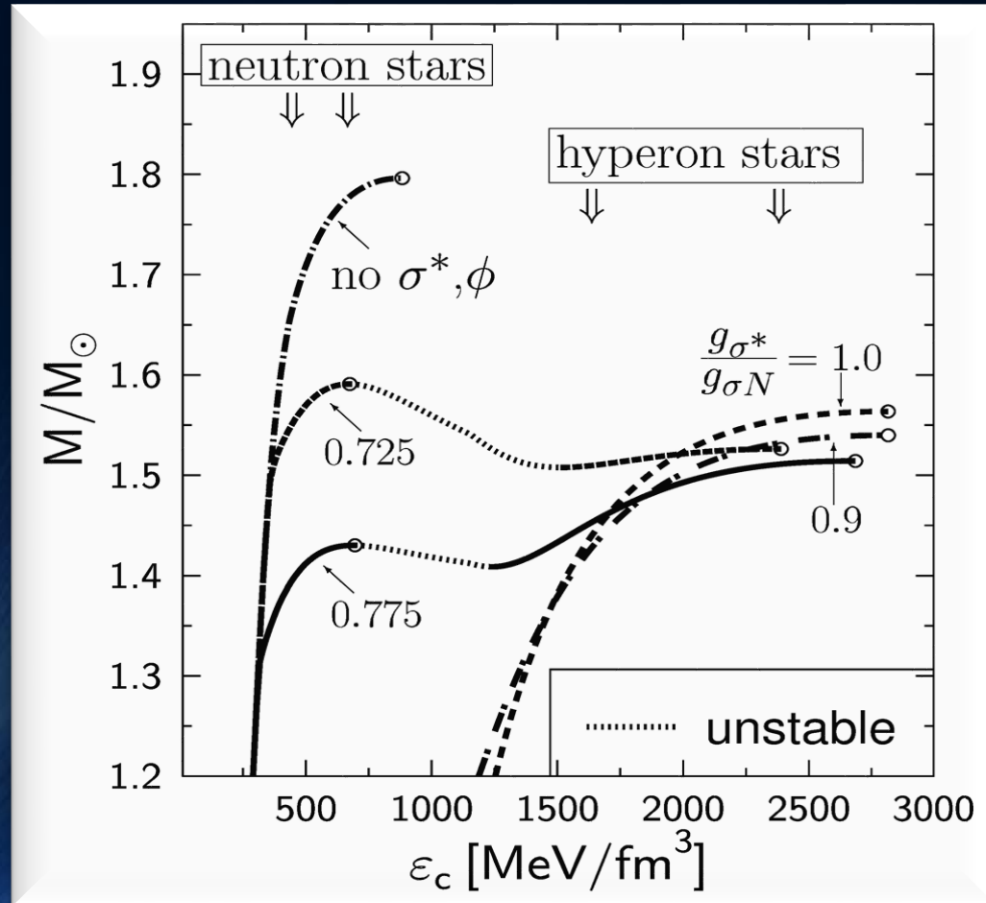


I.N. Mishustin, M. Hanauske, A. Bhattacharyya, L.M. Satarov, H. Stöcker, and W. Greiner,

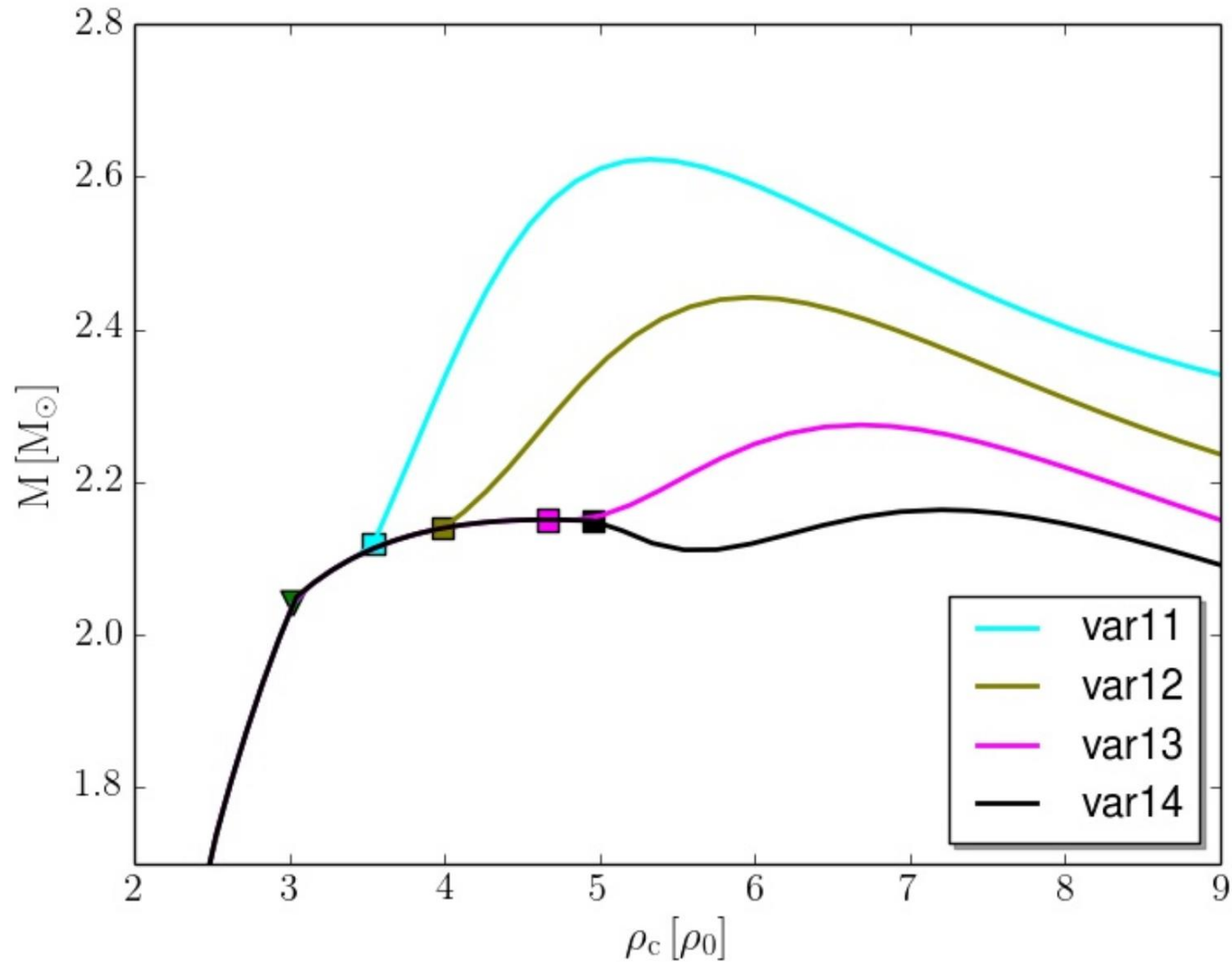
“Catastrophic rearrangement of a compact star due to quark core formation”, Physics Letters B 552 (2003) p.1-8

Exotic Stars

But, unfortunately, twin stars can not be created solely by a Hadron-Quark phase transition. Extremely bound hyperon matter, or kaon condensation could also form a twin star behaviour.

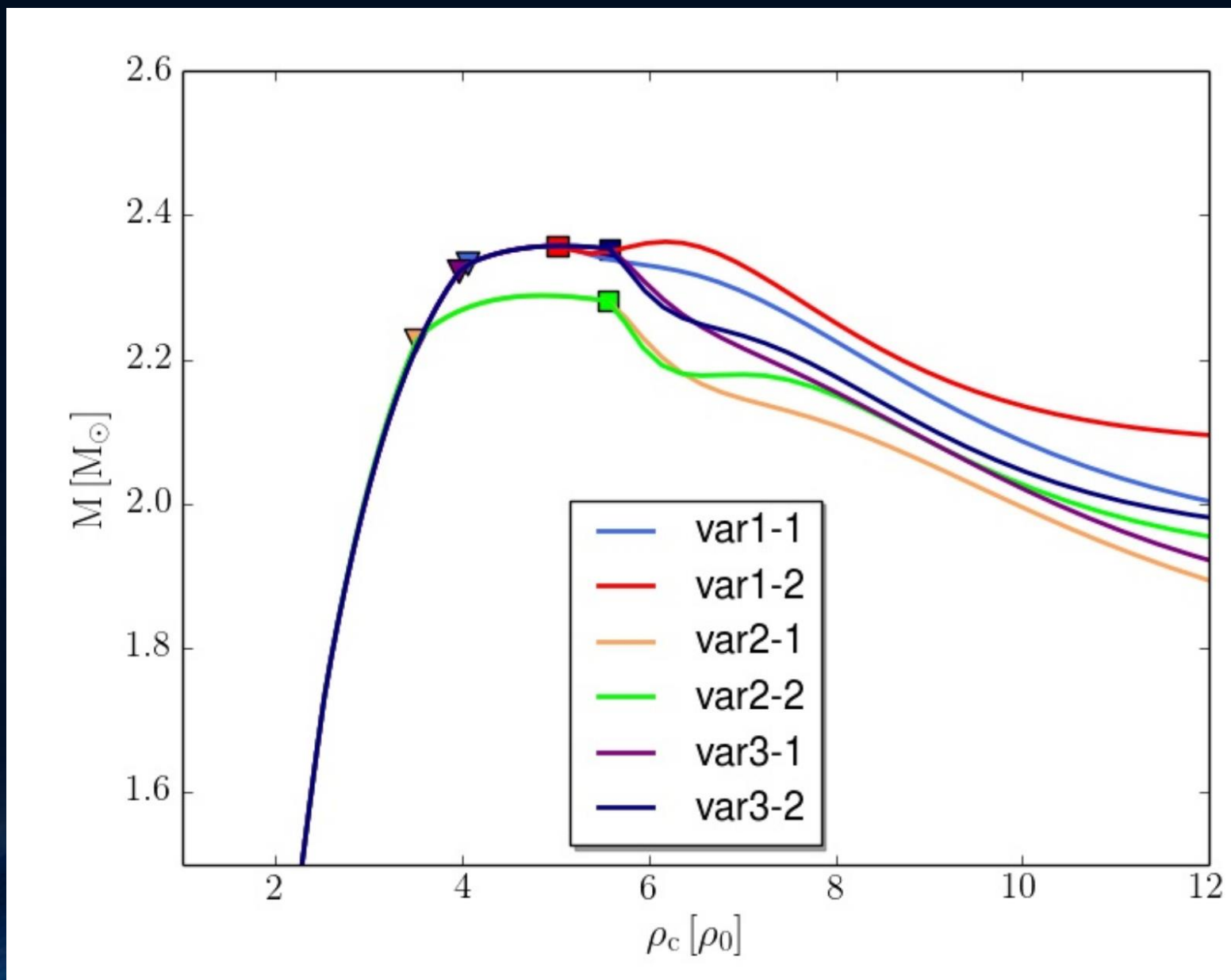


Possibility of Twin Stars in Hybrid Star Models

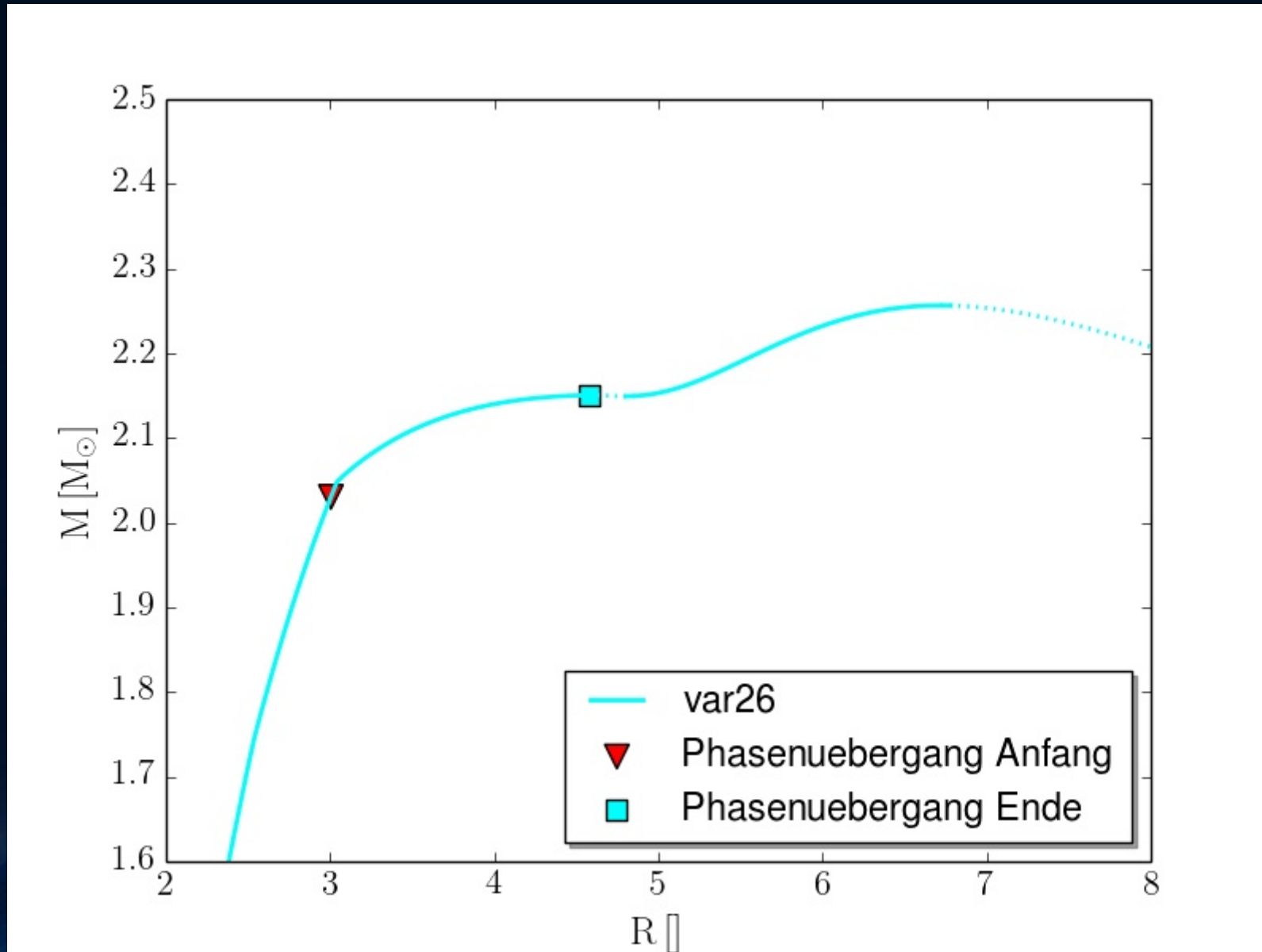


Master Thesis:
“From Neutron Stars to
Hybrid Stars”
by Ms Zekiye Simay Yilmaz

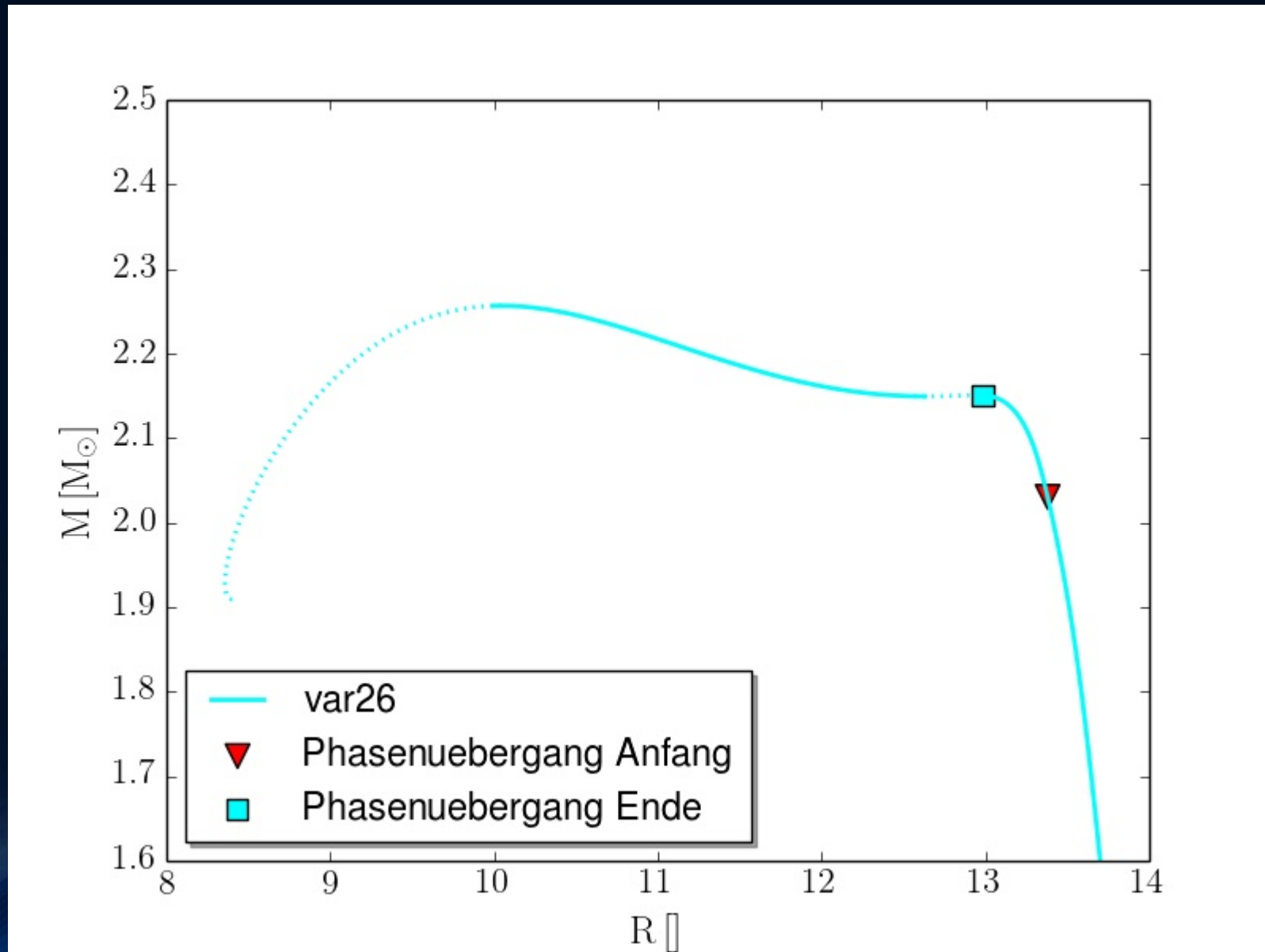
Possibility of Twin Stars in Hybrid Star Models



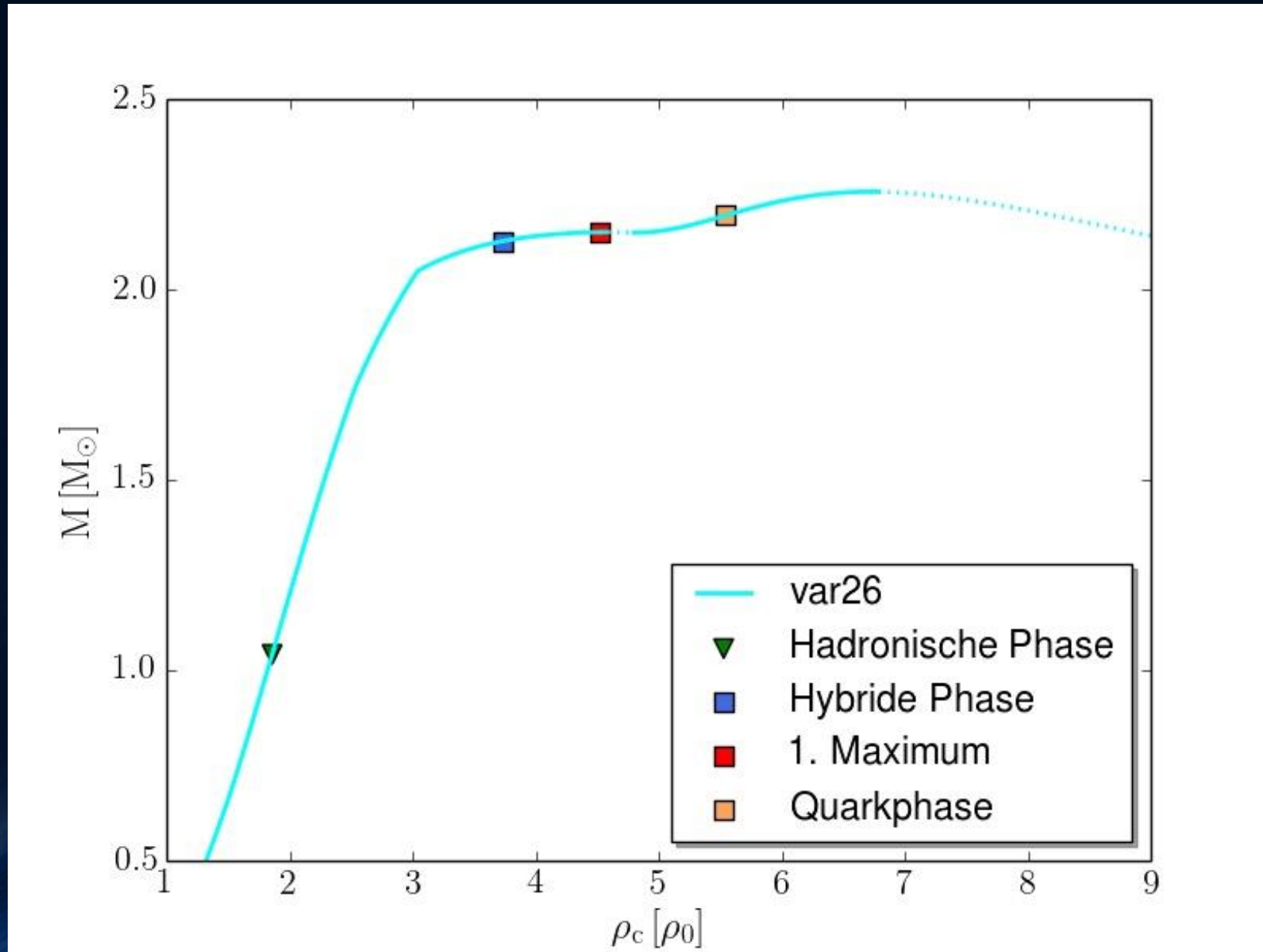
Twin Stars within a Hybrid Model (Gibbs Construction)



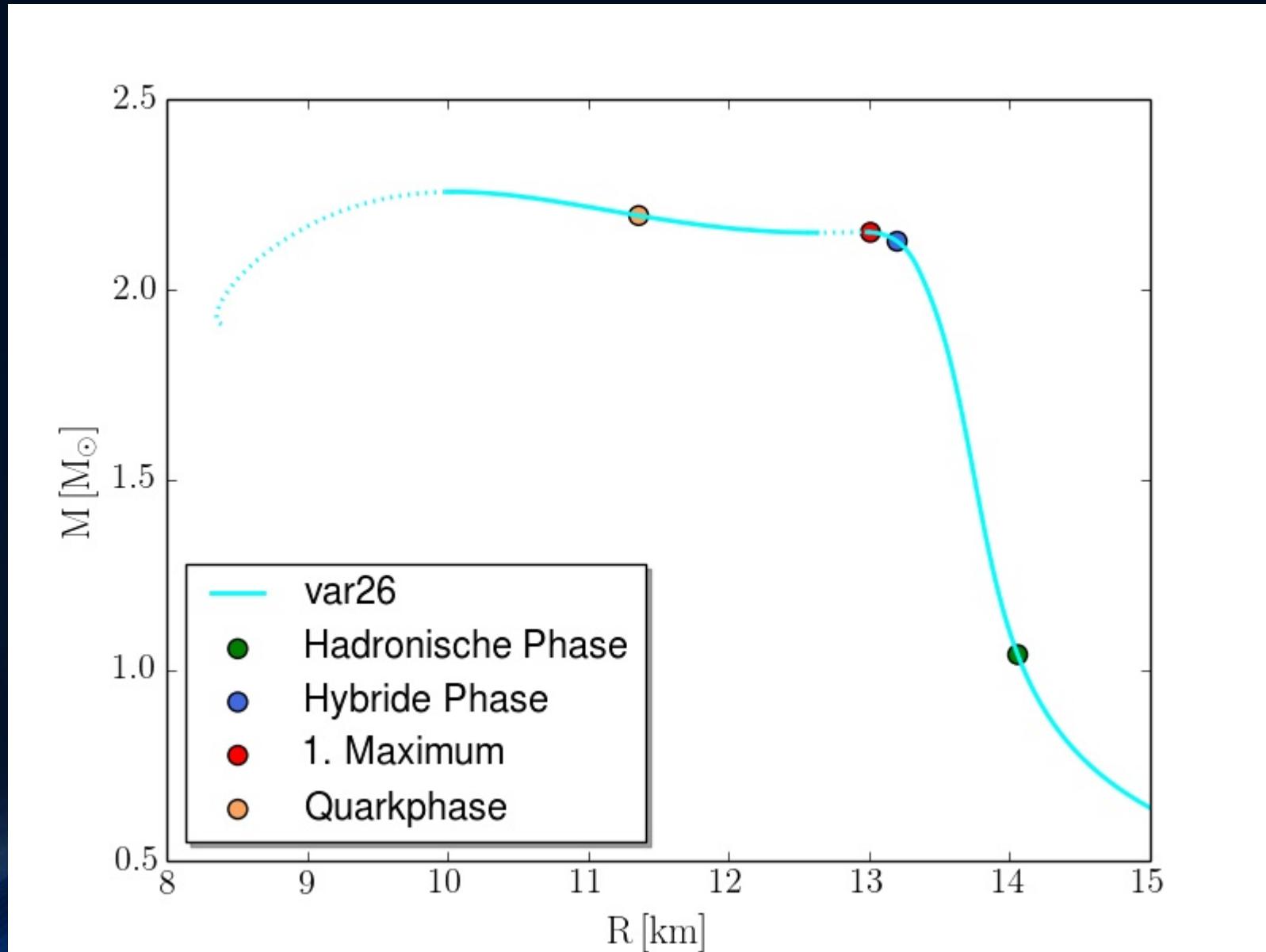
Twin Stars within a Hybrid Model (Gibbs Construction)



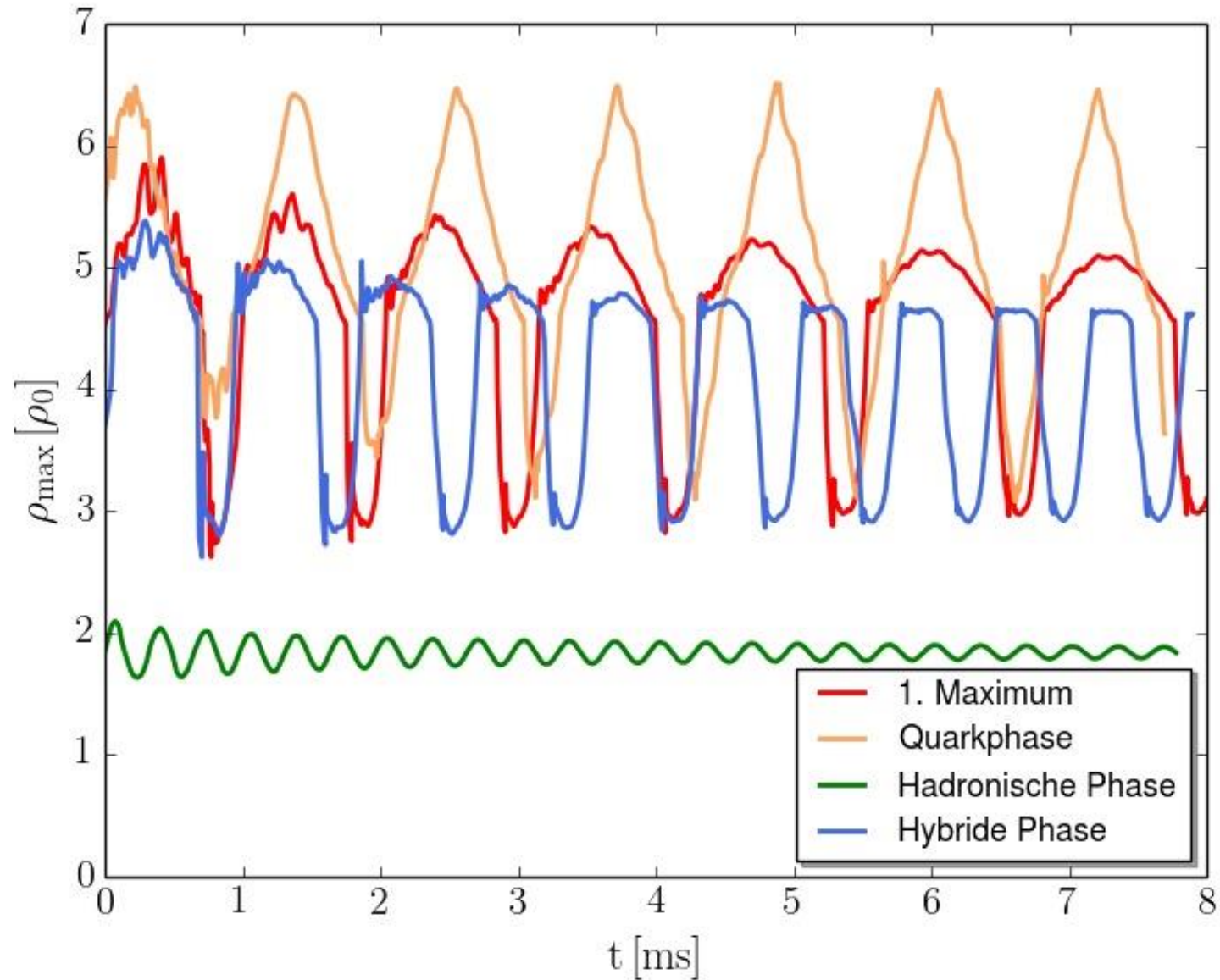
Initial Configuration of the Neutron and Hybrid Stars



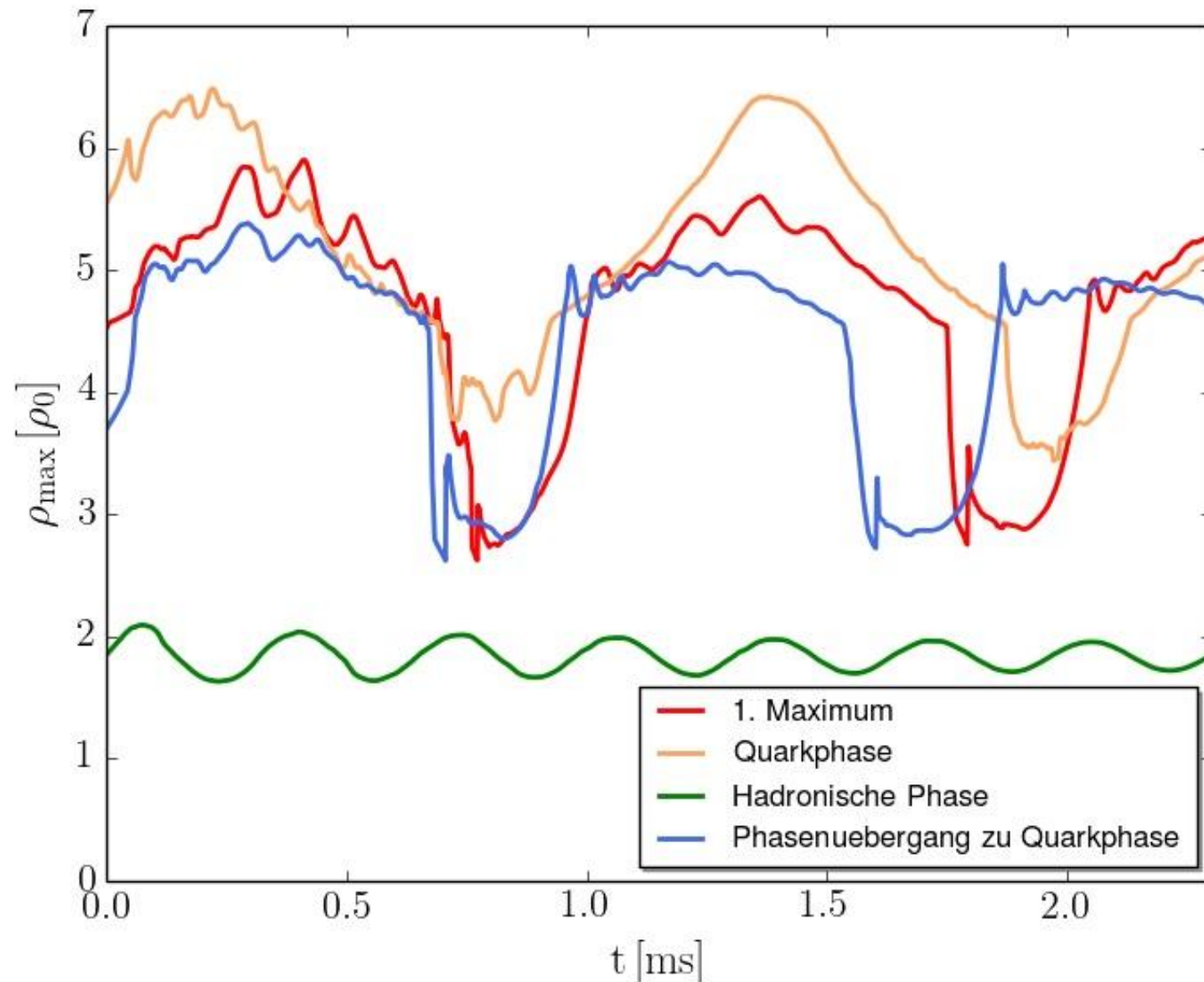
Initial Configuration of the Neutron and Hybrid Stars



The Twin Star Collapse



The Twin Star Collapse



Master Thesis:
“From Neutron Stars
to Hybrid Stars”
by Ms Zekiye Simay
Yilmaz

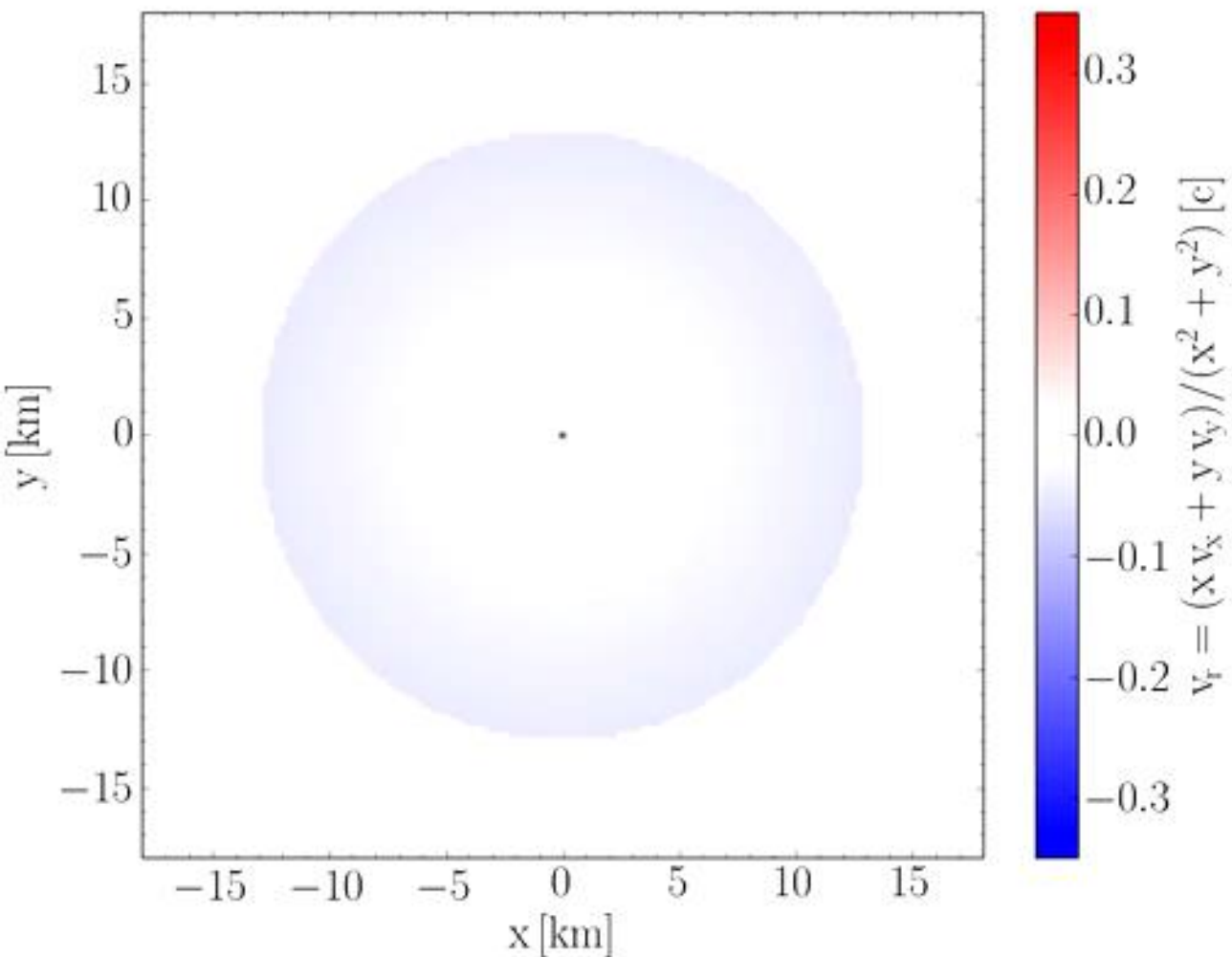
The Twin Star Collapse (red)

Green contour line: Nuclear Matter density

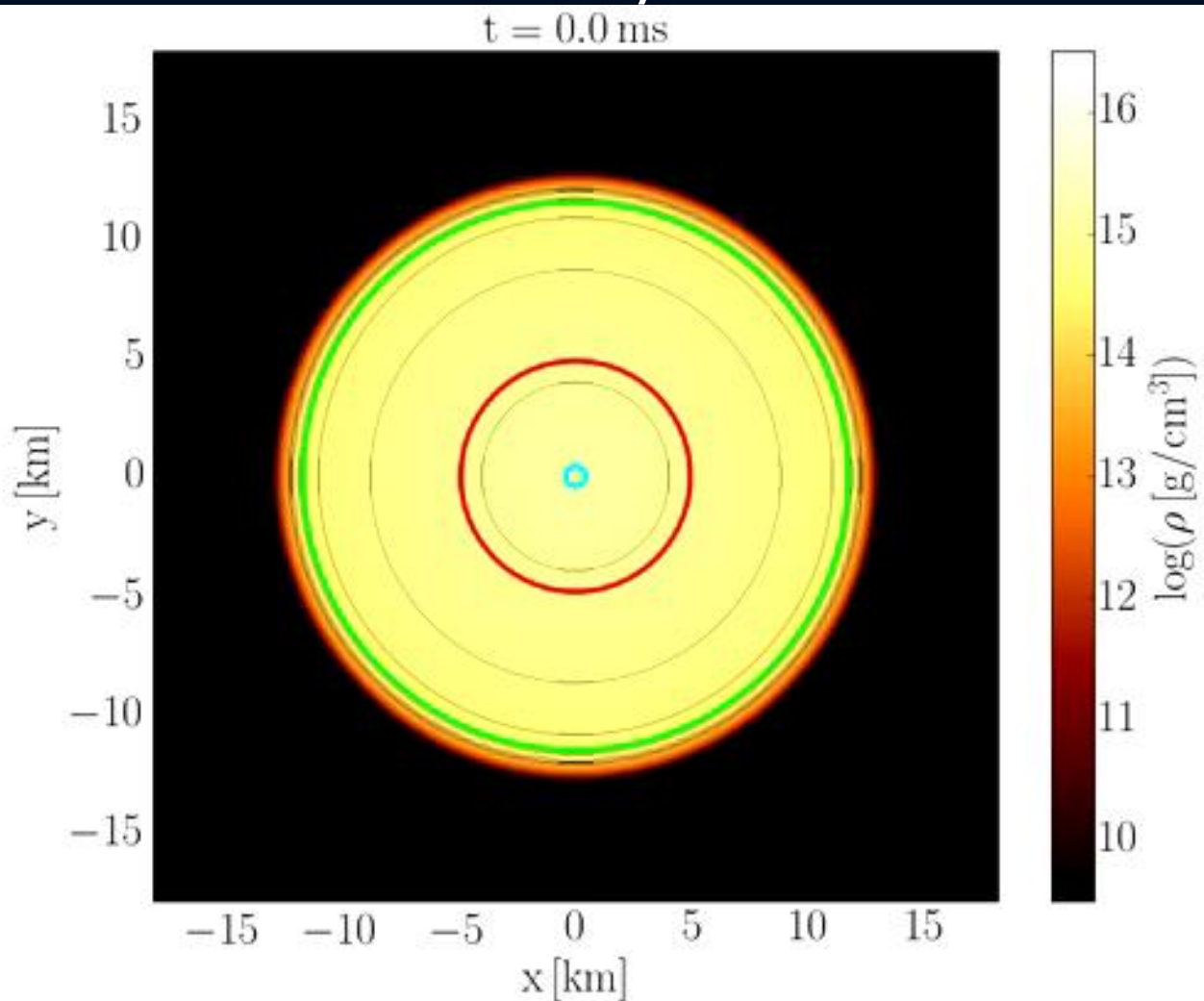
Red contour line: Beginning of PT

Cyan contour line: End of PT

Radial velocity



Density

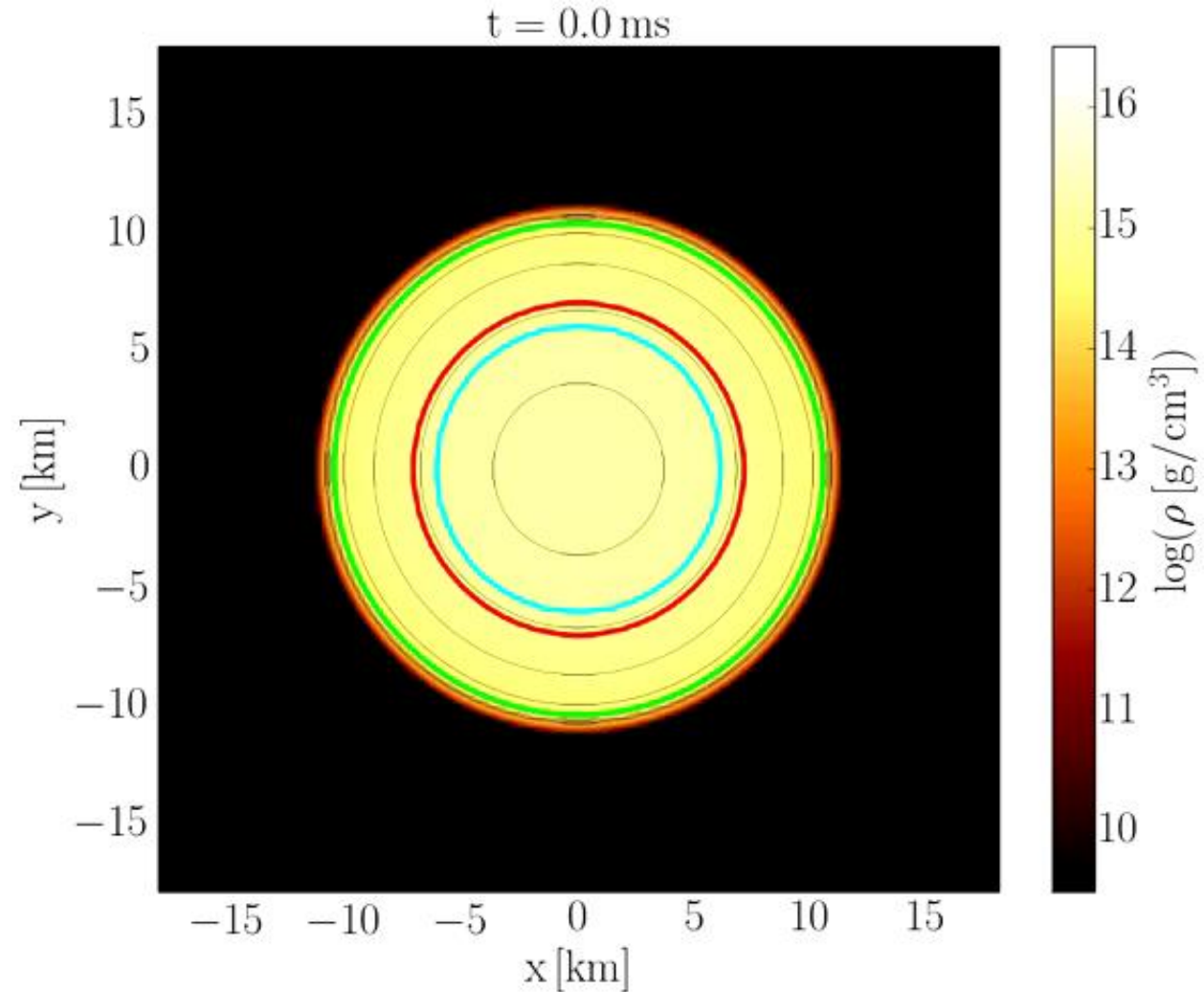
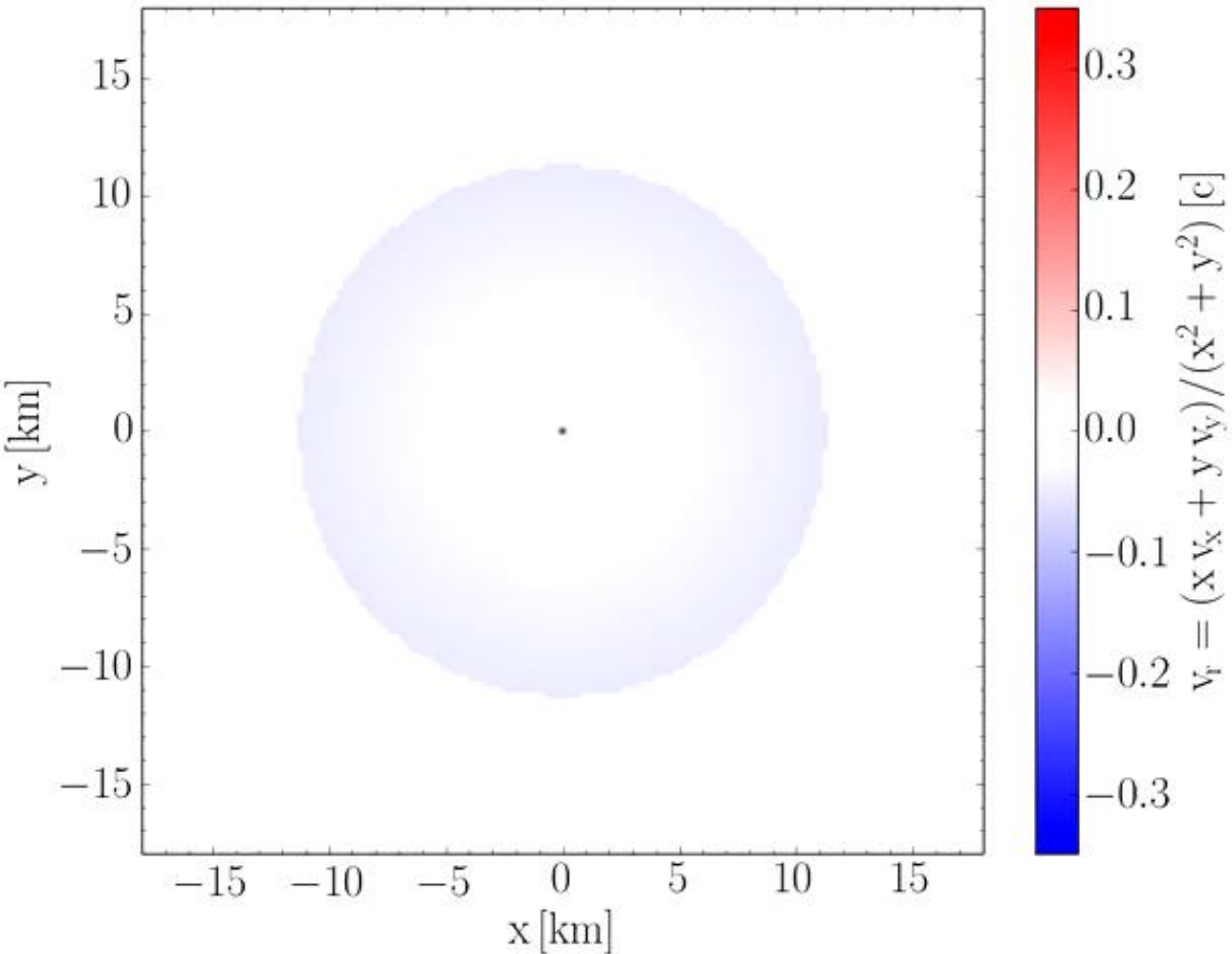


The Twin Star Collapse (brown)

Radial velocity

Green contour line: Nuclear Matter density
Red contour line: Beginning of PT
Cyan contour line: End of PT

Density



Pure Quark Stars including a Chiral Phase Transition

Twin Stars within the SU(3) Chiral Quark-Meson Model

Andreas Zacchi,^{1,*} Laura Tolos,^{2,3,†} and Jürgen Schaffner-Bielich^{1,‡}

¹*Institut für Theoretische Physik, Goethe Universität Frankfurt,
Max von Laue Strasse 1, D-60438 Frankfurt, Germany*

²*Institut de Ciències de l'Espai (IEEC/CSIC), Campus Universitat Autònoma de Barcelona,
Carrer de Can Magrans, s/n, E-08193 Bellaterra, Spain*

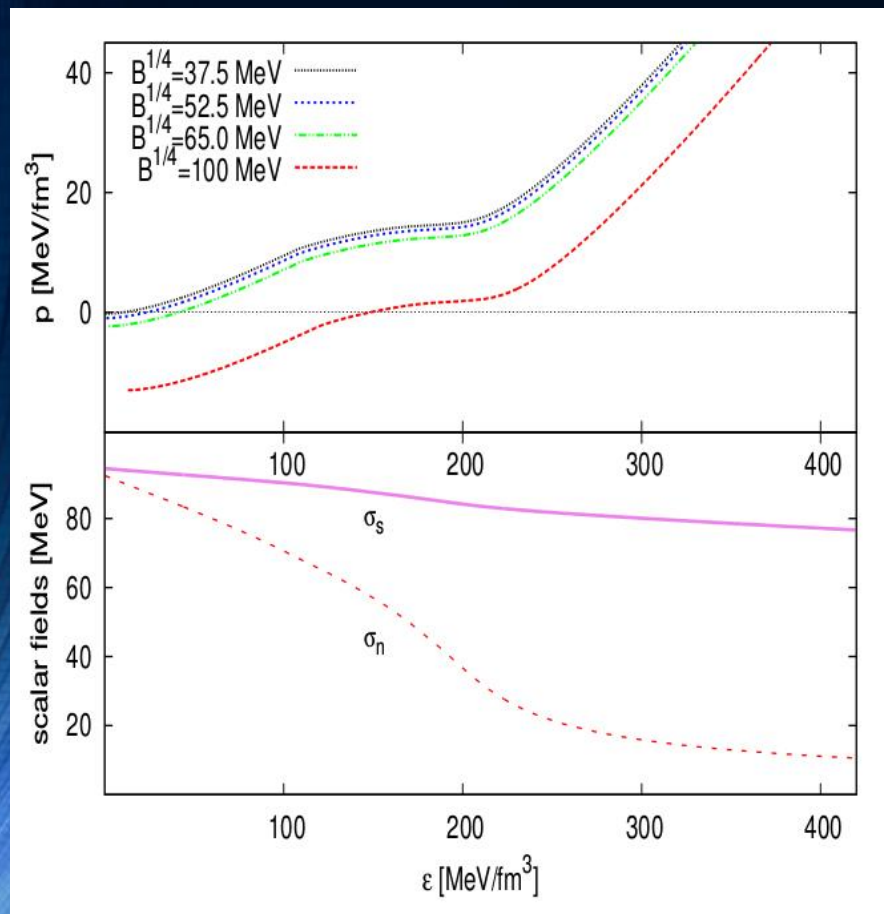
³*Frankfurt Institute for Advanced Studies, Goethe Universität Frankfurt,
Ruth-Moufang-Str. 1, 60438, Frankfurt am Main, Germany*

(Dated: April 27, 2017)

We present new stable solutions of the Tolman Oppenheimer Volkoff equations for quark stars using a quark matter equation of state based on the SU(3) Quark-Meson model that exhibits the onset of the chiral phase transition. These new solutions appear as two stable branches in the mass-radius relation allowing for so called twin stars, i.e. two stable quark star solutions with the same mass, but distinctly different radii. We find solutions which are compatible with causality, the stability conditions of dense matter, the astrophysical constraints of the rotation of the millisecond pulsar PSR J1748-2446ad and the $2M_{\odot}$ pulsar mass constraint.

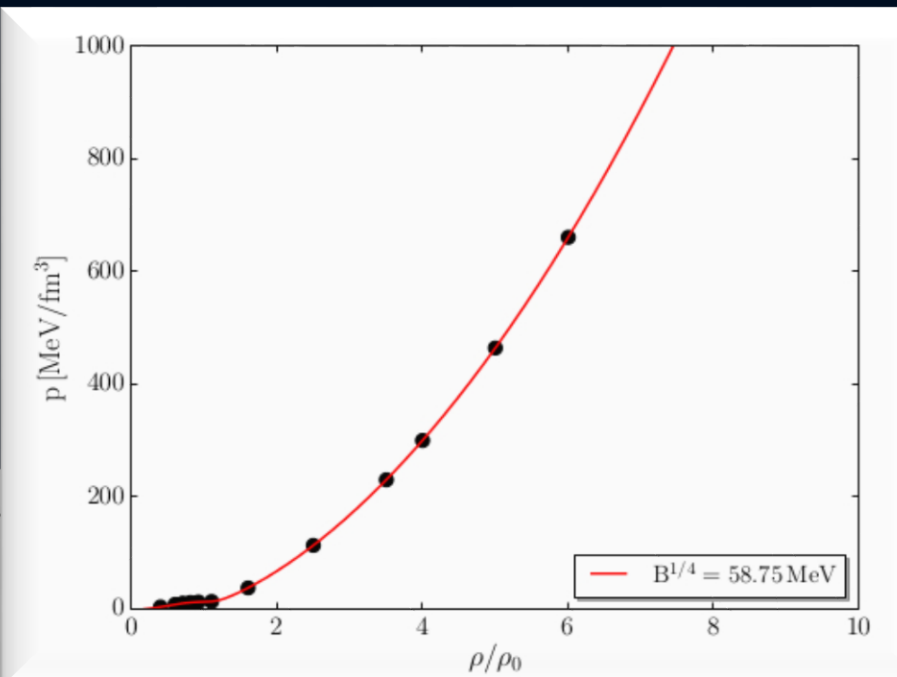
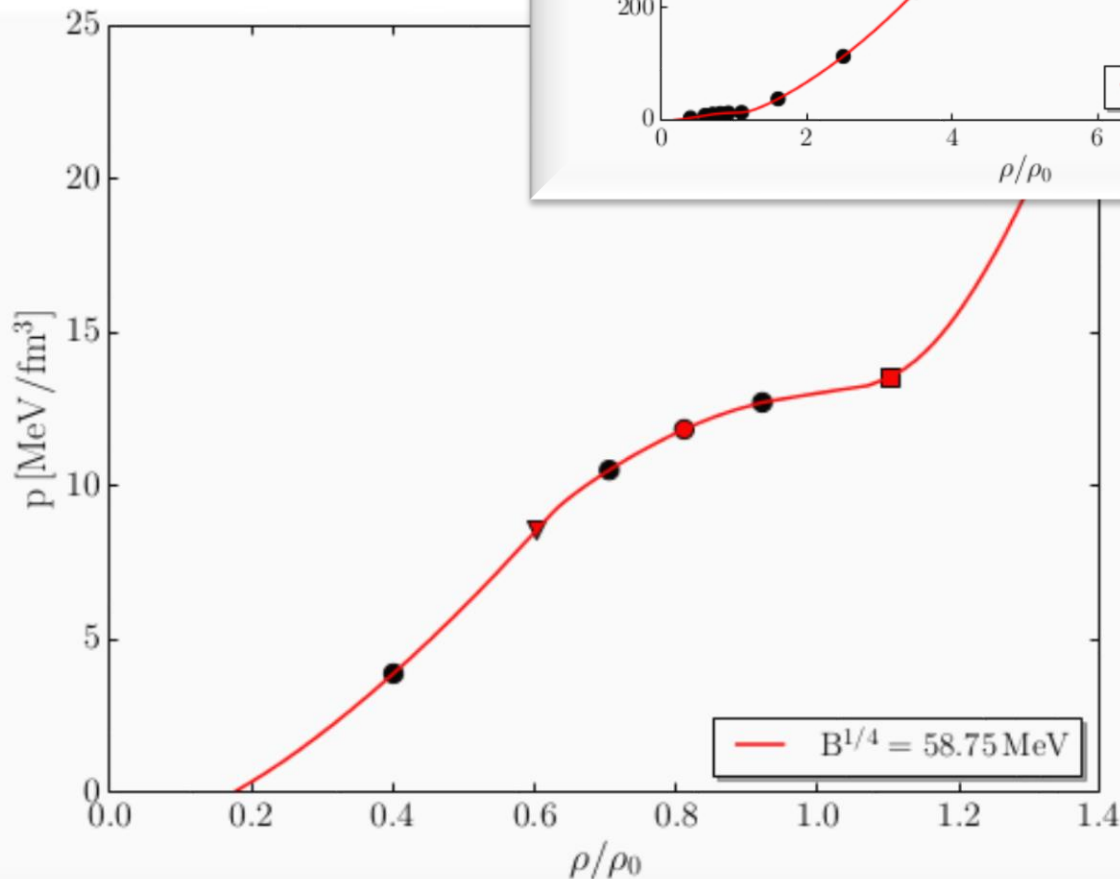
EOS fitted with Piecewise Polytropes

EOSs for different values of the vacuum Pressure (Bag Constant B)

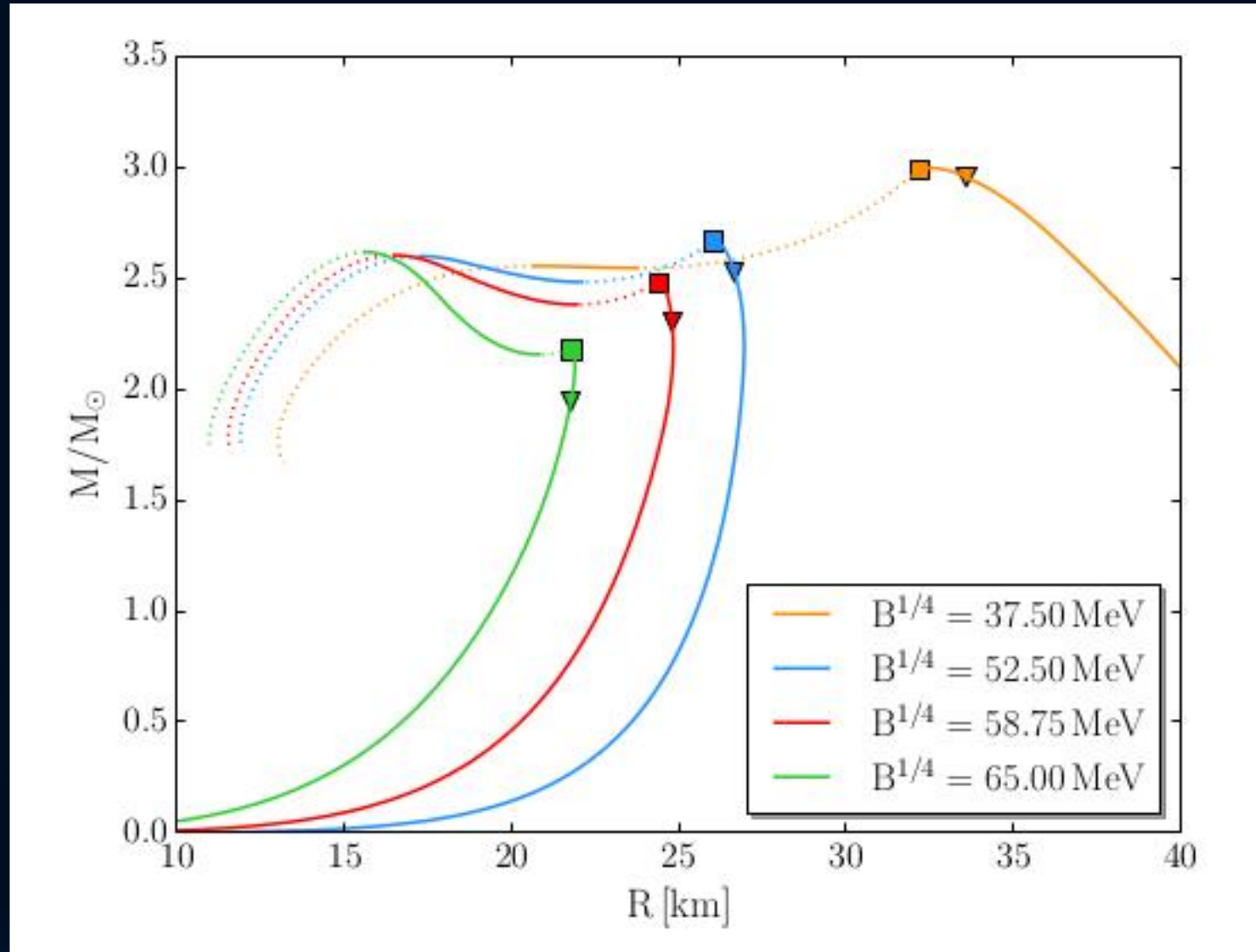
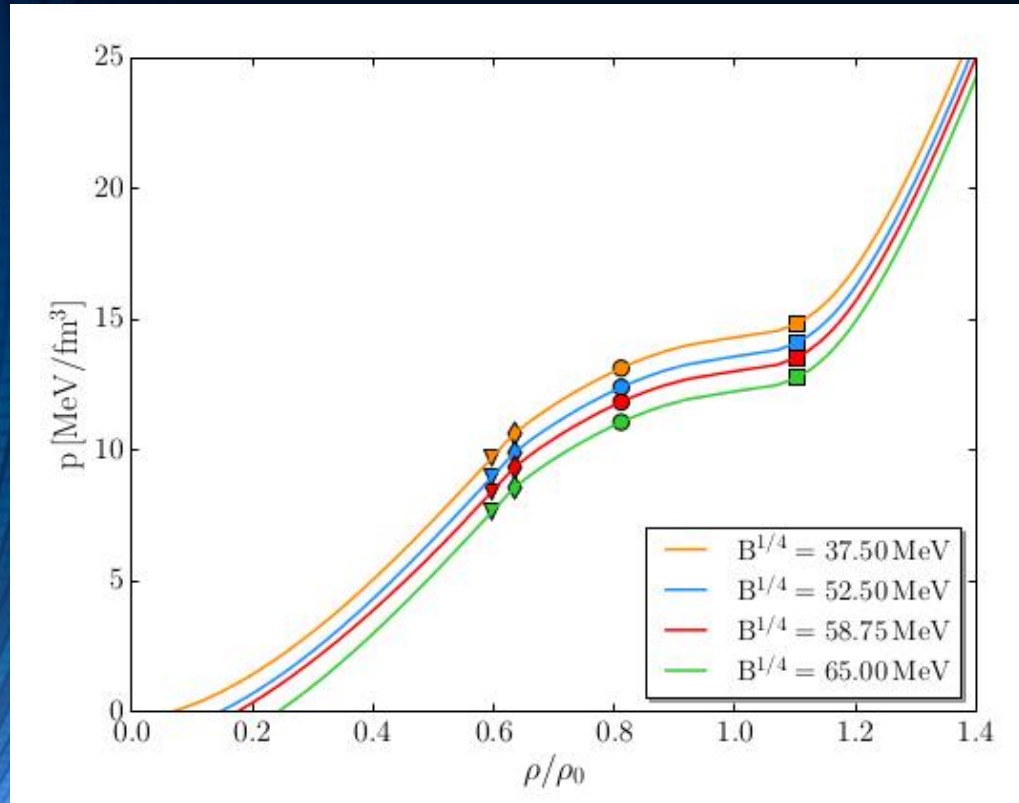


The phase transition to a chirally restored phase

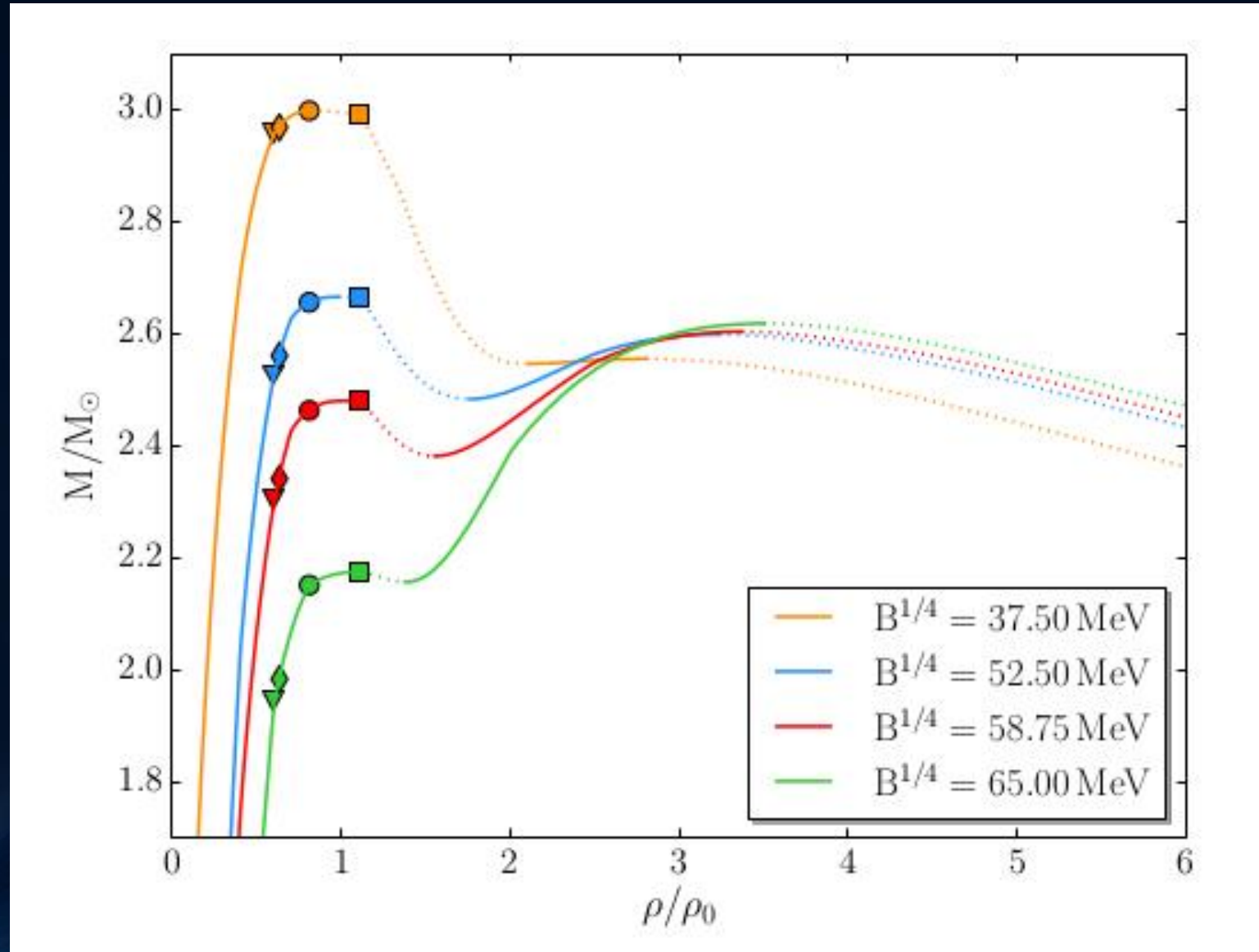
Master Thesis:
Ms Christina
Mitropoulos

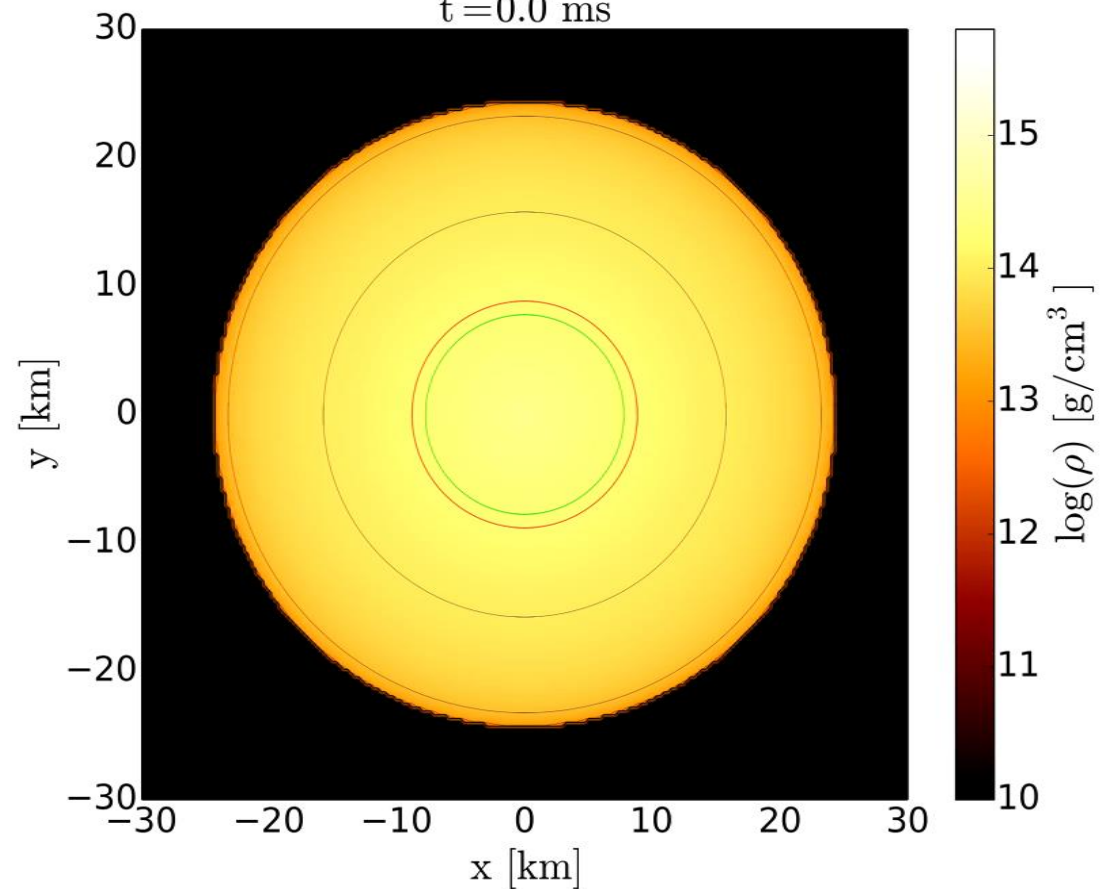
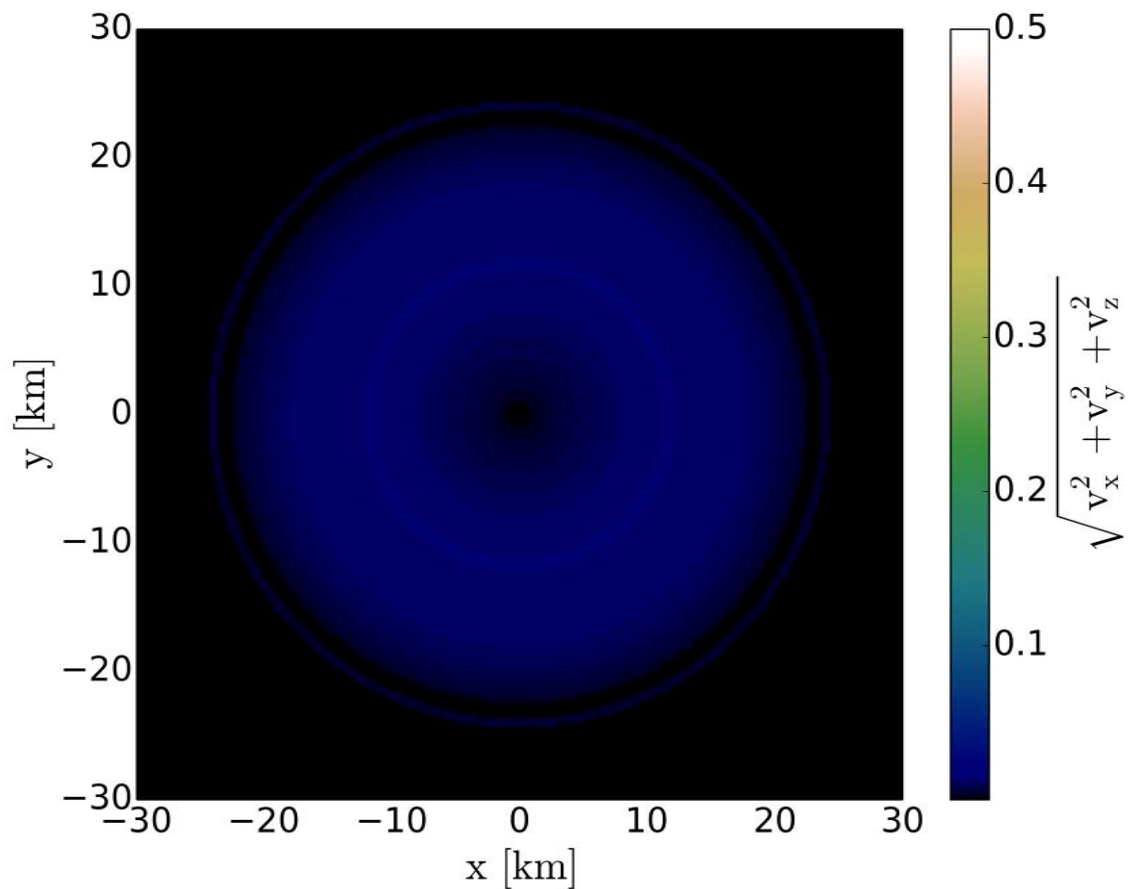


Mass-Radius Relation of TOV Stars

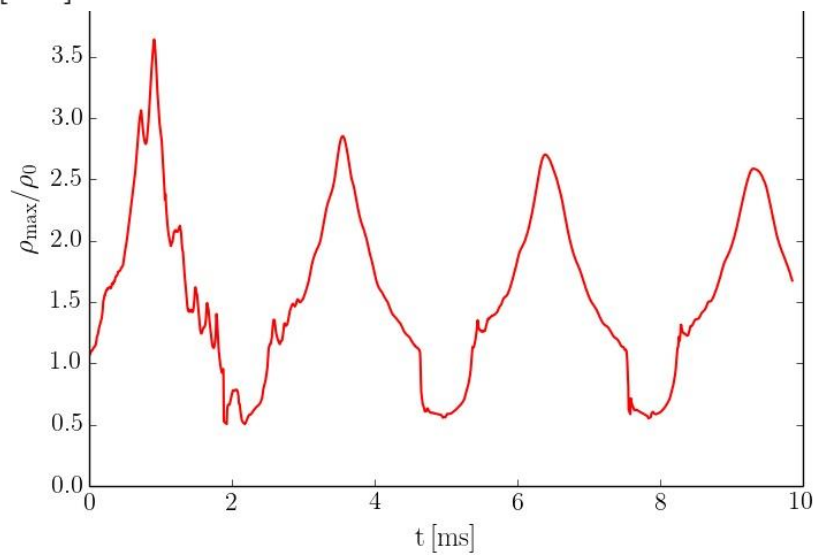


Possibility of Twin Stars in a certain Range of Bag Constant



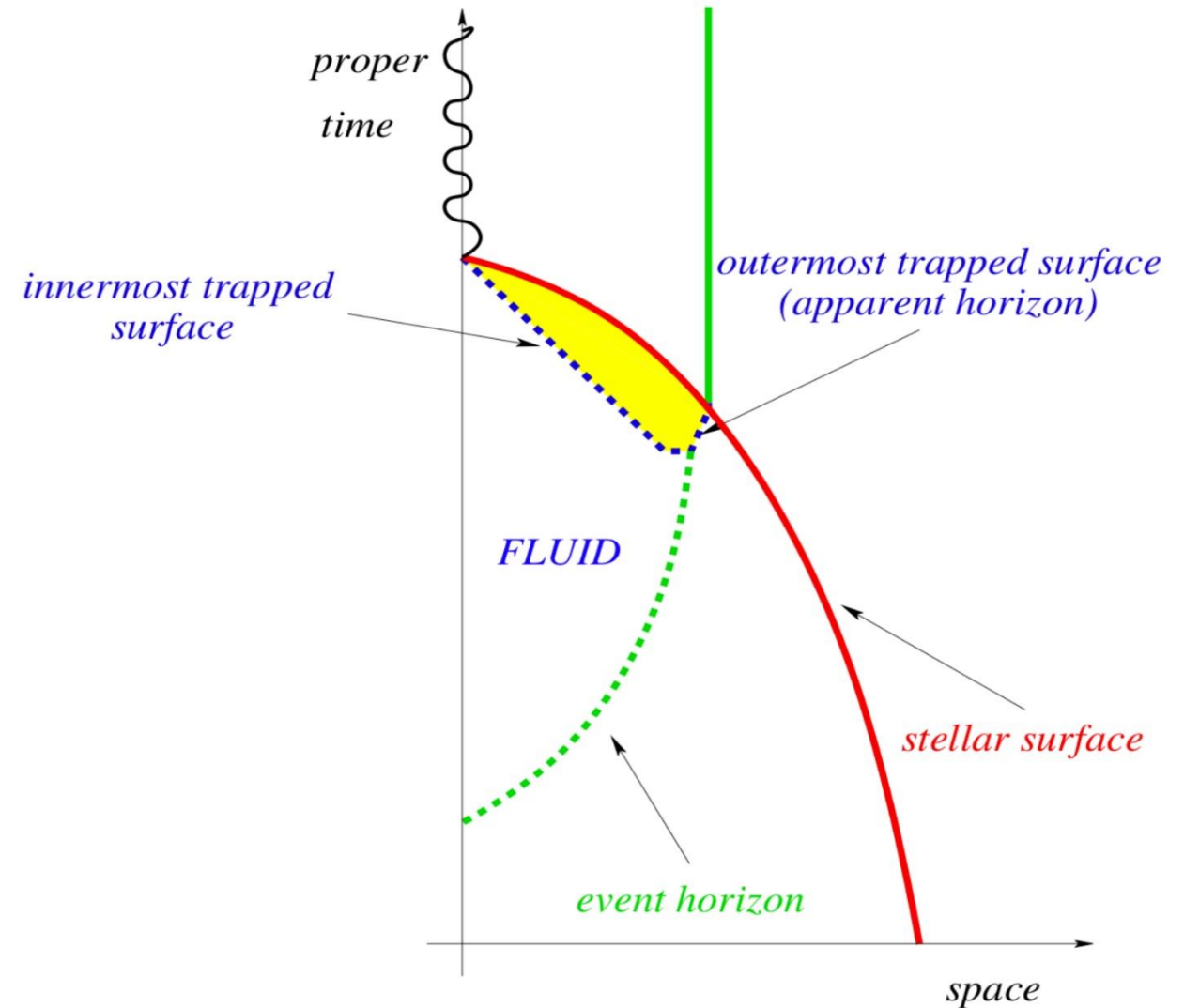
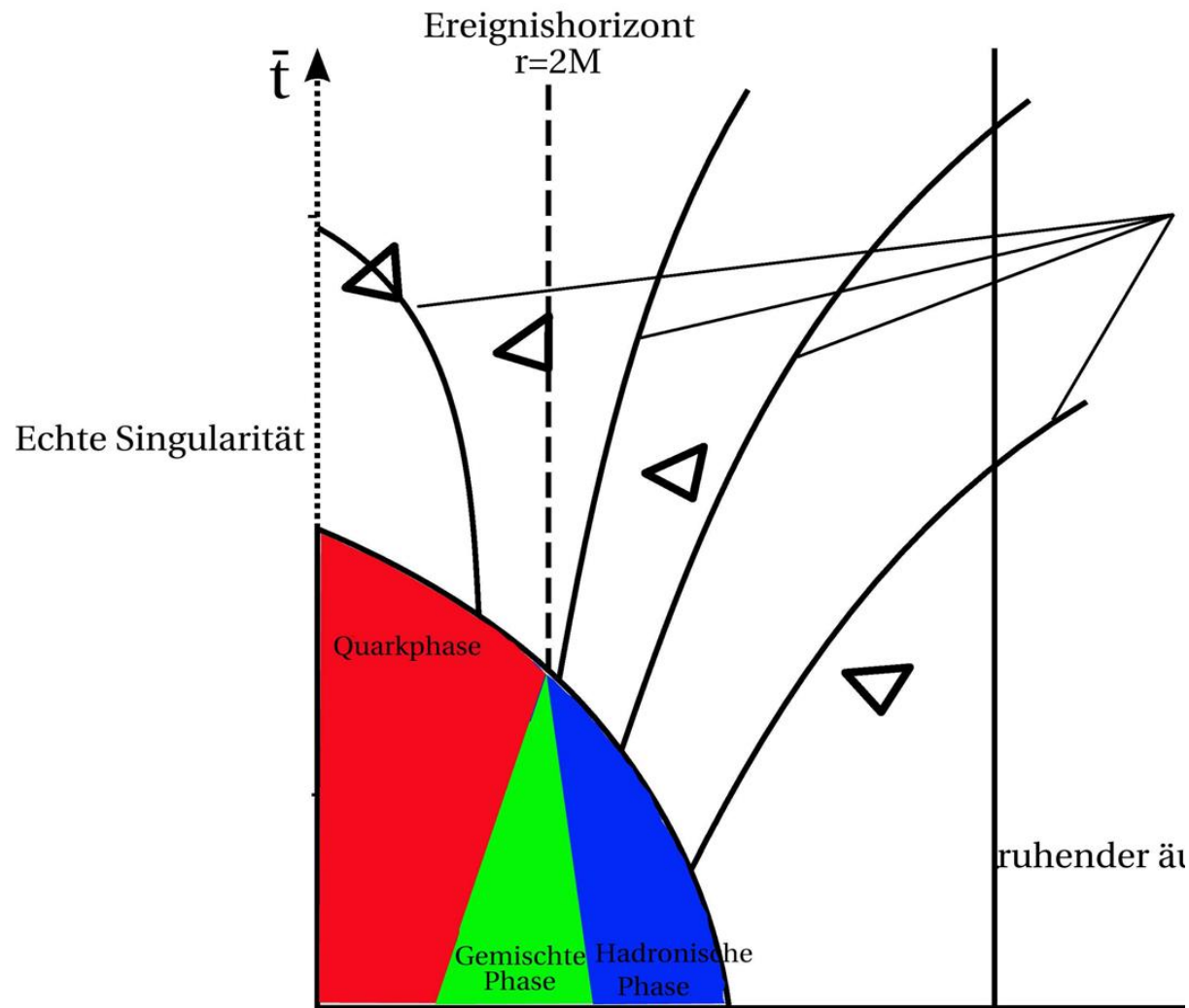


Twin Star Collapse

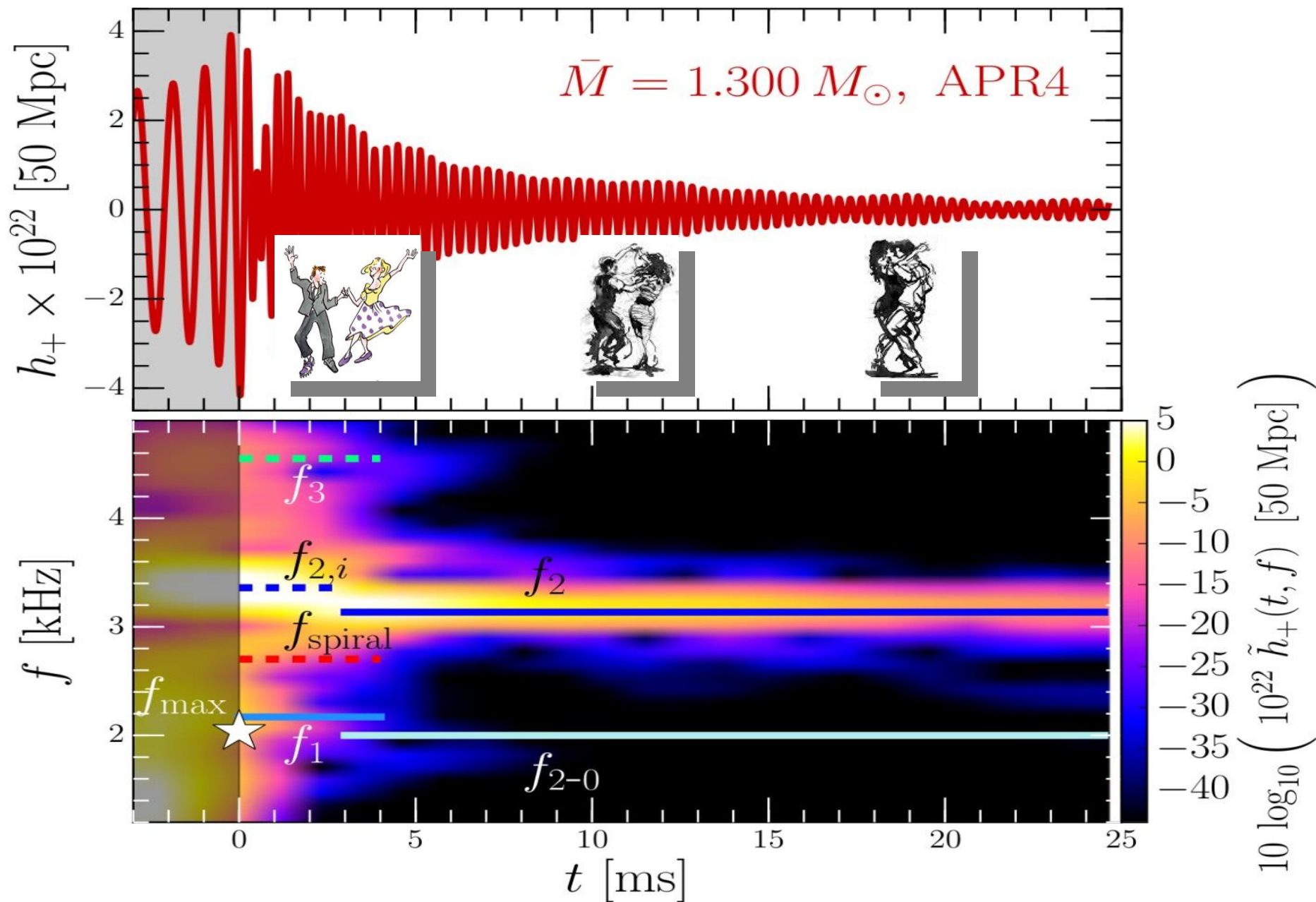


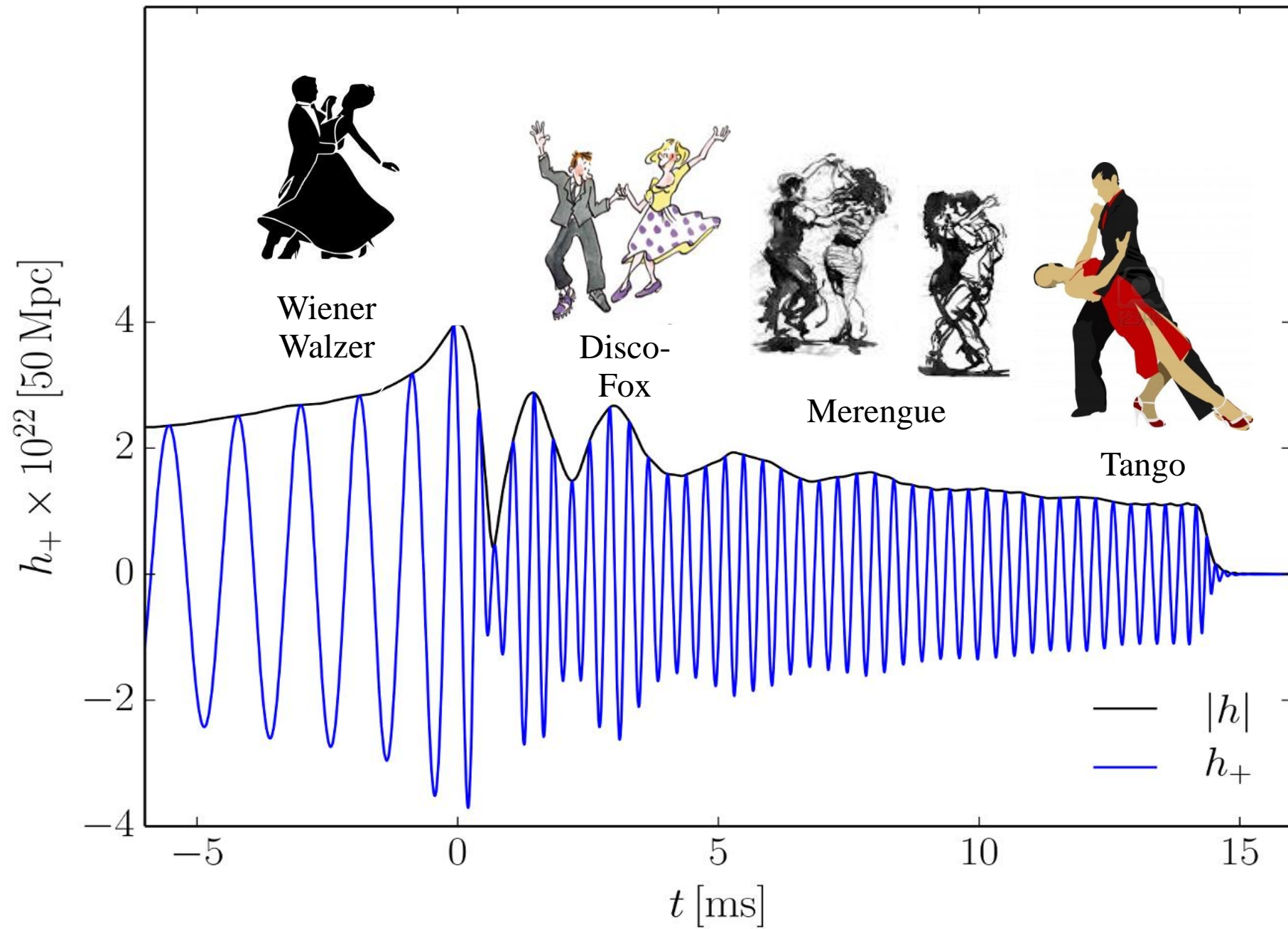
Master Thesis:
 “Quark Stars and the chiral
 Phase Transition”
 by Ms Christina Mitropoulos

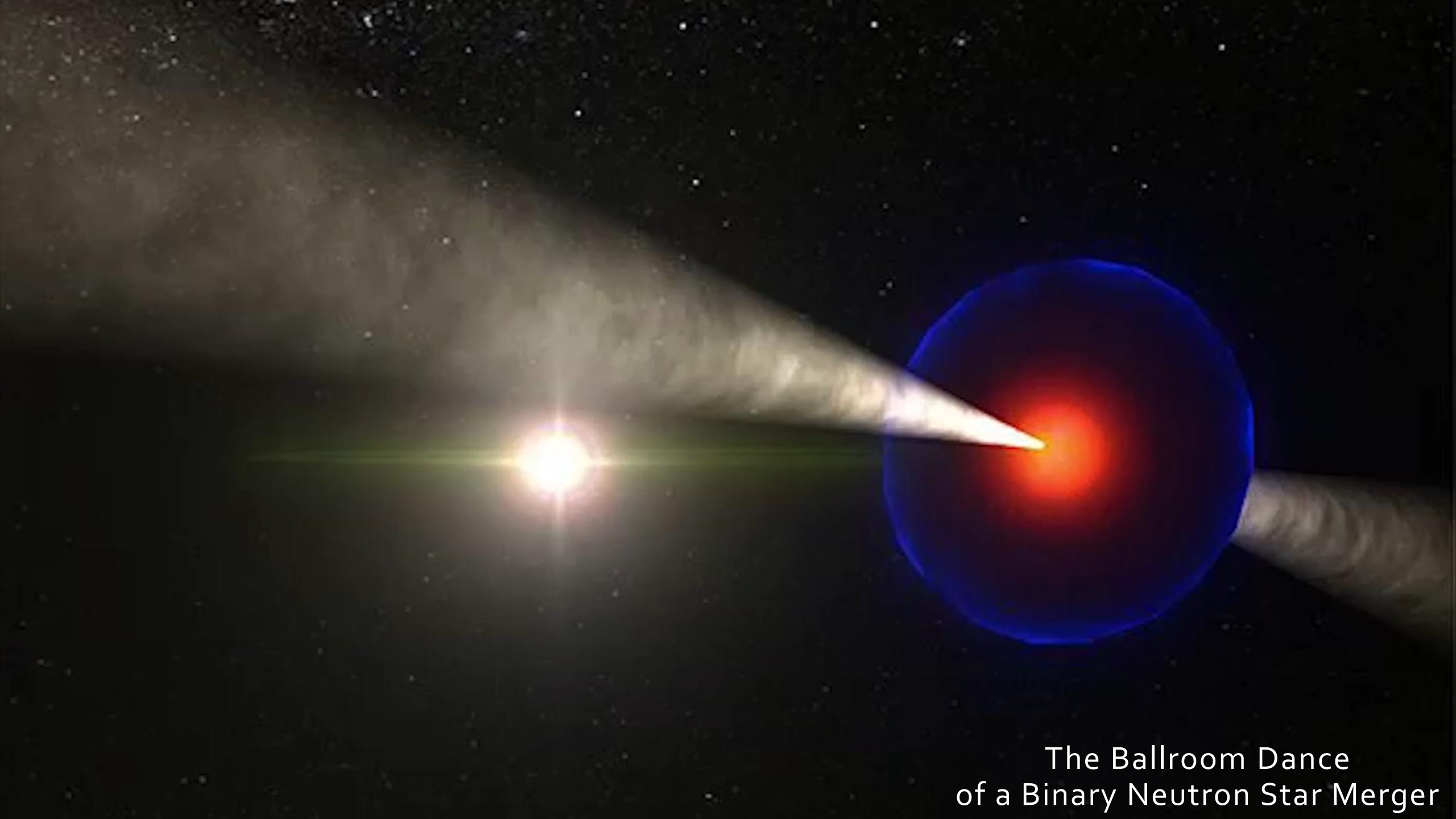
The deconfined Quark Matter will be Macroscopically Confined by the Event Horizon



The different Phases during the Postmergerphase of the HMNS







The Ballroom Dance
of a Binary Neutron Star Merger

Many Thanks to the following Persons who help me showing all the results presented during this Lectures



Prof. Luciano Rezzolla



Prof. Horst Stöcker



Mr. Jens Papenfort



Ms. Natascha Wechselberger



Mr. Elias Most



Mr. Luke Bovard



Ms. Cosima Breu



Mr. Federico Guercilena



Prof. Kentaro Takami

and
Ms Zekiye Simay Yilmaz
Ms Christina Mitropoulos